Pyrolysis of Coals and Biomass: Analysis of Thermal Breakdown and Its Products

ARTICLE *in* CHEMICAL REVIEWS · OCTOBER 2013

Impact Factor: 46.57 · DOI: 10.1021/cr400194p · Source: PubMed

2 AUTHORS:

Trevor J. Morgan
University of Hawai'i at Mānoa
62 PUBLICATIONS **1,067** CITATIONS
SEE PROFILE

R. Kandiyoti
Imperial College London
313 PUBLICATIONS **6,191** CITATIONS
SEE PROFILE

CHEMICAL REVIEWS

Review

pubs.acs.org/CR

Pyrolysis of Coals and Biomass: Analysis of Thermal Breakdown and Its Products

Trevor J. Morgan[‡,*] and Rafael Kandiyoti[†]

[‡]Hawaii Natural Energy Institute, University of Hawaii at Manoa, 1680 East West Road, Post 109, Honolulu, Hawaii 96822, United States

[†]Department of Chemical Engineering, Imperial College London, South Kensington Campus, London SW7 2AZ, United Kingdom

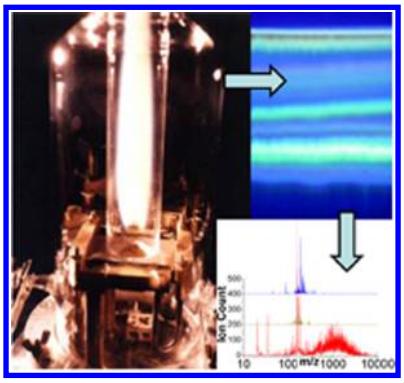

CONTENTS

Special Issue: 2014 Chemicals from Coal, Alkynes, and Biofuels

Received: April 9, 2013
Published: October 25, 2013

   dx.doi.org/10.1021/cr400194p | *Chem. Rev.* 2014, 114, 1547−1607

1. INTRODUCTION

This review presents a survey of experimental data and analytical tools that have served to formulate a conceptual model of thermal breakdown processes taking place during pyrolysis of middle-rank coals and lignocellulosic biomass. Evidence from a variety of sources has been collated to develop an understanding of the initial phases of thermal breakdown and its unfolding stages with rising temperature. Our aim will be to explore reaction pathways as a function of reaction conditions and reactor design. In trying to explain eventual product distributions, evidence relating to covalent bond cleavage will be matched against observable retrogressive recombination reaction patterns of reactive intermediates. Mechanisms of thermal breakdown inferred from this analysis will be tested by examining liquid product formation during pyrolysis and by examining the structures and compositions of the liquid products, observed through the prism of available analytical techniques.

1.1. Lasting Interest in Coal: Still Relevant?

In much of the Western world, coal utilization is commonly thought to be heading for extinction. The perceived link between anthropogenic CO_2 emissions and climate change has generated political traction, and coal appears to have been singled out as an undesirable fuel. Meanwhile, worldwide coal production and utilization is at record levels and rising. In 2010, global total hard coal and brown coal consumption exceeded seven billion tons.[1] The decade-old upward trend continued in 2011, with increases of between 4% and 6%.[2] By 2017, the IEA estimates that coal will rival oil as the world's largest source of energy, primarily through "booming demand for electricity generation and steel and cement production".[3] Demand is projected to increase in every region of the world except in the United States, where cheaper natural gas from hydraulic fracturing is partially displacing coal use in power generation.[4]

Pressures for increasing fuel supplies and improving supply security reflect the global desire for economic growth and better living standards. At present, coal utilization is responding to both requirements, apparently at acceptable cost. However, we have aspirations for a cleaner planet and fear that climate change may be linked to fossil fuel utilization. In effect, our energy-related objectives are inherently at odds with each other. A little disconcertingly, these powerful driving forces appear to act along parallel tracks that have shown little tendency to converge. In addition, there are other worries.

Production and utilization of coal as well as disposal of its waste products pollutes the environment. This is no different from other extractive industries. Everywhere around the globe there is a pressing need to clean up massive legacy pollution, added to our obligation to mitigate the environmental consequences of present and future resource utilization.

In this context, the immediate need for fundamental research aiming to make coal utilization more efficient and less polluting need not be self-evident. The major present-day consumption outlets for coal are combustion for power and steam generation and coke making; gasification is a distant third. These are all mature industries where large throughput volumes do not, in and of themselves, provide an impetus for basic research. At present, fundamental research on coal utilization seems a low-key activity, although gasification technologies are attracting significant *development* effort. Even so, it is possible to highlight some recent technological innovations where basic research has played a useful part, as briefly outlined in the next paragraph.

The study of weakly coking coals described in section 2 (below) touches upon one of several innovations introduced to coke making by Nippon Steel.[5] In an industry of nearly 600 million tons per year global production volume, any improvements in efficiency and/or reductions in pollution may be greeted as significant.[6] In sections 2 and 3, we will review several avenues likely to provide useful starting points for technological development while primarily attending to our objective of pursuing the fundamental study of thermal

dx.doi.org/10.1021/cr400194p | Chem. Rev. 2014, 114, 1547−1607

breakdown in coal and biomass. Section 4 will extend the study to liquid products formed during thermal breakdown while keeping a critical eye on the analytical methods used for characterizing these high-mass, polydispersed materials.

1.2. Coal Pyrolysis

When solid fuels are heated beyond their characteristic threshold thermal breakdown temperatures, irreversible chemical and physical changes are initiated. These processes constitute the first stage of all solid fuel utilization processes, including combustion, coking, liquefaction, and gasification. Pyrolysis itself has often been proposed as a processing step per se in both coal and biomass utilization. The vast amount of early literature on coal pyrolysis and liquefaction will be reviewed only briefly. Much of this work belongs in the pre-World War II era, with a brief but vigorous revival in the late 1970s, as will be explained below. Meanwhile, in the field of biomass pyrolysis, there has been much recent activity relating to process development.[7−11] The dearth of commercially successful projects suggests that there is, as yet, work to be done to make such processes economically attractive. Meanwhile, several process schemes are presently testing at levels between 150 and 400 tons per day.

1.2.1. Coal Carbonization. Coal pyrolysis has a place among important industrial developments of the 19th and early 20th century. Depending on market conditions, "carbonization" has sequentially or simultaneously served as a source of coke and/or coal-derived chemicals. From the 1930s onward, however, chemicals production, which included making ammonia, creosote, and aromatic chemicals, notably including toluene (for making TNT), has been overtaken by the greater production volumes and lower costs of the petroleum industry.

In the aftermath of the 1970s oil shocks, funding by the U.S. government generated new momentum for re-examining many coal utilization routes, designed to produce transport fuels and chemicals from coal liquefaction and from "low-temperature" carbonization. Literature on various applications of coal pyrolysis and its products up to about 1980 has been reviewed in Supplementary Volumes I and II of *Chemistry of Coal Utilization*.[12,13] The coal liquefaction effort of the late 20th century supported by the U.S. Department of Energy has been summarized in a wide-ranging report published in 2001.[14] Both the funding and the momentum generated through the backing of the U.S. government did eventually decline, without any of the major projects leading to economically viable processes. At present, much of the experimentation and process development work is being carried out in China, where coal is viewed as a strategically important indigenous resource.

In the meantime, no new bulk iron-making technology has managed to transplant blast furnaces to any great extent, and these installations consume large quantities of coke. The porous coke matrix interlaid between layers of iron oxides allows both diffusion and convection of reactive gases through the solid mass while providing the necessary structural support for the burden. Meanwhile, the coke also serves as an energy source and as a relatively clean supply of carbon for forming CO, the all-important reducing agent.[15]

While "high-temperature" carbonization (1000−1100 °C) has thus maintained its place within the global steel industry, coke-making technology has also been evolving. Process economics as well as environmental concerns have increasingly led to the use of "nonrecovery" ovens, where some of the heat is raised by introducing air into the oven chambers to combust coal volatiles as they come off the pyrolyzing mass.[16] This development reflects the present-day focus on the specific need to make metallurgical coke, with less attention paid to byproduct recovery.

Within this framework, the rising cost of prime coking coals is a major driving force for blending coals that display a spread of coking abilities. This is still an area that supports basic research as well as technology-oriented development work. Recent innovations include methods to increase the density of the coal mass being charged to the ovens. Moreover, the rapid heating of weakly caking coals has been found effective in enhancing the yields and properties or resultant cokes, as will be discussed in section 2.

1.3. Making Liquid Fuels from Coal and Other Starting Materials

The thermal breakdown phenomena examined in this review are intimately related to processing routes for making synthetic liquids from diverse starting materials that include biomass to liquids (BTL), natural gas to liquids (GTL), coal to liquids (CTL), and wastes to liquids (WTL), collectively referred to as feed to liquids (XTL).[17] At current crude oil price levels, synthetic liquid fuels from coal could probably be made at a profit. However, oil prices have historically proved unstable, which makes the large investment decisions required for coal to liquids processes seem that much riskier. At present, crude oil seems relatively abundant and the price bands quoted for it apparently still affordable. In other words, the overall crude oil supply position does not seem to leave much scope for committing the massive resources and accepting the logistical dislocations that large-scale synthetic liquid fuels production from coal would entail. These potential difficulties are compounded by the distinctly adverse politics of CO_2 generation by utilizing the large amounts of coal that would have been necessary.

There are several important exceptions to this observation. The SASOL *Secunda* plant near Johannesburg in South Africa currently makes about 7 million tonnes of liquid fuels per year by indirect coal liquefaction. Constructed in the early 1980s, the plant produces syngas in SASOL-Lurgi Mark IV moving burden gasifiers.[18,19] Syngas is then converted by Fischer−Tropsch synthesis to a light synthetic crude. The lighter distillation cuts of the tar produced in the gasifiers are blended in with the "diesel pool" to raise the density and calorific value of the product. Similar indirect coal liquefaction technology is being tested in China by the Lu'an Group (Changzhi, Shanxi Province), who installed an array of 6 SASOL-Lurgi Mark IV gasifiers.

The 14 500 barrels per day methanol to gasoline (MTG) plant in New Zealand was operated by ExxonMobil between 1985 and 1997.[20] The plant consisted of a natural gas to syngas unit, a methanol synthesis plant, and the MTG unit. The perceived advantage of decoupling the syngas and methanol production plants from production was to improve the on-stream factor compared to direct coupled operation.

As an aside, several gas to liquids conversion plants have been built around the globe for making more easily transportable liquid fuels from stranded natural gas supplies. At present, a 2500 barrels per day demonstration unit is operating in China (Jincheng, Shanxi Province), based on the technology and operating experience of the plant in New Zealand. Meanwhile, in Qatar (Ras Laffan) SASOL's ORYX GTL plant (34 000 bpd) and the Shell PEARL unit (140 000

dx.doi.org/10.1021/cr400194p | *Chem. Rev.* 2014, 114, 1547−1607

bpd) were built to provide alternative outlets to LNG production for the country's large natural gas reserves.[21]

1.3.1. Direct Coal Liquefaction. As in nearly all areas of research and development on coal utilization, most if not all present-day process development of direct coal liquefaction (DCL) is being carried out in China. A demonstration plant is currently being operated in Inner Mongolia by China Shenhua Coal to Liquid and Chemical Engineering Co. at the level of 24 000 barrels per day.[22]

In section 2, results from several different types of laboratory-scale, direct coal liquefaction experiments will be examined to study covalent bond-cleavage and free-radical recombination reactions taking place during the successive stages of coal thermal breakdown.

1.3.2. Polynuclear Aromatic (PNA) Ring Systems. The size distribution of polynuclear aromatic ring systems is another key parameter that would be useful to evaluate at successive stages of thermal breakdown processes. Indeed, it is of interest to follow the fate of these species during the catalytic hydroprocessing of coal-derived liquids as well.

There seems to be agreement that fused-ring systems naturally grow in size with increasing coalification maturity, i.e., coal rank.[23] In the early 1980s, Mochida et al.[24] signaled that part of the rationale for selecting Yallourn Brown coal (C content = 67.3%) as the starting material in a major Japanese coal liquefaction project was "...because such coals are believed to possess the simplest aromatic structures, i.e., based primarily on isolated aromatic ring systems..." Such observations suggest that it may be worth considering whether hydrocracking other low-rank fuels such as lignin wastes may give a more useful product slate and require less fresh hydrogen input than bituminous coal extracts. More recently, Li Chun-Zhu summarized much of what is known about processing "brown" coals.[25]

In fact, we do not have evidence to show that *any* of the larger fused-ring systems *in the original coal* are actually split during successive extraction and hydrocracking stages. During the 1990s, researchers at the British Coal Liquefaction Project reported observing that during the catalytic hydrocracking of bituminous coal extracts (Point of Ayr, U.K.; carbon content 85.4%), PNA "sheets" would tend to per-hydrogenate rather than crack to give smaller aromatic molecules. In order to recover some of the expensive hydrogen "wasted" in forming these saturated ring systems, it had been proposed to install a saturates-cracking unit in the projected demonstration plant.[26−28] In the event, the plant was not built. Meanwhile, the choice of low-rank bituminous Shenhua Shenfu coal (carbon content 79.8%) at the liquefaction project in Inner Mongolia (PRC) appears to have been based on the magnitude of the local coal reserve and its low ash, sulfur, and phosphorus contents.[29]

Cracking large polynuclear aromatic ring systems through reaction pathways that would produce smaller and more useful aromatic molecules thus remains one of the major challenges of upgrading bituminous coal liquefaction extracts and other predominantly aromatic heavy hydrocarbons.[30] One of the hitherto missing tools for monitoring structural changes during successive stages of coal liquefaction has been a quick and an accurate analytical method for estimating the sizes and distributions of PNA ring systems. In section 4, we will review recent developments based on NMR spectroscopy that have facilitated more accurate estimation of PNA ring system sizes.

1.4. Pyrolysis of Lignocellulosic Biomass

In section 3, we will address fundamental aspects of thermal breakdown in lignocellulosic biomass. Given the large proportions of liquids that may be produced from biomass pyrolysis, we will also review the challenges, methods, and prospects for upgrading biomass pyrolysis tars/oils.

There are compelling reasons for reviewing fundamental aspects of lignocellulosic biomass pyrolysis alongside thermal breakdown in middle-rank coals. As described in sections 2 and 3, coal and biomass respond to increases in temperature in remarkably similar ways. As a result, differences between experimental approaches devised for investigating their behavior are small and the requirements for reactor design often quite similar. Furthermore, it is possible to begin explaining some of the reported "novel" observations from biomass pyrolysis, e.g., the incipient fluid behavior of rapidly heated wood samples, in terms of phenomena already familiar from coal pyrolysis. At the level of basic research, compartmentalization between coal and biomass pyrolysis seems difficult to explain.

Despite the large volume of funding and research devoted to process development, to date there are relatively few applications that have been scaled up beyond pilot plants in the field of biomass to liquids applications.[17] Despite the high costs and difficult logistics that have impeded the commercial acceptance of a plethora of proposed new processes,[7−11] some pyrolysis units appear to have successfully reached the crucial demonstration-plant stage. Several large units are operating in Malaysia, producing bio-oil for cofiring with more conventional fuels in stationary diesel engines. The largest of these is a rapid thermal processing unit based on a fluid catalytic cracker design, the largest with a capacity of 400 tons per day (t/d).[31−33] Another unit being tested in Malaysia is a rotating cone (ablative pyrolysis) device, designed to process 50 t/d of biomass.[34] In Canada and elsewhere, several 100 and 200 t/d bubbling fluidized bed biomass pyrolysis units are currently operating or are under construction.[35] Most of the units dotted around the globe are producing bio-oils for direct combustion, some (as above) in diesel engines. In section 3, we will also present an overview of experimentation on catalytic bio-oil/tar upgrading.

Within this uncertain but modestly optimistic outlook for biomass utilization, it seems useful to take a step back from the pressures of process development to review the possibilities offered by the structures and fundamental behavior of biomass fuels as well as some of the constraints associated with lignocellulosic biomass pyrolysis.

1.4.1. Why Review Basic Research on Thermal Breakdown? We live in an age where prescriptive funding has largely replaced established methods of enquiry with demands for delivery of preconceived work packages at precise intervals. We also know that studies of a fundamental nature rarely lead *directly* to economically viable engineering solutions, let alone to mandatory "game-changing" innovations with prearranged regularity. Reviewing basic research on thermal breakdown phenomena at this time might therefore appear a little wide of the mark. However, in addition to its intrinsic intellectual value of satisfying our curiosity, fundamental research is generally useful in supporting the progress of technological innovation. Small-scale experiments are useful in helping to explain observations from pilot- or plant-scale equipment and have been successfully used in trouble shooting as well as in singling out process routes that appear to have

dx.doi.org/10.1021/cr400194p | *Chem. Rev.* 2014, 114, 1547−1607

relatively little chance of success.[36−38] More important, with the help of judicious experimental design, it is possible to deconvolute (unpack) complex phenomena taking place in larger scale plant and examine likely key parameters in isolation. While striving to develop a more general understanding of the mechanisms of thermal breakdown in coal and biomass, this review will attempt to show that investigating the fundamentals of pyrolytic behavior of solid fuels can be both stimulating and vitally important for future technological innovation.

The next two sections present an overview of experimental work carried out to explore reaction pathways of thermal breakdown in solid fuels. In section 2, thermal breakdown phenomena during pyrolysis and liquefaction of middle-rank coals will be compared, underlining the central role of retrogressive free-radical recombination reactions in shaping the outcomes of thermal processes. Ideas developed from these observations will be tested against the behavior of higher and lower rank coals and coal maceral concentrates. In section 3, we will explore the implications of some of these findings for thermochemical reactions of lignocellulosic biomass and explore the similarities as well as the differences between coal and biomass pyrolysis.

2. FUNDAMENTALS OF THERMAL BREAKDOWN IN MIDDLE-RANK COALS

In reading the next several sections it would be helpful for the reader to know something of coal structure and, to a lesser extent, of coal macerals. Beyond citing several well-known sources, however, no attempt will be made to outline such vast and varied subjects in the space available; these subjects have been widely and encyclopedically described and discussed in the open literature.[12,13,23,39,40]

We begin by examining several elementary questions relating to pyrolysis of middle-rank coals. (1) When does thermal breakdown actually begin? (2) Are there similarities between reaction pathways during pyrolysis and liquefaction? (3) When and how do reaction pathways between these two classes of processes begin to diverge? As allied questions, we will explore the folowing. (4) When and how are pyrolysis product distributions affected by heating rates? (5) What do these results tell us about the way retrogressive recombination reactions tend to work? These questions relate directly to the reaction pathways of thermal breakdown. Any new insights would have implications about the initial phases of all major industrial coal utilization process routes, including combustion, gasification, coke making, and liquefaction.

2.1. Electron Spin Resonance (ESR) Spectrometry of Thermal Breakdown

Singer and co-workers[41−43] carried out much of the pioneering work on the fundamentals of the electron spin resonance (ESR) spectrometry of carbonaceous materials. These researchers were able to show that the stable paramagnetic species observed in the products of low-temperature pyrolysis were indeed free radicals. We now know that the ESR spectra of *untreated* coals reflect stable free-radical populations formed and embedded within coal matrices during the coalification process. Middle-rank coals normally contain on the order of $\sim 10^{19}$ free radicals per gram. Among other advances, Singer and co-workers used ESR spectroscopy to study the kinetics of the transformation of pitch to coke and discussed the relevance to the carbonization process of free radicals observed by ESR.[44]

When pyrolysis experiments are performed within the spectrometer cavity (in-situ), ESR spectroscopy allows observing populations of new unpaired electrons resulting from covalent bond cleavage during heat up. Basically, what is being determined is the number of *stable* free radicals left over from *completed* pyrolytic processes. With appropriate corrections, the change in spin population may be calculated as a function of temperature. However, as in the case of ordinary pyrolysis experiments, the results (in this case, ESR spectra of the pyrolyzing samples) to some degree reflect the design of the experiment and the configuration of the sample.[45,46]

2.1.1. Free Radicals in Coals. The relative reactivities of free radicals in carbonaceous materials depend on whether and how the host molecular structure allows the delocalization of unpaired electrons. Enhanced delocalization tends to reduce the reactivity of free radicals. We also note that observing *reactive* free radicals in coals by ESR spectroscopy is difficult, due to the shorter lifetimes of reactive free radicals (by definition) and their low concentrations, at any given time, relative to the much higher background count of *stable* free radicals.[46]

Figure 1 presents a schematic diagram, typical of spin population vs temperature curves, obtained from experiments

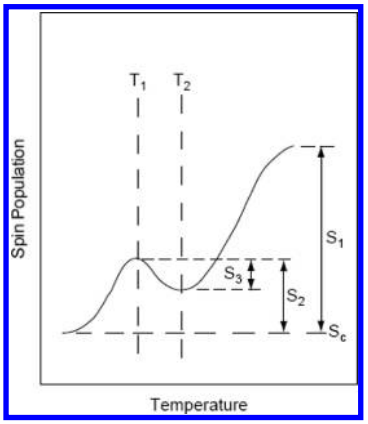

Figure 1. Schematic diagram showing the main characteristics of spin population vs temperature diagrams. (Reproduced with permission from ref 52. Copyright 1989 Elsevier.)

where coal samples are heated in a quartz fixed-bed reactor, placed inside the cavity of an ESR spectrometer. In this configuration, the fixed-bed reactor is equipped with a gas sweep facility to remove evolving volatiles out of the reaction zone and out of the ESR cavity. Sweeping the reactor with an inert gas reduces the residence times of volatile pyrolysis products in the reaction zone and helps suppress likely secondary reactions between primary volatiles and pyrolyzing solids. When coal samples are heated in sealed (i.e., closed) vessels,[47,48] volatile products remain in the vicinity of the pyrolyzing coal and the ESR signal appears to be affected by coal−volatile interactions.[45,49−51]

In Figure 1, three distinct types of thermally induced processes have been identified during coal pyrolysis experiments where the evolving volatiles were swept from the reaction zone by means of a carrier gas stream.[52] In this diagram, spin populations (S) are defined as free radicals per gram of initial sample. Three distinct regions may be identified.

Region I ($T < T_1$). S increases to a relatively shallow maximum (near 200 °C) as signal recovers through desorption

dx.doi.org/10.1021/cr400194p | Chem. Rev. 2014, 114, 1547−1607

Table 1. ESR Parameters of Coals Given as Spin Population × 10^{19} in the Flow Cell[a]

coal	elemental carbon, C (%, daf)	T_1 (°C)	T_2 (°C)	S_C (g^{-1})	S_1 (g^{-1})	S_2 (g^{-1})	S_3 (g^{-1})
Çan[b]	54.2	250	310	0.3	0.8	0.46	0.12
Burning Star	75.5	220	310	0.8	2.9	0.54	0.23
Linby	83.0	205	310	1.07	3.26	1.19	0.33
Point of Ayr	85.4	220	325	1.37	1.98	0.58	0.3
Cortonwood[c]	87.2	250	340	1.36	3.21	0.67	0.23
Cynheidre[d]	95.2			1.72			

[a]Reproduced with permission from ref 52. Copyright 1989 Elsevier. [b]Three region behavior not well developed. [c]Swelling of coking coal forced part of the sample out of the cell. [d]Three region behavior not apparent with this coal.

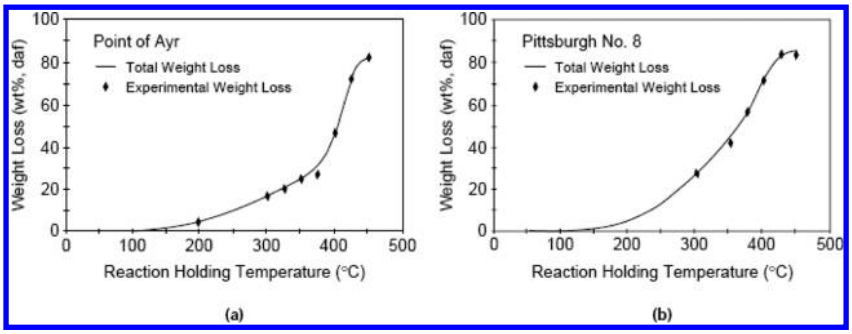

Figure 2. Sample weight loss from Point of Ayr and Pittsburgh No. 8 coals as a function of temperature in the flowing-solvent reactor. Samples were heated at 5 °C s^{-1} to 450 °C with 400 s hold. Tetralin flow rate: 0.9 mL/s at 70 bar. (Reproduced with permission from ref 53. Copyright 1996 American Chemical Society)

of moisture and oxygen, adsorbed on particle surfaces during previous exposure of the sample to air.

Region II ($T_2 > T > T_1$). *S* decreases to a minimum (near 300 °C). This decline is thought to be associated with recombination reactions, resulting from the thermally induced mobility of free-radical-bearing material with sufficiently high reactivity, already residing within the coal matrix.

Region III ($T > T_2$). *S* increases monotonically, signaling an increase in the free-radical population as the temperature rises and coal thermal breakdown commences. It is thought that the temperature T_2 marks the onset of covalent bond-cleavage reactions.

Earlier, Singer et al. pointed out that unpaired spins detected in higher temperature carbons and graphites are primarily conduction electrons.[44] This was useful for interpreting the rise in spin populations at the higher temperatures (Figure 1), where signal increases from unpaired spins due to free radicals (resulting from intensified covalent bond-cleavage reactions) tend to overlap with signal from free conduction electrons.

Table 1 shows data from experiments on six samples, spanning a wide range of coal ranks. In this series, T_2 increased from 310 °C for a lignite to 340 °C for "Cortonwood Silkstone" coal, the highest rank coal for which a result could be obtained (87.2% C content). The Welsh anthracite Cynheidre turned out to be rather inert.

Comparing these results with data from coal *liquefaction* experiments is revealing. The results shown in Figure 2 were from experiments carried out in a "flowing-solvent" reactor, where solvent-soluble coal liquefaction products were continuously removed from the reaction zone. The reactor[53] will be introduced in section 2.4.2.

Figure 2 shows that both coals lost up to one-third of their mass at temperatures below 300–325 °C. These are temperatures that signal the *onset* of covalent bond cleavage for most middle-rank coals. It seems reasonable to expect that weight losses observed up to these temperatures would mostly be due to solvent extraction of the more mobile, relatively low molecular mass material within the coals. Figure 2 shows that above 350–375 °C the rate of weight loss *accelerated* with increasing temperature; the data on Point of Ayr (U.K.) coal shows this more graphically than many other coals. As the temperature rose to between 375 and 400 °C, coal extract yields from two different middle-rank coals reached and exceeded 40%; this increase was accompanied by a broadening of extract molecular mass distributions.[54,55]

The temperature ranges where more significant and rapid release of extracts occurred were clearly well above the 310–340 °C interval, signaled in Table 1 as pinpointing the *onset* of covalent bond cleavage. The temperature difference between the onset of covalent bond scission and the observed massive dissolution after 350–375 °C suggests that several covalent bonds must rupture before fragments of larger molecular mass material (compared to the more easily extractable species) can be released from the solid coal matrix.

Thus, provided an appropriate solvent is used for dissolving and sweeping the extractable material away, solvent-extraction/liquefaction allows recovering a large proportion of the coal mass as a solvent-soluble extract at temperatures up to 400 °C. Meanwhile, sample weight loss during pyrolysis of low- to middle-rank Linby coal (U.K.) at 400 °C was observed to be limited to about 5% or less (Figure 3). Assuming that covalent bond cleavage is primarily a function of the temperature, similar proportions of extractable material would be expected to have detached from the solid matrix, at the same temperature, during both pyrolysis and liquefaction. Clearly, during dry pyrolysis (i.e., in the absence of a solvent), all extractable material that is unable to evaporate at 400 °C remains trapped within heated coal particles.

To summarize, no significant divergences are expected between thermal breakdown reaction *pathways* of pyrolysis and liquefaction/extraction up to about 400 °C. This may be understood in terms of covalent bond rupture being primarily a

dx.doi.org/10.1021/cr400194p | Chem. Rev. 2014, 114, 1547–1607

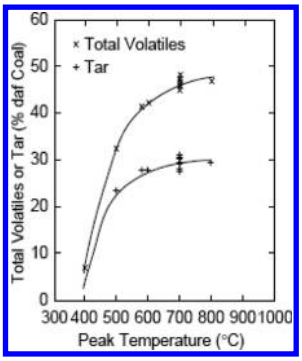

Figure 3. Effect of peak temperature on pyrolysis tar and total volatile yields. Heating rate: 1000 °C s^{-1}. Linby coal. Thirty second holding at peak temperature; sweep gas, helium at 1.2 bar flowing at 0.1−0.2 m s^{-1}. Particle size range: 106−152 μm. (Reproduced with permission from ref 52. Copyright 1989 Elsevier.)

function of the temperature. In the 350−400 °C interval, pyrolysis and liquefaction pathways begin to diverge only in a physical sense: in liquefaction, increasing amounts of extractable material are first detached from the coal matrix and then *removed* from coal particles by the action of the solvent. By contrast, in pyrolysis, weight loss at up to 400 °C represents only a relatively small fraction of the coal mass released *into* the particles. Somewhat less than 5% of the original mass evaporates from the coal particles (Figure 3). Comparison with weight loss during liquefaction (Figure 2) helps us to conclude that during pyrolysis, at up to 400 °C, large proportions of the extractable material (tar precursors) released *within* the coal particles remain trapped there. We will see below that these "trapped" extractables are chemically rather stable at 400 °C for up to 120 s and perhaps longer but begin to degrade significantly above 450 °C.

As the temperature is raised above 400−450 °C in (dry) pyrolysis, extractables trapped within pyrolyzing coal particles become more reactive. Clearly, the course of these reactions directly affects eventual product distributions. However, not all intermediate reaction products necessarily "see" the final temperature. Some of the reaction intermediates become volatile due to cracking of the extractables or may simply become volatile due to the rise in temperature. The composition of the volatile material may still be altered, furthermore, by additional residence time in the heated reaction zone; reactivity would be maintained until the volatiles are cooled down. Thus, pathways dictated by reactor configuration as well as the reaction conditions play a part in determining the eventual product distribution. Furthermore, changing the heating rate usually alters the results of these experiments.

Before discussing the reaction pathways of extractables within coal particles and the effect of the heating rate on pyrolytic processes, it would be instructive to pay attention to experimental design. We will see that careful reactor design may help avoid many of the potential pitfalls presented by the complexity of pyrolytic processes and may help identify "equipment-specific" effects in results from laboratory experiments.

2.2. Design of Bench-Scale Pyrolysis Reactors

The variety of designs on offer for coal/biomass pyrolysis experiments provides testimony that generally acceptable schemes giving unambiguous results have proved elusive. As already signaled, the underlying complication is the chemical reactivity of many of the intermediate products released during thermal breakdown. The outcomes of pyrolytic events are therefore affected by the time−temperature histories of the pyrolyzing solid fuel and the thermal and chemical histories of the occluded intermediates and of the volatile products.

2.2.1. Basic Concepts for Designing Pyrolysis Experiments. The primary requirement in designing a pyrolysis experiment is the ability to characterize the behavior of the fuel, with as little reference as possible to sample or reactor configuration. More formally, we can state that evaluating the fundamental pyrolytic behavior of a solid fuel requires the strict decoupling of observations on sample behavior from effects due to the design of the particular reactor and the shape and dimensions of the sample. This is not in any sense different from requiring the result of *any* measurement to be entirely independent of the method of measurement.

In actual practice, we usually have to make do with results that are *as independent as possible* from the method of measurement. Nevertheless, the importance of striving to *minimize* the effect of sample and reactor configuration on the results of pyrolysis experiments cannot be overstated. In setting up an *actual* experiment, it is essential to establish the elements of design that will allow us to distinguish clearly between the properties and pyrolytic reactions of the fuel and the effects arising from the design of the experiment itself. A case in point is the height and temperature distribution of the freeboard of a fluidized-bed pyrolysis reactor; both parameters would affect the extent of tar cracking in the freeboard.

One practical consequence of the rigid constraints imposed on the design of the experiment is the need to assess the behavior of sample particles, as much as possible, in isolation from one another. It is also important to subdivide the sample particles as finely as is practicable, since *intra*particle reactions of tar precursors tend to influence the amount and composition of tars and other volatiles released from individual particles.[57] Particle diameters much larger than 100 μm may give rise to misleading data. On the other hand, particles with diameters much below 70−80 μm are difficult to handle, due to static electrical effects. The need to make compromises is clear.

The ordinary fixed-bed reactor, where coal particles are stacked together prior to heating, provides several instances of what may go wrong during pyrolysis experiments. In this configuration, contact between evolving volatiles and heated, pyrolyzing solid surfaces seems inevitable. Early experiments by Griffiths and Mainhood have shown that tar molecules move through a heated fixed bed of coal particles in the manner of sample molecules moving through a chromatographic column.[58] Tar molecules sequentially adsorb onto and desorb from a succession of heated particles. However, above 350−400 °C, most coal-derived volatiles are able to react with pyrolyzing bed solids. Tar molecules may polymerize to produce fresh char and/or partially crack to release lighter tars and gases. Compared with products from a wire-mesh reactor experiment (in effect a *very* shallow, monolayer, fixed bed), volatile releases from a fixed-bed reactor may be reduced by as much as 6−8%.[59]

The problems arising from the reactivity of evolved volatiles are complicated by wide differences in reactivity between tars of different origins, largely determined by the chemical makeup of the original fuels. The more oxygenated pyrolysis tars released by cellulose or lignocellulosic materials such as wood are thermally more sensitive and tend to crack thermally at lower

dx.doi.org/10.1021/cr400194p | *Chem. Rev.* 2014, 114, 1547−1607

temperatures compared to tars from lignites or bituminous coals.[60]

Within this framework it is worth noting that thermogravimetric (TG) balances are not designed to suppress or eliminate the secondary reactions of evolving volatiles or prevent tar loss through contact with pyrolyzing solids. While TG balances are effective instruments that have proved useful in diverse applications, they do not allow examining the pyrolytic behavior of solid fuels in a manner that is independent of reactor geometry. By the same token, deriving sets of kinetic parameters from TG analysis cannot be considered an error-free process, since departures from fundamental sample behavior are amplified by differentiating data to arrive at reaction rates. Critical evaluations of pyrolysis experiments in TG balances and calculation of kinetic parameters from such data have been presented elsewhere.[61,62]

Many commercially available pyrolysis devices, e.g., "pyroprobes" attached to pyrolysis-GC-MS systems, are similarly not optimized to produce volatiles with compositions that are independent of device geometry. In addition, pyrolysis-GC-MS systems suffer from similar limitations as all GC-MS instruments, since analyses are necessarily confined to compounds that have sufficient volatility to pass through the GC column. Higher boiling materials tend to remain trapped within the system (cf. ref 62, Chapters 7 and 8)

2.2.2. Wire-Mesh Reactor: Key Features. Figure 4 presents a schematic diagram of the atmospheric-pressure wire-mesh reactor developed at Imperial College London. The instrument is capable of operating at variable heating rates between 0.1 and 10 000 °C s^{-1} and peak temperatures up to 2000 °C. In early work, this instrument enabled observing changes in product distributions with increasing heating rate (Figure 5).[56] Later work described below has shown that sensitivity to heating rate is greatest for middle-rank coals.

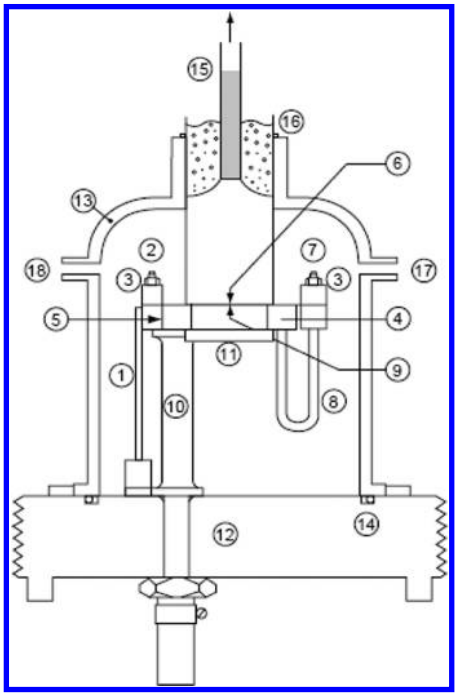

Figure 4. Atmospheric-pressure wire-mesh reactor with the present tar trap designs. Legend: (1) copper current carrier; (2) live electrode; (3) brass clamping bar; (4) sample holder support plate; (5) mica strip; (6) wire-mesh sample holder; (7) electrode; (8) stainless steel tubes; (9) mica layer; (10) brass pillars; (11) sintered pyrex glass disk; (12) base plate; (13) Pyrex bell; (14] O-ring seal; (15) off-take column; (16) o-ring; (17) carrier gas entry port; (18) connection for vacuum pump. (Reproduced with permission from ref 89. Copyright 2004 American Chemical Society.).

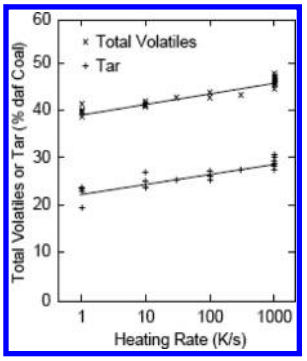

Figure 5. Effect of heating rate on tar and total volatile yields. Wire-mesh reactor data. Peak temperature of 700 °C. Linby coal. Thirty second holding at peak temperature; sweep gas, helium at 1.2 bar flowing at 0.1−0.2 m s^{-1}. Particle size range: 106−152 μm. (Reproduced with permission from 56. Copyright 1989 Elsevier.)

The configuration of this reactor is useful for approximating single-particle behavior during pyrolysis experiments. The wire-mesh reactor concept, originally developed by Loison and Chauvin,[63] is best known through seminal work by Howard and co-workers at the Massachusetts Institute of Technology.[64] Major stages in the evolution of this remarkably versatile instrument by various laboratories have been reviewed elsewhere (cf. ref 62; Chapter 3).

The basic design concept is straightforward. Milligram quantities of sample particles are placed between two layers of folded wire mesh. Spreading the sample particles as less than a monolayer aims to approximate single-particle behavior and minimize the effect of sample and reactor geometry on the outcome of the experiment. The folded wire mesh containing the sample is weighed and stretched between two electrodes. Fine wire thermocouples are attached. The mesh, which also serves as a resistance heater, is heated with a low-voltage current (~80 A). After the sample has been exposed to a preprogrammed time−temperature profile, the weight change of the assembly is determined. Depending on the aim of the experiment, product chars, tars, and/or other volatiles may be recovered and characterized.

The design of both the atmospheric-pressure and the high-pressure versions of the wire-mesh reactor developed at Imperial College London provide for a carrier gas stream flowing normal to the plane of the wire mesh. A brass plate with a central hole was installed underneath the mesh, allowing the gas flow to be directed vertically upward. The stream of gas could then be forced *through* a 3 cm diameter circular area of mesh, where 106−152 μm sample particles (~5 mg) were evenly distributed. The flow served to sweep volatiles released by pyrolyzing sample particles away from the reaction zone into the cold trap (item 15 in Figure 4). One of the electrodes was spring loaded by means of the connecting tubes to take up thermal expansion by the mesh as it heated up; this kept the mesh from distorting. To prevent overheating, the brass plate, electrodes, and connecting tubes (item 8 in Figure 4) were cooled with circulating water. This was particularly useful

during slow heating experiments, when the electrode assembly tended to absorb large amounts of heat.

Once the experiment is triggered, evolving volatiles are continuously swept into the central "chimney", packed with fine strips of stainless steel wire mesh. To quantify tar deposition, the traps were dried and weighed before and after an experiment. Pyrex glass traps could be used at up to 1000 °C for up to 5 s; quartz traps were used for longer runs at 1000 °C or during higher temperature experiments. Applications of this reactor have included pyrolysis experiments under vacuum.[57,65]

The high-pressure version of this reactor has been used for pyrolysis and gasification experiments at temperatures up to 2000 °C (at up to 30 bar)[66] and pressures up to 150 bar[67] (at 850 °C) as well as for high-pressure gasification experiments with pure steam injection, mixed steam/CO_2 injection,[68] or mixed steam/H_2 injection.[69] Injectant coal particle behavior in blast furnace tuyeres and raceways has been mimicked using temperature-staged, successive "nitrogen; O_2-enriched air; carbon dioxide" injection conditions. In this way, the sequential pyrolysis−combustion−gasification stages of blast furnace operation could be simulated during a single wire-mesh reactor experiment.[70]

Despite the flexibility afforded by the basic design, wire-mesh reactors should not be considered as instruments of first resort. Considerable investment is required in reactor and software design, purchasing sensitive balances, and in very substantial operator training. Another major drawback is the small (milligram) sizes of the tar, char, and gas samples generated during individual experiments. The amounts of sample produced do not allow performing standard char porosity measurements or, indeed, provide sufficient sample for tar/oil distillation or tar/oil stability tests. By contrast, a fixed-bed pyrolysis reactor is quickly constructed[59] and may be useful in *comparing* the pyrolytic behavior of distinct samples, even though results are never easy to interpret in detail and the range of possible heating rates is limited. Fluidized-bed[60] and drop-tube ('entrained-flow') reactors[71] provide partial solutions to some of these problems while introducing several difficulties of their own. More detailed discussions of the capabilities and relative advantages of bench-scale pyrolysis reactor types has been presented elsewhere (cf. Chapters 3 and 4 of ref 62).

The pyrolysis tar and total volatile yield data presented in Figure 5 were obtained using the wire-mesh reactor shown in Figure 4. As the heating rate was increased, the tar and total volatile yields increased very nearly in parallel, indicating that the rise in volatiles was due to greater tar evolution. The coal sample used in these experiments was weakly coking Linby coal. At the low heating rate of 1 °C s^{-1}, this particular coal remained morphologically unchanged. However, with increasing heating rate at up to 1000 °C s^{-1} it displayed increasing softening and melting (plastic) behavior.[56] Similar behavior was observed during analogous experiments with middle-rank Pittsburgh No. 8 coal, which also showed no fluidity during experiments at 1 °C s^{-1} but readily softened (melted) when heated at 1000 °C s^{-1}.[72] The Pittsburgh No. 8 sample was obtained from the Argonne Premium Coal Sample Programme (APCSP).[73] Two other samples from the APCSP, Illinois No. 6 and Wyodak-Anderson, gave increasing total volatile yields with increasing heating rate. However, the changes in total volatile release from the semianthracite Pocahontas No. 3 were within experimental scatter.

The plastic/fluid behavior of coals is of interest in most areas of coal utilization. The comprehensive early survey by Habermehl et al.[74] emphasized coke formation but also focused on operating problems in fluidized beds due to coal plasticity. At CSIRO Sydney, Hamilton and co-workers examined the plastic behavior of maceral concentrates as a function of the heating rate.[75−77] The samples covered vitrinite reflectances ranging from 0.2 to 2.0. SEM photomicrographs showed that all vitrinite samples tested had retained their original morphologies when heated at 0.1 °C s^{-1}. However, when heated at 10 000 °C s^{-1}, all vitrinites showed plastic behavior and formed small cavities, except for the vitrinite from an anthracite sample and the "gelinite" fraction from a brown coal. Vitrinites from bituminous coals showed the greatest plasticity. The wire-mesh reactor developed by Hamilton was equipped with an analog feedback control system capable of operating at up to 1000 °C, over a heating rate range from 0.1 to 10 000 °C s^{-1}. Despite the broad operating range that was well ahead of its time, no further work was reported using this instrument.

Below, we will return to the discussion on coal plasticity in the context of the accumulation of extractable materials (tar precursors) inside coal particles during the early stages of pyrolysis. We will also explore how extractable accumulation and eventual tar yields are altered by changing the heating rate.

2.3. Fate of Extractables in Coal Particles at Prepyrolysis Temperatures

2.3.1. Novel Approach to Coke Making. Prime coking coals are usually more expensive and becoming less readily available. Shifting the coke blend composition toward weakly coking coals is therefore commercially attractive. Research on coke making seeks to take advantage of insights that may lead to reducing the proportion of prime coking coals added to coke blends.

At Nippon Steel Corp., experimental observations showing links between heating rates and coal plasticity have led to an interesting pilot-scale application for improving coke production. Crushed coal was rapidly preheated in a riser to about 400 °C. The resulting mass of sticky particles was collected in a retort and slowly heated to 800−900 °C. The effect was to form a stronger coke than would have otherwise been possible from heating the same coal (or blend) in the same retort *slowly* from ambient temperature.[78] The procedure was found to be effective for improving the coking properties of weakly coking coals. For prime coking coals, however, the initial rapid heating step provided no significant improvement in the amount or strength of the coke product.

2.3.2. Extractables in Coals and Coal Plasticity. Solvent extraction of untreated (unheated) coal is known to release solvent-soluble extracts; the amounts extracted reflect the composition of the coal and the effectiveness of the solvent.[79,80] Such extracts have been analyzed by GC-MS and other methods with a view to exploring the structures and compositions of coals. Early work on the subject has been reviewed in detail.[81,82]

More interesting for our present purposes, however, are early findings showing relationships between the measured plastic properties of coals and the proportions of material that could be extracted after heating.[83−86] Dryden and co-workers[84,87] and, a decade later, Brown and Waters[85] described how they recovered increasing amounts of chloroform-extractable material by heating coals (slowly) to between 300 and 400 °C prior to extraction. For any given coal, this inventory appeared to change as a function of the peak heat-treatment temperature and the time at temperature. It was observed, furthermore, that

dx.doi.org/10.1021/cr400194p | Chem. Rev. 2014, 114, 1547−1607

extracting bituminous coals with chloroform *prior to* thermal treatment had a detrimental effect on their subsequent coking behavior. The softening and agglomerating behavior of particular coals (indicators of coking properties) were thus observed to closely correlate with the amounts of chloroform-extractable material recovered from the heated samples.

Howard and co-workers[88] experimented with Pittsburgh No. 8 coal and observed clear relationships between the temperature, the duration of the plastic state at a given temperature, and the extractable content of coal particles *at that temperature*. These researchers monitored the development of coal plasticity and its retrogression with a fast response plastometer; they observed that plasticity correlated with the inventory of pyridine extractables. They showed that plasticity could be quantified in terms of the rates of generation and destruction of pyridine extractables (metaplast) within coal particles.

We will next explore how changing the *heating rate* can affect the extractable content and the plasticity of coals and the impact of these parameters upon the amounts of tar released during pyrolysis. The analysis will lead us to a more detailed view of retrogressive recombination reactions and how they affect the course and eventual outcome of coal thermal breakdown.

2.3.3. Exploring Prepyrolysis Phenomena in Coals. In a study that followed on from the pilot work at Nippon Steel, the extractable materials accumulating within coal particles prior to full-blown pyrolysis were used as a diagnostic tool.[89] The aim was to explore how the extractable contents of heated particles could be altered by changing the heating rate and holding time at the target temperature. The initial experiments were designed to identify (i) the temperature interval within which fast heating was effective in causing discernible changes in the behavior of the samples and (ii) the range of "fast" heating rates, which were effective in enhancing the formation and extended survival of extractables within the coal mass.

Three coal blends from the pilot study at Nippon Steel were used. Weakly coking Newcastle Blend Coal (NCBC) is labeled below as coal A, strongly coking Goonyella as coal B, and the very strongly coking K-9 Blend as coal C. Table 2 presents the properties of the three samples. As will be shown below, K-9 was a blend with some rather peculiar properties.

The atmospheric-pressure wire-mesh reactor used in these experiments (Figure 4) was capable of programmed multistage heat up between several preset temperatures. The initial set of experiments followed one of two sequences[89]

Sequence I. Step 1: Fast heating (1000 °C s^{-1}) to 400 °C. Step 2: 30 s holding at 400 °C. Step 3: Slow heating (1 °C s^{-1}) to a target temperature between 400 and 500 °C. Step 4: 30 s holding at the target temperature followed by cooling and extraction with NMP (1-methyl-2-pyrrolidinone).

Sequence II differed from Sequence I only by application of slow (1 °C s^{-1}) heating up to 400 °C during Step 1.

Sequence II. Step 1: Slow heating (1 °C s^{-1}) to 400 °C. Step 2: 30 s holding at 400 °C. Step 3: Slow (1 °C s^{-1}) heating to a target temperature, between 400 and 500 °C. Step 4: 30 s holding at the target temperature followed by cooling and extraction with NMP.

The 106−150 μm particle size range was used for volatile and tar yield measurements in the wire mesh reactor. This size range was partly determined by the smallest size of stainless steel mesh able to accommodate the relatively easy to handle 50 μm diameter thermocouple wires. However, when *chars* from coals ground to 106−150 μm were extracted in the solvent

Table 2. Characteristics of Three Australian Coal Blends Used in the Study[a]

	coal A	coal B	coal C
volatile matter, %	35.2	24.1	17.9
fixed carbon, %	52.4	65.1	72.3
ash, %	9.0	9.3	8.9
crucible swelling no.	3.5	6.5	8.0
C (%, db)	83.6	87.7	90.7
H (%, db)	5.6	5.0	4.6
S (%, db)	0.55	0.57	0.15
N (%, db)	1.8	1.7	0.8
O (%, db)	8.3	4.8	3.3
vitrinite (vol %, mmf)	72.60	61.48	82.33
liptinite (vol %, mmf)	3.12	0.98	0
inertinite (vol %, mmf)	26.80	37.90	20.82
Giesler plastometry			
softening temperature (°C)	392	399	444
max fluidity temp. (°C)	430	455	485
resolidification temp. (°C)	457	493	505
max fluidity[b]	2.0	3.0	1.3

[a]Reproduced with permission from ref 89. Copyright 2004 American Chemical Society. [b]Maximum fluidity, given as log [1/DDPM (dial divisions per minute)].

NMP, some solid sample was observed to escape through the mesh (63 μm × 63 μm aperture size). The problem was side stepped using a larger sample size fraction, 212−250 μm, in experiments where heating in the wire-mesh reactor was to be followed by extract yield determinations. Using a 25 μm diameter thermocouple wire would have allowed the use of mesh with smaller aperture sizes. However, compared to 50 μm, handling the 25 μm diameter thermocouple wire turns out to be disproportionately difficult. It normally requires manipulation under a microscope, which was impractical for performing a large number of experiments.

Figure 6 shows the amounts of extractable material recovered from coal A particles heated to 400 °C rapidly (1000 °C s^{-1})

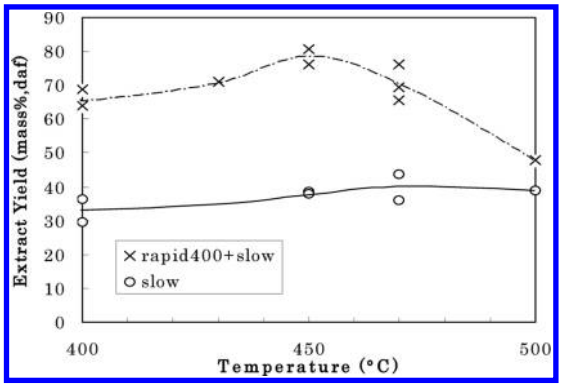

Figure 6. Comparison of NMP extractables recovered from coal A particles treated by one of two heating sequences: Fast (1000 °C s^{-1}) or slow (1 °C s^{-1}) heating to 400 °C in Step 1. (Reproduced with permission from ref 89. Copyright 2004 American Chemical Society.)

and slowly (1 °C s^{-1}) during Step 1. In both sets of experiments, the samples were then heated slowly (1 °C s^{-1}), from 400 °C to target temperatures between 400 and 500 °C, before cooling to ambient temperature.

The key finding from these experiments was the large difference between extract yields from chars recovered after fast

dx.doi.org/10.1021/cr400194p | *Chem. Rev.* 2014, 114, 1547−1607

and slow heating to 400 °C. Samples rapidly heated to 400 °C at 1000 °C s^{-1} gave about 66% extract, compared to about 33% extract from the samples heated slowly (1 °C s^{-1}) to 400 °C. The extract yield from *untreated* (unheated) coal A was about 35%. As the temperature was raised from 400 °C at 1 °C s^{-1}, the amount of extractable material accumulated within the particles that had initially been heated rapidly increased slowly to about 80% near 475 °C, before declining due to char formation above 475 °C. The slow upward drift of extractable content in the initially slowly heated sample was not much greater than experimental scatter.

Two further questions need to be answered regarding how these differences arise during heat up to 400 °C. First, was there a critical target temperature above which differences between fast (1000 °C s^{-1}) and slow (1 °C s^{-1}) heating became apparent and below which differences in extractables were not observed? Second, how fast did fast heating need to be for differences to begin to emerge between slow and fast heating?

2.3.4. Critical Base Temperature for Fast Heating To Begin Making a Difference. To answer the first question, coal A particles were heated at 1000 °C s^{-1} to temperatures between 350 and 400 °C followed by cooling and extraction with NMP. Figure 7 shows a fairly clear transition to greater

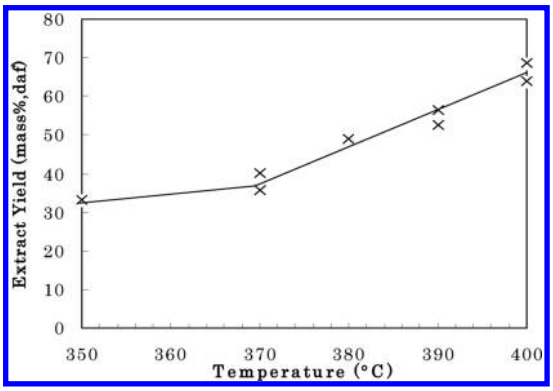

Figure 7. Extractables accumulating in particles of coal A during "fast" heating (1000 °C s^{-1}) to temperatures between 350 and 400 °C. (Reproduced with permission from ref 89. Copyright 2004 American Chemical Society.)

extractable accumulation above 370 °C. Near 400 °C, the extractable yields rose toward the same point (~65%) reported in Figure 6, showing satisfactory internal consistency within the data.[89]

The faster rise in extractables above 370 °C was consistent with the temperature for the onset of massive breakdown inferred from ESR-spectroscopy-based observations discussed above and from the liquefaction data in Figure 2. Recalling that results from ESR spectroscopy indicated the *onset* of individual bond rupture in the 310−340 °C range, data in Figure 7 appear consistent with the proposition that several bonds need to break before larger molecular mass materials can detach from the solid matrix to be released *within* the pyrolyzing coal particles.

The extractable material within initially slowly heated particles appeared to be surprisingly inert between 400 and 500 °C. Figure 6 shows that, above 400 °C, no clear char formation trend could be observed for particles heated initially at 1 °C s^{-1}.

Recalling the assumption that covalent bond-cleavage reactions are functions of the temperature alone, the smaller extractable yield from particles heated slowly to 400 °C (Figure 6) suggests that a greater number of free-radical *recombination* reactions must have taken place during *slow* heat, up to 400 °C. The greater extractable inventories within the rapidly heated particles indicate that during rapid heating such recombination reactions must have taken place to a lesser extent. Meanwhile, the *less reactive* free radicals that survived the heat-up process to 400 °C (at either heating rate) within the extractable mass are observed to be stable at 400 °C for at least 120 s (Figure 8) and

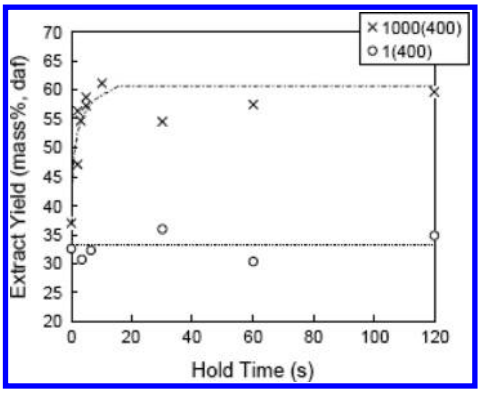

Figure 8. Effect of holding time at 400 °C on NMP-extract yields for coal A samples heated at 1 and 1000 °C s^{-1}. (Reproduced with permission from ref 89. Copyright 2004 American Chemical Society.)

to produce char rather slowly *above* 450 °C (Figure 6). These observations give us a preliminary handle on how to distinguish between Type-A (fast) and Type-B (slow) free-radical recombination reactions and by inference the reactions of the more reactive and less reactive free radicals during coal pyrolysis. We will return to this point.

Meanwhile, the larger pool of extractables (tar precursors) contained in rapidly heated particles goes some way toward explaining the higher tar yields from middle-rank coals during rapid heating. As temperatures are raised by rapid heating above 400−450 °C, e.g., to 700−800 °C, some tarry material begins to evaporate directly while heavier tar precursors may crack to give more volatile tar precursors and gas as well as some fresh char. As first suggested by V. R. Gray,[90] it is likely that some tarry material is ejected due to steep internal pressure gradients generated by the high speeds of heating. This suggestion is consistent (i) with larger tar yields and (ii) with size exclusion chromatography (SEC) showing broader molecular mass distributions for tars recovered from faster heating rate experiments.[57,65] The broader molecular mass distributions would correspond to heavier tars, rapidly ejected from coal particles, presumably before some tar precursors could undergo further cracking and/or charring reactions. In section 4 (below) we will outline analytical methods for characterizing high-mass, highly polydispersed samples that provide tools for monitoring the progress of these thermochemical processing steps.

It may be noted, meanwhile, that tar yield enhancement through rapid heating is not a very large effect. Tests on many coals have shown that maximum differences observed in tar yields between slow and fast heating are in the 4−8% range (cf. ref 62, p 70). This is not a large difference, compared to over 30% difference in extractable (tar precursor) accumulation observed between heating samples from the same coal slowly and fast to 400 °C (Figure 6). Even greater accumulations of plasticizing mass have been observed in "good" coking coals (cf. Figure 10a and 10b below). Meanwhile, Figure 5 shows that for

dx.doi.org/10.1021/cr400194p | Chem. Rev. 2014, 114, 1547−1607

Linby coal, which was more heating-rate sensitive than many coals, the difference in tar yields between heating at 1 and 1000 °C s^{-1} was about 6%.[56] Thus, when temperatures are raised above 500 °C, char formation rather than tar evaporation or explosive ejection remains the *dominant* (but clearly not the only) tar reaction pathway, irrespective of the heating rate.

Returning to Figure 8, the extractables accumulated within coal A particles showed remarkable stability for up to 2 min and possibly beyond. In retrospect, the duration of the experiment should have been prolonged. This level of chemical stability of the extractables appears consistent with the work of Fong et al.[315] For the higher temperature interval of 540−800 °C, these researchers reported a depletion rate for pyridine extractables ("metaplast depletion") characterized by the first-order reaction rate constant

$$k = 1.9 \times 10^{10} \exp(-21\,200/T)\ (s^{-1})$$

The numerical value of this rate constant calculated using this equation for depletion of extractable materials at 400 °C is rather small. As depletion of extractables by evaporation is not a significant factor at 400 °C, in this context it appears to be almost entirely due to char-forming radical recombination reactions.

These data lead to the observation that relatively rapid char-forming recombination reactions take place between *more reactive free radicals* during slow heat up to 400 °C and that these recombination reactions are partly blocked during rapid heating, leaving larger amounts of material intact as fairly stable extractables. Below, we will suggest that when fast heating is applied internally released hydrogen, native to the coal, may be entering the reaction mixture to quench *some* of the more reactive free radicals and block *some* of the potential retrogressive char-forming recombination reactions.

2.3.5. Heating Rate: How Fast Is Fast Heating? Experiments were also carried out to determine how fast fast heating had to be for differences in extractables yields begin to emerge. In the new set of experiments, sample particles were heated to 400 °C at increasing heating rates, between 1 and 1000 °C s^{-1}, while holding all other parameters constant. Chars from these experiments were then extracted with NMP. Figure 9 shows how the amounts of extractables (tar precursors) accumulated in the heated particles changed as the heating rate was increased. The transition at and above 500 °C s^{-1} was sharp and repeatable. The total weight loss (total volatiles) data from these experiments showed a similar qualitative trend including the transition at and above 500 °C s^{-1}.[89]

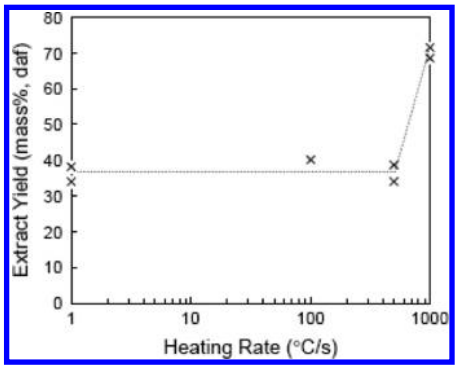

Figure 9. Relationship between heating rate and NMP-extract yield; final experimental temperature: 400 °C in all cases. Transition above 500 °C s^{-1} was sharp and repeatable. (Reproduced with permission from ref 89. Copyright 2004 American Chemical Society.)

It was thus observed that the sample must be heated to 375 °C or above before larger amounts of extractables may be released within the coal particles and that for fast heating rates to be effective *for this coal* samples must be heated at or above 500 °C s^{-1}. The level of accumulation of extractables was thus observed to be directly affected by the heating rate. While we should be hard put to explain why the particular heating rate threshold value of 500−1000 °C s^{-1} turns out to be the critical one, it seems sufficient for present purposes to note that a high heating rate at or above 500 °C s^{-1} is required for recovering larger amounts of extractables from coal A particles.

Meanwhile, it seems possible to arrive at a working explanation regarding the questions raised by results from the pilot-plant work at Nippon Steel. We know from previous work that coal plasticity and extractable contents are linked. Work at MIT expanded on earlier observations and showed that minimum viscosity and maximum pyridine-extractable contents occurred within the same temperature interval.[89] Characterization work within the Nippon Steel project also showed that the temperature of maximum extractables accumulation in coal A was near its temperature of maximum thermoplasticity, between 400 and 430 °C.[78] Finally, the stability of extractables during at least 2 min (Figure 8) and possibly longer appears to allow sufficient time for particles emerging from the riser tube in a plastic state to form coherent lumps when stacked within the retort and heated to 800−900 °C.

Rapid heating is observed to lead, therefore, to improved coke strength via the related increase in extractables content and the resulting enhanced thermoplasticity of coal A. However, we still need to explain how and why faster heating rates (≥500 °C s^{-1}) give rise to formation of greater amounts of extractable material. To explore this further, let us recall that coal A was a "weakly" coking coal. At this stage, it is of interest to observe how good coking coals behave during analogous experiments.

2.3.6. Prepyrolysis Behavior of Strongly Coking Coals. Coal B was a prime coking coal with a volatile matter content of 24.1% and a maximum Gieseler fluidity of 3.0 (Table 2). Extract yields from coal B chars were determined following one of three time−temperature profiles: (i) slow (1 °C s^{-1}) heating directly to the target temperature, (ii) rapid (1000 °C s^{-1}) heating to 350 °C followed by slow heating to the target temperature, and, finally, (iii) rapid (1000 °C s^{-1}) heating to 400 °C followed by slow heating to the target temperature.

Figure 10a shows that as the target temperature was raised, extractables yields from coal B chars increased, reaching a maximum between 400 and 450 °C, and then declined, giving near-total resolidification at about 600 °C. When heated to 400 °C, the coal displayed highly plastic (fluid) behavior and over 85% of the sample mass could be dissolved in NMP, irrespective of the heating rate. No measurable effect of heating rate on extractables yields was observed.

This finding contrasts with the behavior of coal A, which only softened when heated at or above 500 °C s^{-1} and *not* when heated at 1 °C s^{-1}. On the basis of the behavior of coal A, we would have expected to observe more rapid char-forming recombination reactions in the 350−400 °C interval during slow (1 °C s^{-1}) heating to 400 °C of coal B compared to rapid heat up. Whatever the internal processes of coal B, however, such a reduction of solvent-soluble material to char was not observed. With help from pyrolysis tar yield data from a wider

dx.doi.org/10.1021/cr400194p | Chem. Rev. 2014, 114, 1547−1607

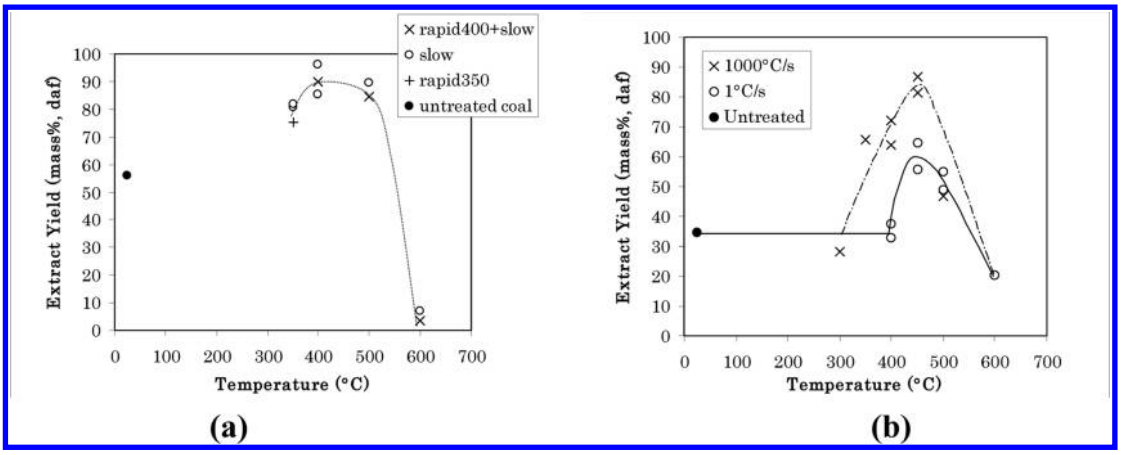

Figure 10. Relationship between NMP-extract yield and temperature for samples of (a) Goonyella (coal B) and (b) K-9 (coal C), both prime coking coals, heated at 1 and 1000 °C s^{-1} to 400 °C, followed by heating at 1 °C to a variable peak temperature up to 600 °C (30 s holding at peak temperature). (Reproduced with permission from ref 89. Copyright 2004 American Chemical Society.)

range of samples (ref 62, cf. Chapter 3) it seems possible to arrive at a more general tentative conclusion that high heating rates appear to improve the plastic behavior of ordinarily nonmelting coals, i.e., coals that do not melt at slow heating rates. However, little difference is observed for coals showing good plastic behavior at low as well as high heating rates. Below, we will examine evidence suggesting that the melting behavior of coals is associated with the local availability of hydrogen, serving to quench (cap) free radicals. The process appears to be helped along when the availabilities of hydrogen scavengers, such as oxygen and sulfur in the pyrolyzing mass, are relatively low.

The coal C blend, the second good coking coal sample used in the study, showed similar but not identical behavior to coal B. Despite a VM content of 17.9% and a maximum Gieseler fluidity of 1.3, coal C behaved as a good coking coal, albeit with somewhat peculiar properties. It was observed to have a relatively high softening temperature (~450 °C) compared to ~400 °C for the two other samples in the study. The elemental carbon content of this blend (90.7%) was high, but the contents of potential hydrogen scavengers, i.e., sulfur (0.15%) and oxygen (3.3%), were relatively low.

A small but measurable effect of heating rate could be observed for this unusual coal, from approximately its softening point onward. The long (~400 s) holding times required at 450 °C for these effects to become apparent are consistent with slow depolymerization of a highly cross-linked coal blend of 90.7% carbon content.

Figure 10b presents extractable yields from coal C chars heated at 1 or 1000 °C s^{-1} directly to the target temperature. For a heating rate of 1 °C s^{-1}, the extractable yield at 400 °C was similar to that from untreated coal C. Above 400 °C, the extractable yield traced a sharp maximum at about 450 °C, with resolidification reaching completion somewhat above 600 °C.

By contrast, when samples were heated at a rate of 1000 °C s^{-1}, the extractable yield remained similar to that of untreated coal C up to 300 °C but increased sharply from 350 °C onward, reflecting a little of the behavior of coal A. The shape of the curve was similar to that obtained for heating at 1 °C s^{-1} in Figure 10b, tracing a sharp maximum at about 450 °C and declining rapidly at higher temperatures. However, extractable yields were enhanced by ~30% of the coal mass in response to rapid heating. Meanwhile, almost identical results were obtained when NMP-extractable yields from rapid heating to 400 °C followed by slow heating and the slow heating programs were investigated.[89] Taken together, the pyrolytic behavior of coal C seemed to be intermediate between coal A and coal B with the added peculiarity of a high softening temperature and slow development of pyrolytic reactions at 450 °C. Recalling that coal C was a proprietary blend of several coals, there is insufficient evidence to comment further.

2.4. How Does Fast Heating Work? Considering Possible Mechanisms

Higher tar yields during fast heating were previously explained by the explosive ejection of tar precursors (i.e., extractables) from pyrolyzing coal particles. In this sense, rapid heating may be viewed as reducing the probability of repolymerization reactions of tar precursors through their rapid removal from pyrolyzing coal particles.[90] However, explosive ejection can only work on (i.e., eject) tar precursors that are already in some sort of fluid/plastic state. Observations summarized in Figures 6–9 indicate that a larger pool of tar precursors develops when coals that have marginal coking ability are heated rapidly. The question that remains to be answered is *how* the larger pool of extractable material came into being (and remained intact) when particles of the marginally coking coal A were heated rapidly. Answering this question would provide us with the link between faster heating and higher extractable and tar yields.

To try and answer this question, it is necessary to revisit ideas earlier proposed by Brown and Waters[85] and Wiser.[91] Developing these ideas, Neavel[92] formulated a consensus view of plasticity in coals, suggesting that pyrolytic processes prior to tar evaporation may be viewed as a hydrogen-donation stage and that H-donating activity by the plastic phase provides a medium analogous to liquefaction in a hydrogen-donor solvent (e.g., tetralin). Within this framework, the coal itself is viewed as *supplying* the solvating and hydrogen-donating vehicle. Work by Howard and co-workers[88] contributed to these views by providing a direct *transient* link between plasticity and the inventory of extractables (metaplast) within coal particles. According to Neavel's argument, the hydrogen-donor ability within the pyrolyzing mass was held to reside in the hydroaromatic (alicyclic) component of the plasticizing phase. Broadly, the latter term corresponds to what we have called extractables (tar precursors) in this review and to Howard et al.'s metaplast.[88]

dx.doi.org/10.1021/cr400194p | *Chem. Rev.* 2014, 114, 1547–1607

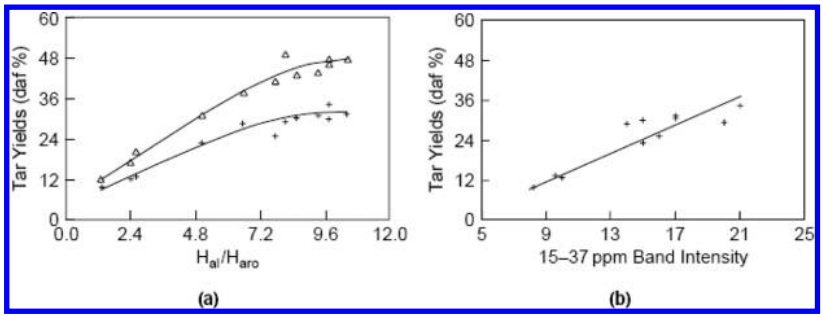

Figure 11. (a) Pyrolysis tar and total volatile yields as a function of FT-IR-derived aliphatic:aromatic hydrogen ratios. Rank-ordered series of Northern Hemisphere coals: (+) tar, (Δ) total volatile. Pyrolysis in atmospheric-pressure helium at 1000 °C s^{-1} to 700 °C with 30 s holding time. Nonmelting coals: Taff Merthyr, Emil Mayrisch, Tilmanstone. Melting coals: Heinrich Robert, Santa Barbara, Longannet, Candin, Bentinck, Thoresby, Gedling, Linby, Illinois No. 6. (b) Pyrolysis tar yields as a function of ^{13}C-NMR-derived 15−37 nm aliphatic band intensity for a rank-ordered series of Northern Hemisphere coals. Coals and pyrolysis conditions as in a. (Reproduced with permission from ref 94. Copyright 1994 Elsevier.)

Within this formulation, therefore, the extent of coal softening and the magnitude of tar yields are thought to depend on local hydrogen availability and be directly proportional to hydroaromatic hydrogen content. Before the onset of tar evaporation (above 400−450 °C), pyrolysis is considered to work as an internal liquefaction process, where free radicals are quenched and stabilized *by internally released hydrogen*. Clearly, this action would block *some* (but not all) free-radical recombination reactions. We also know that when middle-rank coals are heated, small amounts of hydrogen are released from about ∼285−300 °C (e.g., cf. ref 93). It is within this framework that the observed role of the heating rate finds an explanation.

During fast heating experiments, we observe that pyrolytic events (e.g., tar evaporation) are compressed into a shorter time frame and pushed up the temperature scale. Experiments with Linby (U.K.) coal clearly showed that the level of weight loss achieved by heating at 1 °C s^{-1} was matched during rapid heating (1000 °C s^{-1}) only at temperatures that were about 100 °C higher (cf. Figure 4 of ref 56). This difference continued up to 600 °C, after which volatiles evolution from the slowly heated sample tended to slow down. Temperature differences between analogous pyrolytic events during the fast and slow heating of Pittsburgh No. 8 coal (APCSP)[73] were greater, closer to 130−140 °C.[72]

Although Neavel and the sources he drew on were not particularly concerned with the effect of heating rate, the sequence of events just described draws on and is consistent with the Neavel model outlined above.[92] The telescoping together of pyrolytic events and shifting to higher temperatures during faster heating would tend to improve the probability that internal hydrogen release overlapped with covalent bond cleavage at higher temperatures. Both the donatable alicyclic hydrogen and the internally released hydrogen are thus more likely to enter the pyrolyzing mix and quench (cap) freshly formed free radicals, blocking many more recombination reactions, compared to slow heating. In other words, the model suggests that the hydrogen transfer process within the coal mass coincides more completely with greater covalent bond cleavage when coals are heated rapidly and pyrolytic processes are telescoped closer together in time.

While we have no direct proof for this sequence of events, the model we outlined is able to explain diverse phenomena and the data presented above. (i) Figure 6 shows coal A maintaining a greater inventory of extractable material during heat up to 400 °C at 1000 °C s^{-1} compared to heat up at 1 °C s^{-1}. (ii) Figure 5 shows increasing tar and volatile yields with increasing heating rate. The model is also able to provide an explanation for observations on marginally hydrogen-deficient coals such as Linby (U.K.), NCBC blend (Australia), and Pittsburgh No. 8 (U.S.), which do not melt when heated slowly (∼1 °C s^{-1}) but show plastic behavior when heated rapidly (1000 °C s^{-1}).

It thus appears that no strict dividing line exists between melting and nonmelting coals. These low- to middle-rank bituminous coals appear to be transitional between subbituminous and high-volatile bituminous coals (less mature coals that would melt with greater difficulty) on the one hand and the readily melting and swelling coking coals on the other. At the higher end of the rank scale, finely divided anthracite samples might partially respond to very fast heating rates if at all.

We can now begin to explain the behavior of coals like Goonyella (coal B, above) or indeed the behavior of other H_2-rich specimens, such as liptinites, which show far less sensitivity to heating rate, than Linby coal or the NCBC blend, discussed above. Samples such as liptinites, or indeed the Goonyella coal, present relatively high elemental H_2 and relatively low contents of hydrogen scavenger species (oxygen and sulfur). Evidently, this provides a combination of factors capable of swamping the internal liquefaction process with sufficient hydrogen to block some of the recombination reactions, regardless of the applied heating rate. In other words, the greater presence of hydrogen allows them to show melting and swelling behavior during fast *or* slow heating. By comparison, marginally hydrogen-deficient vitrinites show more pronounced heating rate sensitivity during pyrolysis with respect to both plastic behavior and tar yields[65,57,78,94] due to their greater dependence on the hydrogen-enhancing effects of fast heating rates.

Later in this review we will use data on the pyrolytic behavior of coal *maceral concentrates* to test some of the ideas brought together in this part of the review. Before that, however, it would be useful to focus on the hydrogen-donor function attributed to aliphatic structures and distinguish between the actions of saturated aliphatic groups and hydroaromatic (alicyclic) structures in coals during pyrolytic processes.

2.4.1. Tar Yields and Aliphatic Structures in Coals. Figure 11 presents data for a rank-ordered but otherwise nearly randomly selected set of Northern Hemisphere coals. Data show reasonably smooth trends of increasing tar yields with

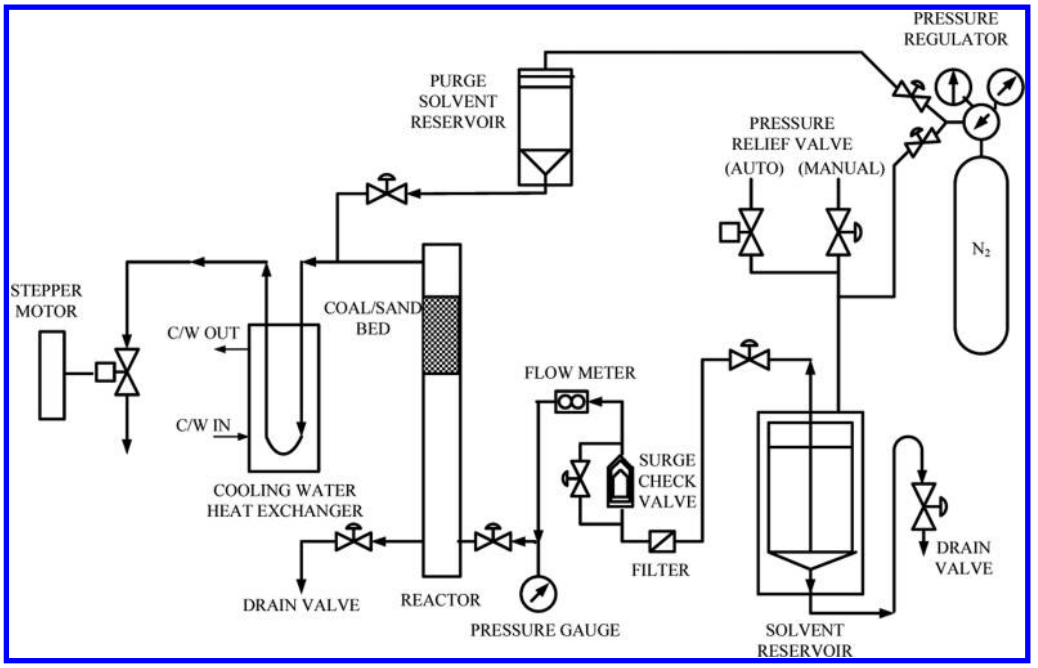

Figure 12. Schematic diagram of the flowing-solvent reactor system. Solvent from the solvent reservoir is forced through the fixed bed of coal placed inside the reactor and sweeps dissolved products away from the reaction zone and into the heat exchanger. Letdown valve is attached to a computer-controlled stepper motor and serves to control the flow rate. (Reproduced with permission from ref 53. Copyright 1996 American Chemical Society.).

increasing aliphatic content in the coal samples, as determined by FT-IR and solid-state ^{13}C NMR spectroscopy. Both sets of data lump together signals from alkyl and hydroaromatic (alicyclic) structures.

We already considered that the H-donor ability of pyrolyzing coals during the internal liquefaction process is thought to reside in the hydroaromatic component.[85,92] Hydroaromatic content in coals generally decreases gradually with increasing elemental carbon content, i.e., coal rank, up to about 87−88%; above this level it is observed to decrease rapidly with increasing coal rank.

Meanwhile, there is a need for a reasonably direct and preferably practical method for determining hydroaromatic contents in *solid coals*. The work up to about the late 1970s has been summarized by Dryden.[82] Estimates of hydroaromatic carbon content based on dehydrogenation of coal using benzoquinone[95] indicated about 29−30% hydroaromatic carbon for vitrinites of 82.5% C content, declining to 20% for 87.5% C content. Using a broadly similar approach, Reggel et al.[96−98] catalytically dehydrogenated vitrinites in an organic vehicle (phenanthridine) with various formulations of palladium and rhodium catalysts mounted on $CaCO_3$, alumina, or charcoal supports. Their results were broadly in line with hydroaromatic contents found using the benzoquinone method by Peover.[95]

Both past and some more recent work aiming to quantify hydroaromatic content in coals has focused on coal-derived liquids rather than on solid coals. In solution-state ^{1}H NMR, the difficulty consists in distinguishing between the α-hydrogens of hydroaromatic (alicyclic) structures and the α-hydrogens of alkyl substituents of aromatics in the chemical shift region of 2.45−4.45 ppm. Similarly, studies based on solution-state ^{13}C NMR have not provided new routes for distinguishing between $C_{\alpha 2}$ carbons in bridging structures from $C_{\alpha 2}$ carbons in hydroaromatic groups.[99] The lines of approach and challenges faced are similar to characterization of hydroaromatic structures in petroleum-derived heavy fractions.[100,101] Arriving at simple straightforward methods for determining hydroaromatic carbon contents in complex liquids as well as in solid coals remains a desirable objective. In section 4.3.4, we will review relatively recent attempts to resolve this enduring problem.

Returning to the data in Figure 11, we do not therefore have a direct method for distinguishing, with reasonable accuracy, between the roles of cyclic and alkyl groups in solid coals during pyrolysis. That said, we do not *expect* alkyl groups within the plasticizing mass to donate hydrogen to reactive free radicals. It would therefore seem reasonable to conclude provisionally, but difficult to prove, that the observed increases in tar and total volatile yields in Figure 11 correspond to the progressively increasing hydroaromatic component within the coal sample sequence.

Meanwhile, what *can* be shown with reasonable clarity is the absence of any contribution by long chain aliphatic species, when used as the liquid medium during coal liquefaction. Data presented below shows that the straight chain alkane, hexadecane (n-$C_{16}H_{34}$), contributes little to the coal liquefaction process in terms of either solvent power or H-donor activity. In fact, when coal samples are liquefied in hexadecane, conversions differ little from pyrolysis in an inert gas environment at similar temperatures.

In order to examine how alkyl and hydroaromatic solvents/vehicles interact with coals during liquefaction, however, we first need to describe the design of a reactor that allows removal of liquefaction products from the reaction zone immediately after being released from the reacting coal particles.

2.4.2. Flowing-Solvent Liquefaction Reactor. Most laboratory liquefaction reactors consist of closed vessels where only batch experiments can be performed. In this type of experiment, the reactants as well as the products formed

dx.doi.org/10.1021/cr400194p | *Chem. Rev.* 2014, 114, 1547−1607

during the reaction remain within the reaction zone until termination of the experiment. It is possible to arrive at a clearer picture of the processes involved when liquefaction *products* are rapidly removed from the reaction zone, diluted, and cooled to suppress secondary reactions while the reacting coal sample remains in the reaction zone.

Figure 12 presents a schematic diagram of the flowing-solvent liquefaction reactor system developed at Imperial College London.[53] During an actual experiment, the solvent is preheated in the lower part of the reactor body and forced through a fixed bed, composed of coal particles mixed with inert sand. Products released by coal particles are diluted by excess solvent and swept out of the reaction zone into a water-cooled heat exchanger. The basic device consists of a 0.95 cm o.d. reactor tube made of Haynes 230 alloy, designed to operate at 70 bar and up to 1000 °C. The lower (preheating) section of the two-stage reactor was set to deliver solvent to the upper (reaction) section at the temperature of the latter. The power supplied to the two sections was controlled separately, supplied by direct electrical heating, using copper electrodes clamped to the reactor body. Temperature control was done by sheathed thermocouples positioned immediately above and below the coal sample bed. The original system[102−104] was subsequently revamped to extend the temperature range and provide greater ease of experimental control.[53,105] Residence times of dissolved products in the heated zone were estimated at between 6 and 10 s. By limiting residence times of products in the reaction zone and diluting the products of thermal breakdown by excess solvent this configuration helps suppress coal−product interactions as well as secondary reactions between dissolved products.[53] When the liquid medium is a hydrogen donor as well as a good solvent for coal-derived material (e.g., tetralin) it serves to block some of the potential retrogressive reactions by chemically quenching reactive free radicals.

2.4.3. Alkyl and Hydroaromatic Solvents in Coal Liquefaction. Table 3 presents data from liquefaction experiments in three distinct types of liquid media: (1) a hydrogen-donor solvent, tetralin, (2) a mixture of non-H-donor solvents, quinoline and phenanthrene, which are known as effective solvents for coal-derived materials, and (3) hexadecane, a straight chain alkane, which is neither an H-donor solvent nor an effective solvent for coal-derived materials. Experiments were carried out using samples of Point of Ayr coal (U.K.) and a vitrinite concentrate from the same coal. Conversion data from flowing-solvent reactor liquefaction experiments were compared with data from pyrolysis experiments done at similar temperatures.

Table 3. Comparing Conversions in Different Solvents: Liquefaction Experiments with Solvent Flow Rate of 0.9 mL s^{-1} at 70 bar (g)[a]

	heating rate, °C s^{-1}	holding time, s	ambient medium	weight loss, % w/w (daf basis) 350 °C	450 °C
Point of Ayr	1000	150	helium	3.3	20.5 (2)[b]
vitrinite concentrate	5	400	tetralin	28.8[c]	77.6 (2)
	5	400	Q/P[d]	38.0	73.8 (2)
	5	400	quinoline	n.a.[e]	72.7 (2)
	5	400	*n*-hexadecane	12.5	27.3 (2)
Point of Ayr whole coal	5	400	tetralin	24.6	82.5 (4)
	5	400	quinoline	39.5	74.7 (2)
	5	400	*n*-hexadecane	n.a[e].	24.0 (2)

[a]All data are given on % w/w dry ash free basis. (Reproduced with permission from ref 54. Copyright 1994 American Chemical Society.) [b]Number of repeated runs used for calculating the average conversion value. [c]Holding time: 500 s. Weight loss from 100 s experiments under the same conditions was 29.2%, within experimental error (±2%). [d]Q/P: (2.5:1 w/w) mixture of quinoline and phenanthrene. [e]n.a.: not available.

Table 3 shows that at up to 350 °C greater amounts of coal-derived material could be removed by quinoline or the quinoline−phenanthrene mixture compared to tetralin. ESR spin population measurements as well as the liquefaction experiments described above suggest that weight loss up to 350 °C *mostly* represents extraction of already soluble material native to the coal. The larger amount of extract removal at up to 350 °C by nondonor (but stronger) solvents is consistent with the dominant process being one of dissolution rather than removal of material *made* soluble through thermal breakdown.

Liquefaction in nondonor solvents at 400−450 °C in closed reactors such as minibombs (see below) produces an initial onrush of dissolved coal-derived product. However, in closed reactors, the products are kept at reaction conditions for the duration of the experiment. In the absence of hydrogen donation by the solvent (or externally supplied hydrogen), dissolution of the coal-derived material is eventually reversed after 10−30 min (depending on the coal:solvent ratio). After the initial dissolution step, this combination of reaction parameters leads to increasing *char* formation due to retrogressive free-radical recombination/repolymerization reactions.[106] The analogous reversal of the liquefaction process is not observed in the flowing-solvent reactor since only the solid reactant particles remain in place throughout the experiment. Dissolved coal products are continuously diluted and removed from the reaction zone and cooled. The product solution normally contains less than 200 mg of coal-derived material in approximately 700−1000 mL of solvent.

Table 3 also shows, however, that at 450 °C *lower* conversions were observed in the nondonor solvents compared to liquefaction in tetralin. These results are consistent with data from experiments with another nondonor solvent, 1-methylnaphthalene, discussed below.[107] At temperatures above 350 °C, the positive contribution made by tetralin in dissolution of the samples showed what we already thought we knew: that in addition to its solvent ability the hydroaromatic molecule, tetralin, performs an H-donor function. This is thought to help quench reactive free radicals and block a proportion of retrogressive reactions. Potentially important clues relating to rates of retrogressive reactions are provided by the comparison of conversions at 350 and 450 °C in tetralin and in the two more powerful solvents. The implications of these data will be discussed in section 2.5.

The properties of Linby and Point of Ayr coals and the Point of Ayr vitrinite concentrate are presented in Table 4

Finally, the data in Table 3 allow comparing liquefaction conversions in hexadecane and pyrolysis in helium at similar temperatures. Using the non-H-donor hexadecane (also a poor solvent for coal-derived materials) as the liquefaction medium, 24% and 27% conversions were observed using the Point of Ayr coal and vitrinite samples. Meanwhile, the total weight loss observed from pyrolysis in helium at 450 °C was 20.5%. This result was somewhat counterintuitive. It might have been

dx.doi.org/10.1021/cr400194p | *Chem. Rev.* 2014, 114, 1547−1607

Table 4. Elemental Analysis of Point of Ayr (U.K.) Coal and Its Vitrinite Concentrate[a54,55]

sample	C[b]	H[b]	N[b]	S[b]	O (by difference)	ash (dry basis)
PoA whole coal	84.5	5.4	1.8	1.5	6.1	9.6
vitrinite concentrate	84.8	5.0	1.9	2.3	5.7	2.3
Linby whole coal[c]	82.3	6.0	1.9			4.8

[a]Point of Ayr coal (84% vitrinites, 6% liptinites, 10% inertinites) softens on heating but does not coke. (Reproduced with permission from ref 54. Copyright 1994 American Chemical Society.) [b]Dry ash free. [c]Linby coal 73% vitrinites, 15% liptinites, 12% inertinites.

expected that mass transfer between the solid and the liquid (coal to hexadecane) would have been more efficient than mass transfer from coal to an inert gas stream. However, in the absence of solvent power for coal-derived materials the presence of hexadecane *as a liquid* appears to have been only marginally advantageous compared to pyrolysis in helium.

Data presented in Table 3 may therefore be understood in terms of the coal (or vitrinite concentrate) sample depolymerizing quite substantially during heating to 450 °C. The outcome of the experiment then appears to depend on whether a large fraction of the depolymerized material can be chemically quenched by a hydrogen donor and/or moved out of the coal particles by dissolving in a liquid with the appropriate solvating properties. The role of the density (i.e., gas or liquid) of the surrounding fluid medium seems far less relevant than its chemical properties.

At this point it seems appropriate to discuss the contribution of alkyl and alicyclic groups during coal thermal breakdown. We observed that hexadecane plays *nearly* no role during the liquefaction experiment with the possible exception of removing small amounts of free alkanes and labile alkyl groups from the solid matrix. The closeness of the result to that of pyrolysis in helium suggests that it is unlikely to have either helped or hindered extractables (tar precursors) formation and accumulation within the coal particles. It is also unlikely to have assisted any possible hydrogen transfer process. It seems reasonable to infer that saturated alkyl species play little role during thermal breakdown. Similarly, the observed increases in tar and volatile yields shown in Figure 11 are far more likely to have been assisted by the increasing abundance of hydroaromatic structures native to the coal than by the presence of alkyl groups.

2.5. Fast and Slow Recombination Reactions during Pyrolysis and Liquefaction

As already noted, the shorter lifetimes of reactive free radicals and their consequently low concentrations make it difficult to observe them against a far greater background count of stable free radicals.[46] Nevertheless, in section 2.3.5 we were able to identify relatively rapid free-radical recombination reactions in terms of greater char formation during the slow heat up of coal particles to 400 °C. In the absence of direct measurements, identification of these reactions and that of the presence of reactive free radicals was based on what must be described as indirect evidence.

Similarly, the extractables that had survived heat up and reached 400 °C appear to undergo relatively slow char-forming reactions when the temperature was raised above 450 °C (Figure 6). The fast and slow char-forming radical recombination reactions were labeled as Type-A and Type-B reactions, respectively.

We do not know how fast the retrogressive reactions we labeled as Type A (fast) really are. We do know that these recombination reactions were observed during slow heating (1 °C s^{-1}), a heating rate which translates into 100 s duration for every 100 °C of heat-up. That may or may not imply very fast retrogressive reactions. However, the transition point between the low and high extract regimes (low and high heating rates) was observed around 500 °C s^{-1} (Figure 9). For instance, we envisage retrogressive reactions to be faster around, say, 100–200 °C s^{-1}, which is still below the observed transition rate at around 500 °C s^{-1}. What is clearer, however, is that Type-A reactions occur at far faster rates than the reactions we observed above 450 °C in Figure 6, which we have labeled as Type-B reactions.

In the next section, we will present analogous experimental evidence from coal liquefaction experiments that allows distinguishing between slow and fast retrogressive, char-forming, free-radical recombination reactions.

2.5.1. Rapid Retrogressive Reactions in Liquefaction.

We have seen in Table 3 that at 350 °, greater amounts of coal had been extracted by the nondonor solvents compared to extraction with tetralin. We explained this in terms of the process at 350 °C being *mainly* one of dissolution, where quinoline and phenanthrene clearly had an advantage. We also saw that when the peak experimental temperature was raised from 350 to 450 °C, (i) the conversions increased significantly in the presence of both tetralin and the nondonor solvents but that (ii) systematically higher conversions were recorded at 450 °C in the presence of tetralin, compared to conversions in the nondonor strong solvents.

In a separate set of flowing-solvent reactor experiments about 10–12% higher conversions were obtained in tetralin compared to liquefaction in the strong (but) non-H-donor solvent 1-methylnaphthalene at 400 and 450 °C, Figure 13.[107] We will

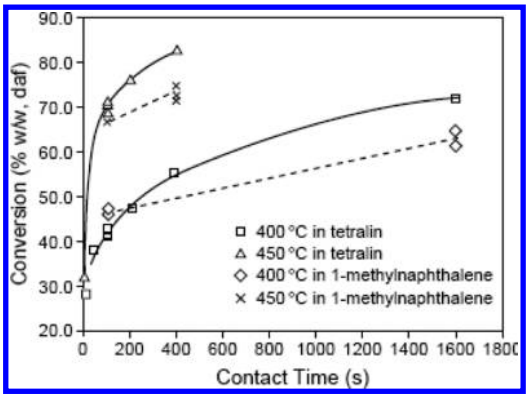

Figure 13. Effect of solvent type on conversions in the flowing-solvent reactor. Heating at 5 °C s^{-1}; solvent flow rate 0.9 mL/s at 70 bar. (Reproduced with permission from ref 107. Copyright 1991 Elsevier.)

next examine the reasons why the trend in Table 3 was reversed between 350 and 450 °C and why the donor-solvent tetralin gave systematically higher conversions at the higher temperature compared to the three strong (but) nondonor solvents.

Much of the present discussion is based on the premise that covalent bond-cleavage reaction rates during thermal breakdown depend primarily on the temperature. In this instance, the experiments consist of heating similar coal samples to

dx.doi.org/10.1021/cr400194p | Chem. Rev. 2014, 114, 1547–1607

similar temperatures. We expect therefore broadly similar rates of covalent bond cleavage and release by the solid matrix of similar amounts of extractables irrespective of whether the liquid medium is an H-donor or a non-H-donor solvent. In the flowing-solvent reactor the solvent stream sweeps away all extractable material that has been dissolved in the liquid medium (and diffused out of the coal particles). Furthermore, we also found higher conversions in the presence of tetralin, the H-donor solvent with less solvent power, despite bond-cleavage reactions releasing broadly similar amounts of extractables. We are led to think that any extractables not carried away by the *stronger* (non-H-donor) solvents must be no longer soluble. In other words, data in Table 3 strongly suggests that more frequent (and probably rapid) retrogressive reactions occur during heat up in the nondonor solvents, between 350 and 450 °C, compared to heating in tetralin.

The higher conversions in tetralin at 450 °C are therefore consistent with the H-donor ability of tetralin being better able to block what appear to be rapid retrogressive reactions during heat up compared to the nondonor solvents that are unable to provide this function. The analogy between the role of tetralin in these experiments and the internal liquefaction process posited for coal pyrolysis is clear.

It must be noted that the design of liquefaction reactors plays a key role in determining the course of the liquefaction process. In the flowing-solvent reactor high conversions may still be maintained in the presence of non-H-donor solvents, as products are diluted and rapidly removed from the reaction zone (~10 s). In the next section, we will see that when coal was liquefied in a closed (batch) reactor conversions in a non-H-donor solvent went through a maximum and then *declined*. We will be focusing on the (low) speed of these retrogressive char-forming reactions. Analytical characterization of some of these coal extract fractions has been discussed in section 4.2.1 of the present review.

2.5.2. Slow Retrogressive Reactions during Liquefaction Experiments. During initial experiments in the batch ("minibomb") reactor using a tetralin to coal ratio of about 4:1 only minor differences were found with conversions observed in the flowing-solvent reactor.[107] In the flowing-solvent reactor a heating rate of 5 °C s^{-1} was used as standard. Sample weight loss was found to be insensitive to heating rates between 0.3 and 10 °C s^{-1} at 400 and 450 °C. In the bomb reactor, quoting from the original publication, "...A heat-up period of 3 min in the sand fluidized bed was allowed for reaching the target temperature...", resulting in an *averaged* (estimated) heating rate of between 2.1 and 2.4 °C s^{-1}.[103,104,107] However, in the batch reactor it took far longer, about 1 h, to reach the level of conversion, which could be achieved in the flowing-solvent reactor within several minutes. The difference appears due to slower diffusion of extracts out of coal particles in the batch reactor caused by the gradually increasing extract concentration in the fluid surrounding the particles and the resulting diminishing concentration driving force for extract molecules to diffuse out of coal particles.

Conversions in the two reactors were also compared using the non-H-donor 1-methylnaphthalene as liquid medium (Figure 14). In the flowing-solvent reactor, conversions increased monotonically with contact time at both 400 and 450 °C. At 400 °C, conversion in the minibomb also increased monotonically with time but was nearly 30% lower than in the flowing-solvent reactor.

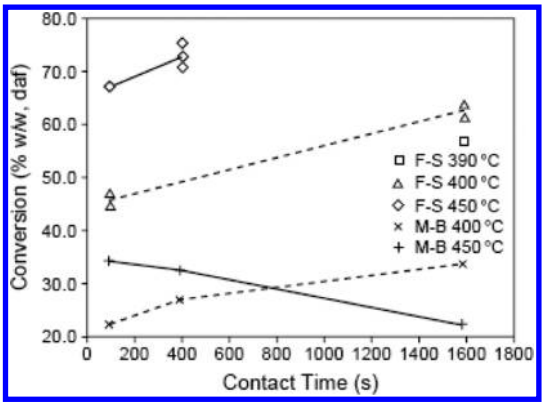

Figure 14. Flowing-solvent reactor and minibomb reactor comparison using 1-methylnaphthalene as the liquefaction medium. Solvent/coal ratio in minibomb reactor: 4/1 by weight. Flowing-solvent reactor: heating at 5 °C s^{-1}; solvent flow rate 0.9 mL s^{-1} at 70 bar. (Reproduced with permission from ref 107. Copyright 1991 Elsevier.)

Conversion loss in the minibomb reactor at 400 °C may be due to one (or both) of two reasons. Part of the difference is probably due to rapid recombination reactions in the *batch* reactor, where products cannot be removed from the reaction zone before termination of the experiment. Part of the difference between conversions in the two reactors *may* also be due, however, to slower diffusion of product molecules out of the coal particles, as outlined above. In the case of tetralin it had taken nearly 1 h for conversion in the minibomb to come up to the level found in the flowing-solvent reactor (cf. ref 107). Experiments reported in Figure 14 were taken to a little under 27 min. With the data at hand, it seems difficult to distinguish between the two effects.

However, at 450 °C, Figure 14 shows clear evidence of retrogressive char-forming reactions in the minibomb reactor. Any increase in filtered solids would be due to fresh char formed during the experiments and is measured as a function of time. At contact times longer than 100 s conversions diminished and the proportion of residual solids increased. This aspect of the data is consistent with trends observed during earlier work (e.g., cf. ref 106). The relevance of these results in the present context is the demonstration of the slow, indeed very slow, speed of char-forming reactions. Figure 14 showed a loss of 12−13% soluble material in about 25 min (1500 s). These slow char-forming reactions contrast sharply with the inferred relatively rapid rates of retrogressive reactions during heat up in nondonor solvents during experiments in the flowing-solvent reactor. The latter are only apparent when conversions in the nondonor solvent are compared with liquefaction in a donor solvent.

2.5.2.1. Even Slower Retrogressive Reactions: Sample Aging. On the face of it, coal extracts catalytically hydrocracked in tetralin under high-pressure hydrogen should be quite stable. In order to test this proposition, a sample of Point of Ayr (U.K.) coal extract was hydrocracked for 10 min in distilled tetralin at 440 °C under 190 bar H_2 pressure and in the presence of a presulfided $NiMo/Al_2O_3$ catalyst. As soon as the liquid product was filtered from the solid material in the reactor, a sample was taken for characterization by SEC and UV-fluorescence spectroscopy. The rest of the sample was separated into two parts. One part was kept under nitrogen in a freezer at −22 °C; meanwhile, the second part of the sample was kept exposed to air at room temperature. Samples were

dx.doi.org/10.1021/cr400194p | *Chem. Rev.* 2014, 114, 1547−1607

examined by SEC and UV-fluorescence spectroscopy every 2 h during the first day, once a day during the first week, once a week during the first month, and then once a month for the rest of the year.[108]

Sample aging was assessed in terms of shifts to shorter elution times in SEC and parallel changes in UV-fluorescence spectra. Both stored products showed significant structural evidence of aging over the first week of storage. Subsequent changes observed in the samples were within the range of variability of the polystyrene standards, routinely used for checking internal consistency in SEC. Aging was attributed to the presence of low-reactivity free-radical species undergoing fairly slow recombination reactions during storage.

2.5.2.2. Aging in Biomass Tars/Oils. Similar aging tests were carried out on tars/oils from pyrolysis of samples of beech wood and rice husks. Tar/oil samples were stored under different sets of conditions: (i) 5 °C with nitrogen headspace; (ii) laboratory ambient temperature with nitrogen headspace; (iii) laboratory ambient temperature with air headspace; (iv) 40 °C with nitrogen headspace. Evolution of the samples was tracked using size exclusion chromatography and UV-fluorescence spectrometry.[109]

The broadening of the SEC chromatograms was observed to be fastest during the first four days and level off during the subsequent 3 months. The changes in the SEC chromatograms of the rice husk bio-oils showed only slight differences from those of beech wood tars/oils. These results are in qualitative agreement with earlier work based on viscosity measurements.[110] The observed broadening of SEC chromatograms is likely to have involved aldehyde polymerization reactions and formation of phenolic resins. It was observed that higher temperatures tend to accelerate the aging process, although the process could also be observed in bio-oils stored at a relatively low temperature. Oxygen in air did not seem to affect sample aging. A more detailed account of sample aging reactions in tar/oil from coal biomass coprocessing can be found elsewhere[111] using the recently developed multitechnique analytical approach described in section 4.4.

2.6. Overview of Coal Thermal Breakdown

In this section we reviewed experimental evidence relating to reaction pathways during the thermal breakdown in coals and the effect of the heating rate on coal behavior. Data from pyrolysis and liquefaction experiments with different configurations have enabled observing effects due to more reactive and less reactive free radicals created and destroyed during successive stages of thermal breakdown processes. Overall, these observations provide evidence for the presence of free radicals with broad ranges of reactivities during thermal breakdown processes in the reacting solid phases and in the "liquid" products recovered from them.

2.6.1. Initial Stages of Thermal Breakdown. The onset of covalent bond cleavage identified by electron resonance spectroscopy (ESR) was observed near 310 °C for a lignite, rising to 340 °C with increasing coal rank. As coal samples were heated the initial stages of pyrolysis and liquefaction presented similar patterns of covalent bond cleavage. The findings are understood in terms of covalent bond cleavage being a function of the temperature alone for any given sample. Clearly outcomes may differ between samples with different structural characteristics.

During the liquefaction of middle-rank coals, greater mass loss was observed above 350−375 °C. This temperature range is consistent with several bonds rupturing before larger molecular mass fragments can detach from the solid matrix to be released *within* the coal particles. In this review this material has been labeled as extractables or tar precursors. The terms extractables, tar precursors, plastic phase, and metaplast commonly refer to broadly the same solvent-soluble mass, although nuances of meaning are found in reports on diverse approaches to analyzing coal thermal breakdown.

The pathways of pyrolysis and liquefaction begin to diverge during accumulation of solvent extractables (tar precursors) within the coal particles. In liquefaction, the solvent (vehicle) serves to remove most of the extractables from reacting coal particles. By contrast, during the early stages of pyrolysis in an inert gas medium accumulated extractables remain *mostly* inside the coal particles. At 400 °C, weight loss by evaporation in dry pyrolysis rarely exceeds several percent of the initial mass. Yet the extractables content of the particles (dry) heated to about 400 °C was found to be as high as 65−80%, depending on the coal.

Meanwhile, we observed that greater contents of extractable materials tend to improve the plasticity of coal particles. Moreover, greater prepyrolysis extractable (tar precursor) contents and the resulting greater plasticity of coal particles closely correlate with larger tar yields observed during pyrolysis experiments driven to 700 °C and beyond. Observations on middle-rank coals indicate that high heating rates (≥500 °C s^{-1}) simultaneously enhance all three effects, namely, proportion of solvent extractables (tar precursors) within coal particles, coal plasticity, and, as the temperature is raised, eventual tar yields.

2.6.2. Effect of Rapid Heating. There is clear and consistent experimental evidence that far larger proportions of the initial mass of weakly coking coals end up as extractable material if the sample is heated rapidly to 400 °C compared to slow heating to the same temperature. As covalent bond cleavage is primarily a function of the temperature, similar patterns of bond cleavage are expected to occur during fast and slow heating. We expect therefore that similar amounts of potential extractables are initially released inside coal particles, irrespective of the heating rate. The observed differences in extractable yields between fast and slow heating may be explained in terms of many more char-forming recombination reactions taking place during *slow* heating to 400 °C. On their own, however, these observations do not explain *why* fewer retrogressive reactions take place during rapid heating.

Fast heating tends to telescope the sequence of pyrolytic events into a narrower time frame and shift the temperature scale of pyrolytic events to higher temperatures. For the several coals tested, we observed this upward temperature shift to be on the order of between 90 and 140 °C. It is thought that, during rapid heating, the internal release of hydrogen may temporally overlap (more) with processes of covalent bond cleavage. The pyrolyzing mass may thus be able to assimilate internally released hydrogen more effectively and quench (cap) more of the reactive free radicals. This action would effectively block more of the potential rapid recombination reactions.

There are two likely sources for internally released hydrogen. During slow heating, low-level release of molecular hydrogen from pyrolyzing coals can be measured relatively easily from about 285 to 300 °C. During fast heating, the released hydrogen is more likely to remain in contact with the pyrolyzing coal mass at higher temperatures. It is likely that the hydrogen would be fairly reactive when first breaking off

dx.doi.org/10.1021/cr400194p | *Chem. Rev.* 2014, 114, 1547−1607

from the parent coal mass, although we have no *proof* that it is actually assimilated into the pyrolyzing coal mass during rapid heating.

We also considered that during pyrolysis internally released "donatable" hydrogen plays a role that is analogous to donor solvents (e.g., tetralin) during liquefaction in effectively blocking *rapid* potentially char-forming free-radical recombination reactions. Donatable hydrogen in coals and coal-derived materials is thought to reside in the hydroaromatic component of the plastic phase. Such hydrogen transfer would more effectively block free-radical recombination reactions when thermal activation of hydrogen-donor activity and covalent bond cleavage overlap during rapid heating. More efficient hydrogen release to the pyrolyzing coal would explain the enhanced plasticity of weakly coking coals during rapid heating and the resulting enhanced tar and total volatiles yields. Supporting data has been presented indicating direct links between hydroaromatic content and increasing tar and total volatile yields.

The accumulated evidence indicates that weakly coking coals show greater sensitivity to increasing heating rates. Such coals tend to be marginally deficient in hydrogen. Greater proportions of extractables accumulate and greater plasticity is observed during the fast heating of these coals, giving rise to improvements in plastic behavior and enhanced product yields. In the work outlined above, the effect was clearly observed at heating rates greater than 500 °C s^{-1}.

Meanwhile, good coking coals present high proportions of accumulated extractables and show high levels of plasticity irrespective of the heating rate. The conceptual model developed suggests that such coals initially contain sufficiently high amounts of donatable hydrogen and probably also relatively low contents of hydrogen-scavenging elements such as oxygen and sulfur.

2.6.3. Fast and Slow Free-Radical Recombination Reactions in Thermal Breakdown. As thermally induced bond-cleavage reactions and depolymerization of coals accelerate above 350 °C, the more reactive of the free radicals have greater potential to undergo either retrogressive or quenching (capping) reactions. The evidence presented suggests that the outcomes of these processes are determined by the relative abundance of locally available internally released hydrogen.

2.6.3.1. Rapid Recombination Reactions in Pyrolysis. During slow heating (up to about 500 °C s^{-1}), internally released hydrogen may escape before intense covalent bond-cleavage reaction temperatures are reached. The more rapid recombination reactions taking place during *slow* heating tend to produce more char and less extractable material compared to rapid heating. The effect is observed more clearly in coals that are marginally deficient in hydrogen.

2.6.3.2. Slow Recombination Reactions in Pyrolysis. During pyrolysis, some of the extractable mass survives the heat-up stage to 400 °C, irrespective of the heating rate. For weakly coking coal A, this was found to be about 35% after slow heating to 400 °C and about 65% after fast heating. However, once 400 °C was reached and the rapid recombination and/or quenching reactions of the reactive free radicals were completed, the remaining extractables content identified within the coal particles was remarkably stable for 120 s and possibly longer. Slow recombination reactions making fresh char were observed to proceed only slowly as the temperature was raised to 450 °C and beyond.

2.6.3.3. Rapid Recombination Reactions in Liquefaction. The difference in conversion between donor and nondonor solvents is thought to arise from the outcome of short-range interactions, as extractables detach from the coal matrix within the coal particles. In the absence of sufficient locally available hydrogen, char-producing recombination reactions would preferentially result from such short-range interactions. During liquefaction at up to 450 °C in the flowing-solvent reactor, non-H-donor strong solvents allowed more of the rapid repolymerization reactions to take place during heat up, reducing the extract yield by about 5−10% compared to liquefaction in the donor solvent tetralin under otherwise identical experimental conditions.

2.6.3.4. Slow Recombination Reactions in Liquefaction. It may be recalled that in the flowing-solvent reactor rapid removal of products from the reaction zone and far greater dilution of soluble products in excess solvent minimize opportunities for secondary reactions. During liquefaction in non-H-donor solvents in batch reactors, however, the initial rapid dissolution of coal-derived material results in rising concentrations of partially reactive products in close proximity in the non-H-donor solvent. With increasing time at temperature and increasing solute concentration retrogressive char-forming reactions are observed, reducing the proportion of dissolved product. During liquefaction in 1-methylnaphthalene already dissolved extracts were observed to form solids at 450 °C at a very slow rate (12−13% in 25 min). These reactions appear distinct from and slower than the rapid recombination reactions taking place during heat up. The latter were inferred from flowing-solvent reactor data by comparing conversions in H-donor and non-H-donor solvents.

2.6.4. Wide Spectrum of Free-Radical Reactivities in Coal Pyrolysis. It is not surprising that free radicals generated by a multiplicity of covalent bond-cleavage reactions during the thermal breakdown process should display a wide range of reactivities. The evidence presented above helps identify wide ranges of free-radical reactivities and wide ranges of radical recombination reaction rates. Admittedly, the framework that has been presented seems a relatively blunt instrument for a detailed analysis (exact structures? precise rates?) of free-radical formation and retrogressive reactions in coals. However, we may now be a little closer to understanding how and why coals respond to different heating patterns in different ways. We may thus be a little closer to explaining some technologically relevant aspects of coal behavior, possibly useful in what appears to be the coming age of expanded coal utilization.

3. REFERENCE POINTS FOR BIOMASS PYROLYSIS: COMPARISON WITH COAL THERMAL BREAKDOWN

As outlined in the Introduction, pyrolysis experiments involving coal and biomass samples present a level of similarity that is unusual among nominally distinct fields of research. Both activities involve heating solid fuels to broadly similar temperature ranges, and both sets of samples tend to release intermediate products that are reactive. The designs of the experimental reactors usually are, or should be, pretty much interchangeable. In both cases the aim is to determine product distributions as well as achieve a measure of control over the time−temperature histories of the volatile products and of the solid residues. Even so, much past research on coal and biomass pyrolysis has been conducted with relatively little reference to the many common aspects and shared challenges.

dx.doi.org/10.1021/cr400194p | *Chem. Rev.* 2014, 114, 1547−1607

This section will briefly trace the contours of biomass pyrolysis experiments and define points of reference for comparison with coal pyrolysis. We will focus on what may be learned about the properties and thermal breakdown of lignocellulosic biomass from work on both sets of samples.

3.1. Plastic Behavior of Pyrolyzing Biomass: A Quick Look over the Shoulder

An excellent recent review of biomass pyrolysis research by Mettler et al.[112] provides an example of how the compartmentalization of coal and biomass pyrolysis has led to missed opportunities. Among the topics suggested for more detailed investigation, the review rightly discusses the significance of a transient liquid phase observed during rapid heating of wood samples. The article made no reference to similarities with transient plastic and fluid phases observed during pyrolysis of many coals. It seems reasonable to expect that comparing fluid phases of heated coals with those of pyrolyzing biomass would provide clues relating to mechanisms of thermal breakdown in woods.

Furthermore, there are other highly oxygenated samples that display plastic behavior. Solomon et al.[113] reported on the transient plastic deformation of North Dakota Zap *lignite* particles (oxygen content 26.5%) during pyrolysis in the high-heating rate environment of an entrained flow reactor. They noted "...This behaviour is not observed at lower heating rates..." and speculated that "...the high heating rate may have reduced the cross-linking reactions responsible for lack of fluidity". In other work, photomicrographs of solid residues from pyrolysis of lignin at high heating rate (1000 °C s^{-1}) deposited on wire-mesh lattices showed clear evidence of fluid behavior on the part of the pyrolyzing Kraft lignin sample (C, 53.5%; hydrogen, 6.0%; oxygen content (estimated by difference), 37−38%).[114]

There is a second effect that is directly related to the softening (fluidlike) behavior of both coals and biomass during pyrolysis. As observed earlier in this review, when heating rates are increased, many coals show more pronounced plastic behavior as well as releasing increasing amounts of volatile matter and tar. Tables 5−7 present evidence showing clear increases in volatile and tar yields with increasing heating rate during pyrolysis of three biomass samples: silver birch wood, sugar cane bagasse, and a Kraft lignin sample (Holmen AB, Sweden). In fact, increasing volatile and tar/oil yields from biomass pyrolysis with increasing heating rate have previously been widely observed and reported (see below). However, the effect has rarely been considered in relation to the plastic behavior of rapidly heated biomass, still less studied in the context of the analogous knowledge base deriving from coal pyrolysis, outlined earlier in this review.

Table 5. Tar and Total Volatile Yields from Atmospheric-Pressure Pyrolysis of Silver Birch Wood Determined Using the Wire-Mesh Reactor[a]

	heating rate					
	total volatiles % daf basis[b]		tar/oil yield % daf basis[b]		char residue % daf basis[b]	
temp, °C	1 °C s^{-1}	1000 °C s^{-1}	1 °C s^{-1}	1000 °C s^{-1}	1 °C s^{-1}	1000 °C s^{-1}
400	77	89	43	56	23	11
500	89	96	49	58	11	4
700	93	99	54	57	7	1
900	93	99	52	57	7	1

[a]Helium was used as ambient gas in all experiments; 30 sec holding at the peak temperature.[114,115] (Reproduced with permission from ref 115. Copyright 1991 Elsevier.) [b]daf: dry ash free.

Table 6. Tar and Total Volatile Yields from Atmospheric-Pressure Pyrolysis of Sugar Cane Bagasse Determined Using the Wire-Mesh Reactor[a]

	heating rate					
	total volatiles % daf basis[b]		tar/oil yield % daf basis[b]		char residue % daf basis[b]	
temp, °C	1 °C s^{-1}	1000 °C s^{-1}	1 °C s^{-1}	1000 °C s^{-1}	1 °C s^{-1}	1000 °C s^{-1}
400	74.3	88.3	37.0	49.2	25.7	11.7
500	86.1	93.7	42.4	56.4	13.9	6.3
600	89.1	96.1	45.4	54.4	11.1	3.9
700	87.5	96.9	45.6	53.7	12.5	3.1
900	88.8	96.9	45.4	53.7	11.2	3.4

[a]Helium used as ambient gas in all experiments.[114] [b]daf: dry ash free.

Table 7. Tar and Total Volatile Yields from Atmospheric-Pressure Pyrolysis of Kraft Lignin Determined Using the Wire-Mesh Reactor[a]

	heating rate					
	total volatiles % daf basis[b]		tar/oil yield % daf basis[b]		char residue % daf basis	
temp, °C	1 °C s^{-1}	1000 °C s^{-1}	1 °C s^{-1}	1000 °C s^{-1}	1 °C s^{-1}	1000 °C s^{-1}
400	44.7	50.6	37.6	40.0	55.3	49.4
600	57.2	65.5	42.0	44.9	42.8	34.5
900	58.7	68.3	43.2	45.0	41.3	31.7

[a]Helium was used as ambient gas in all experiments; 30 sec holding at the peak temperature.[114] [b]daf: dry ash free.

Within this framework it is not inconceivable that the fluid (plastic) phase identified during biomass pyrolysis is related to a transient local abundance of native hydrogen, as in the case of pyrolyzing coals discussed in the previous section of this review. The very short lifetimes reported for the liquid phase in pyrolyzing biomass[112] would be consistent with the fiercely hydrogen-scavenging, oxygen-rich environment of pyrolyzing wood. In summmary, while the short-lived plastic stages observed during biomass pyrolysis clearly require further careful examination, the body of related knowledge developed within the ambit of coal pyrolysis research looms large as a resource that has yet to be fully exploited.

3.2. Designing Biomass Pyrolysis Experiments: Reactor Configurations and Reaction Parameters

In section 2.2.1 we suggested that evaluating the fundamental pyrolytic behavior of a solid fuel requires strict decoupling of observations on sample behavior from effects due to design of the particular reactor and the shape and dimensions of the sample. This condition is consistent with the more general requirement that data from the measurement of *any* fundamental property be entirely independent of the method of measurement.

Within this framework, a measure of care is required in assessing data and trends in the literature. A recent review quoted 12% char recovery from pyrolysis of 3 mm diameter finely ground wood particles as the observed limit of solid fuel conversion to volatile products.[7] We will see below that by manipulating reaction parameters it is possible to reduce char

dx.doi.org/10.1021/cr400194p | Chem. Rev. 2014, 114, 1547−1607

yields from some woods to near zero. While the char yield quoted in the cited review is probably reasonable for the stated particle size distribution (3 mm diameter), the necessity to discriminate between fundamental fuel behavior and discussions of data from pilot-scale or larger scale process development equipment seems self-evident.

Looking beyond similarities, observed *differences* between the behavior of coals and biomass during pyrolysis also provide valuable insights. Compared to thermal breakdown in coals, lower temperatures are needed for the onset of pyrolysis for most biomass materials. Similarly, most lignocellulosic biomass tend to release tars at lower temperatures and produce higher overall tar yields. These differences reflect the more highly oxygenated, thermally labile, and reactive makeup of lignocellulosic biomass. The same properties are reflected in the structures of the tars, which are generally more volatile than coal tars and thermally crack at lower temperatures. The greater reactivity of lignocellulosic biomass and their tars tend to make product distributions more sensitive to changes in sample and reactor configuration.

In the rest of section 3.2 we will review the behavior of several common biomass samples under a variety of experimental conditions.

3.2.1. Altering the Product Slate by Design: Vagaries of Cellulose Pyrolysis. Fred Shafizadeh and co-workers[116] were pioneers in research on the pyrolysis of polymeric materials and biomass. They reported that the linear polymer cellulose may be thermally decomposed to give a product mixture containing a large proportion of laevoglucosan (1,6-anhydro-β,D-glucopyranose), the single-ring product released when the linear cellulose chain breaks down. In the absence of secondary reactions leading to thermal degradation, cellulose pyrolysis may be expected to give a theoretical yield of nearly 100% laevoglucosan. However, in the days when standard laboratory practice involved introducing little metallic boats laden with powdered sample into horizontal furnaces, Shafizadeh and Fu could only attain laevoglucosan yields of about 50% from pyrolysis of pure cellulose.[117] The rest of the condensable product they collected presented a complex mixture of oxygenated compounds.

Clearly, projecting near-100% laevoglucosan yields implies that *no* (or nearly no) char residue would be expected from cellulose pyrolysis. Indeed, such a result may be approached, but much depends on sample and reactor configuration. At the opposite end of the conversion spectrum, Antal and co-workers found no record of a fixed-carbon yield from biomass that exceeds the thermodynamic equilibrium value for the carbon yield and also that the pyrolytic yield of carbon from biomass approaches the thermochemical equilibrium 'limit' for the carbon yield from below.[118]

Table 8 presents char yields from cellulose pyrolysis experiments at broadly similar temperatures, ranging from near-zero to 26%, from experiments using different heating rates, distinct reactor and sample configurations, as well as different reactor operating regimes.

3.2.1.1. Experimenting with Cellulose. As part of a wider investigation aiming to maximize charcoal yields from wood and other lignocellulosic biomass, Zaror and co-workers pyrolyzed samples of pure cellulose in two reactors with different geometries.[119] A McBain thermogravimetric balance was used for heating strips of filter paper at 14 °C min^{-1} to 480 °C under a stream of flowing nitrogen. In a parallel set of experiments, similar samples were heated in a Gray-King retort[120] at 5 °C min^{-1} to the same temperature (480 °C), again under a stream of flowing nitrogen. Table 8 shows that broadly similar char yields (about 12%) were observed in the two experiments. However, when the nitrogen flow sweeping over the sample was interrupted during experiments in the Gray-King retort (other parameters remaining unchanged), the char yield in the resulting stagnant atmosphere more than doubled to 26%. In the absence of a carrier gas stream, a significant proportion of tar vapors (aerosols), which would have otherwise been removed from the reaction zone, appear to have reverted to char.

Table 8. Cellulose Pyrolysis Char Yields in Four Different Reactor Configurations[a]

reactor configuration	char yield (% w/w)	temperature program
Gray-King retort (without carrier gas)[119]	26.0	5 °C min^{-1} to 480 °C
Gray-King retort (with carrier gas)[119]	12.5	5 °C min^{-1} to 480 °C
McBain thermogravimetric balance[119]	12.0	14 °C min^{-1} to 480 °C
fluidized-bed reactor[60]	<3%[b]	fast (est. > 1000 °C s^{-1}) to 450 °C
wire-mesh reactor[114]	<1%[b]	1000 °C s^{-1} to 500 °C

[a]A 100 μm thick strip of pure cellulose filter paper was used as sample in the McBain thermogravimetric balance and the Gray-King retort; 106−152 μm particles were used in the fluidized-bed and wire-mesh reactors. [b]Below limit of the determination.

Table 8 also shows that using rapid heating *and* a stream of inert gas to remove volatiles from the reaction zone the outcome of cellulose pyrolysis experiments could be radically altered. Negligible char residue was recovered in a wire-mesh reactor[114] (Figure 4) and in a fluidized-bed pyrolysis reactor,[60] which will be described in section 3.2.3. Clearly, very different outcomes may be encountered during pyrolysis of this thermally sensitive biomass component, depending on reactor and sample design and choice of reaction conditions.

3.2.2. Pyrolyzing Silver Birch Wood and Sugar Cane Bagasse in a Wire-Mesh Reactor. Tables 5 and 6 present tar/oil and total volatile yields from pyrolysis of silver birch wood[115] and sugar cane bagasse[114] particles (106−152 μm diameter), respectively, in the wire-mesh reactor of Figure 4. The silver birch gave char yields of less than 5% during fast heating (1000 °C s^{-1}) to 500 and 600 °C. At 700 °C, the amount of char residue recovered was below the limit of detection of the determination; just 0.2% char could be recovered. Even slow (1 °C s^{-1}) heating rate experiments in the same apparatus produced just short of 90% total volatiles (i.e., conversion) of silver birch wood.

During fast heating experiments, silver birch wood tar yields of 56−58% were recorded at an end temperature of 400 °C. The analogous experiments on sugar cane bagasse samples gave qualitatively similar results, although the volatile and tar yields were slightly lower. In addition to highlighting the sensitivity of tar yields to the heating rate, the wire-mesh reactor data of Tables 5 and 6 show that smaller particle sizes lead to significantly smaller char yields than the 12% char yield from wood mentioned earlier.

The pyrolysis behavior of middle-rank coals differs significantly from these data. Middle-rank coals rarely release more than 5−7% volatiles at around 400 °C (e.g., Figure 3). This is a low temperature for coal thermal breakdown. At these temperatures, reactions are slow and longer holding times (as in

dx.doi.org/10.1021/cr400194p | Chem. Rev. 2014, 114, 1547−1607

the fluidized bed at the same temperature) may release up to 20% volatiles. During rapid (1000 °C s^{-1}) heating many coals require temperatures nearer 650−700 °C for reaching *peak* tar yield values, which rarely exceed 28−30% (Figure 3; also cf. ref 62, Chapter 3). However, even at these higher temperatures total volatile release from middle-rank coals rarely exceeds 45%, corresponding to char yields of about 55%. Further heating to 1800 °C and beyond appears to squeeze several more percent volatiles.[64]

3.2.2.1. Pyrolysis or Gasification? Do We Need Reactive Gases? On the face of it, the low *char* yields from biomass shown in Tables 5−7 might suggest that there is not much need to *gasify* lignocellulosic biomass with reactive gases such as steam, air, or oxygen in order to convert these solid fuels more completely into volatile products.

However, operators of pilot- and plant-scale equipment would likely reject the idea of finely grinding the usually fibrous lignocellulosic biomass to the range of particle sizes used in these experiments, which were meant for sample characterization (106−152 μm), on account of the energy and money costs involved for fine grinding. When fluidized beds are used at the pilot or plant scale, furthermore, some kind of provision must be made to suppress fuel loss (or loss of fuel residence time) through sample elutriation. The standard response to such problems is to increase the particle size distribution, which, in turn, tends to increase the amount of residual char. Reactive gases are then needed to react with the extra char to boost conversions.

The link between particle size and char yield is easily explained. Howard and Anthony[121] calculated that when heating at 1000 °C s^{-1} the maximum diameter of coal particles (of higher thermal conductivities than wood particles) that could reasonably be expected to show nearly uniform temperature profiles is about 100 μm. Within larger particles, the slower temperature front, resulting from the lower thermal conductivity of biomass materials, would lead to more char formation and probably also provide a barrier to the outward passage of tar vapors on their way out toward the particle surfaces.

Furthermore, relatively slowly heated solids/chars lose reactivity due to longer exposure to higher temperatures during heating to the target temperature, particularly above 800−850 °C. The effect is akin to annealing carbons and chars at higher temperatures, and the loss of reactivity is surprisingly rapid. Coal particles heated at 1000 °C s^{-1} to 1000 °C were observed to lose nearly 70% of their reactivity within 10 s at 1000 °C.[122]

The use of steam, with high heat-transfer coefficients coupled to reactivity, is usually helpful in improving the conversion of larger feedstock particles. Thus, in pilot- and plant-size gasifiers, use of reactive gases partially compensates for the secondary effects of the fluidization parameters that have to be selected. Cracking of evolved tars is another useful action by reactive gases such as steam. The absence of tars or tar-cracking products in the British Coal ABGC fluidized-bed reactor exit streams (work Imperial College, unpublished work) indicated that the action of steam at 900−950 °C is useful in destroying residual tar vapors given sufficiently long residence times (∼1 s).

3.2.3. Biomass Pyrolysis in Bench-Scale Fluidized-Bed Reactors. We discussed at length how pyrolysis tar/oil yields may be determined under conditions that minimize secondary reactions of evolving volatiles. However, wire-mesh reactor experiments provide no clues regarding the thermal sensitivity (reactivity) of the tars/oils themselves, precisely because these experiments were designed to suppress extraparticle secondary reactions.

We now turn to a fluidized-bed reactor design which aims to induce controlled extents of thermal cracking of released volatiles in the reactor freeboard. In these experiments sample particles are usually gravity fed into a preheated reactor, where achieving stable temperatures is usually straightforward. Given the high rates of heat transfer in bubbling fluidized beds, sample heating rates are also estimated to be high, although the actual rates cannot be measured directly.

Much of the early biomass pyrolysis work in fluidized-bed reactors was done by Scott and Piskorz, who explored product distribution trends from finely divided (<500 μm) sample particles, mostly between 400 and 700 °C.[123−125] Up to 65% of the original fuel mass could be recovered as tar/oil. As the reactor temperature was increased, more of the tar/oil could be cracked to gaseous products. In these rigs, cracking of volatiles takes place both inside the fluidized bed (in contact with the fluidizing bed material) as well as in flight, in the reactor freeboard. The highly oxygenated nature of biomass tars/oils could be clearly observed in the work of Scott and Piskorz from increasing CO and CO_2 concentrations in the gas product as reactor temperatures were raised. The same researchers scaled up their reactor to pilot scale and, like so many other researchers since, attempted to find uses for the liquid products.[126] In section 3.4, we will briefly review developments associated with the catalytic upgrading of biomass tars/oils.

In general, the fluidized-bed reactor configuration allows examining the thermal cracking propensities of pyrolysis volatiles by exposing them to the temperature of the bed and the reactor freeboard. However, a conventional fluidized bed design would not allow independent manipulation of the temperature and residence time of volatiles in the reactor freeboard without altering the fluidizing conditions inside the bed.

3.2.3.1. Imperial College Fluidized-Bed Pyrolysis Reactor. Figure 15 presents the schematic diagram of a reactor designed to fix the fluidizing conditions and vary the temperature and/or

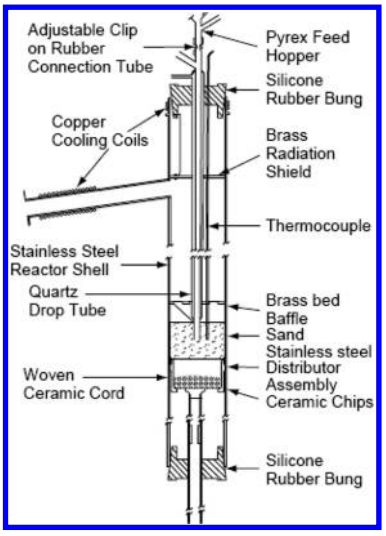

Figure 15. Fluidized-bed pyrolysis reactor with movable support plate, where volatile residence times in the freeboard may be varied without altering fluidizing conditions. (Reproduced with permission from ref 60. Copyright 1989 Elsevier.)

dx.doi.org/10.1021/cr400194p | *Chem. Rev.* 2014, 114, 1547−1607

the freeboard residence times of volatiles independently of the fluidizing conditions.[60]

The reactor consists of a stainless steel tube (76 mm i.d.; 1000 mm high), serving as the body of a bubbling fluidized bed composed of acid-washed sand particles. Sample is introduced by gravity through the inner of two concentric tubes running down the center of the already heated reactor. The annular space of the downcomer carries a stream of inert gas (in this instance nitrogen) to keep the sample particles from heating up before they drop into the bubbling fluidized bed. The original design concept is due to Ralph Tyler at CSIRO in Sydney,[127,128] who pyrolyzed coal particles in a smaller sized reactor made of silica. The design shown in Figure 15 incorporates several additional features.

First, the bed of sand particles was placed upon a support plate, which could be moved up and down between experiments, enabling residence times of evolved volatiles in the reactor freeboard to be changed without altering fluidizing conditions. In this way, the design allows decoupling the effect of temperature and residence time in the reactor freeboard and enables examining their effects on the extents of thermal cracking independently of other parameters. In this version of the reactor the volatile residence times could be changed between 0.8 and ~4 s when using a gas flow corresponding to 3−3.7 times that of incipient fluidization velocity. In the original work, overall conversion data collected as a function of temperature and residence time were used for calculating kinetic constants for tar cracking reactions.[129]

The second major modification of the original design was introduced for solving an operating problem encountered during trial runs with biomass particles. It was observed that tar and char yields were distorted by solid particle carryover into the quench zone. The effect was severe during operation at shorter freeboard residence times and during runs with lower density substrates, such as cellulose and wood particles. A wire screen (denoted as brass bed baffle in Figure 15) was placed above the fluidized bed to suppress the escape of solid particles from the reaction zone. The cold-trap design was also improved to stop lighter biomass tars/oils (compared to coal tars) from escaping through the filters alongside light hydrocarbons.[60]

Figure 16 presents tar/oil yield data from pyrolysis of silver birch wood in the fluidized-bed reactor, showing the extent to which cracking due to exposure to any given temperature may be controlled by altering volatile residence times in the reactor freeboard. The asymmetric bell-shaped curves are typical of pyrolysis tar yields in fluidized beds. Yields increase with rising temperature until, near the maximum, tar production begins to flatten out and thermal cracking begins to destroy increasing proportions of the tar/oil produced.

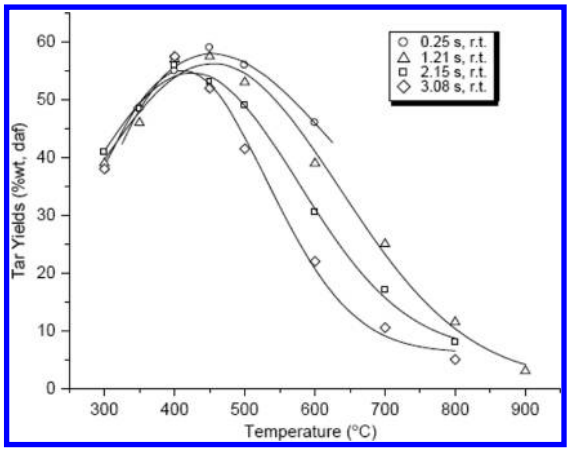

Figure 16. Silver birch pyrolysis tar yields as a function of temperature and freeboard residence times. Operation at atmospheric pressure. (Reproduced with permission from ref 60. Copyright 1989 Elsevier.)

Data in Figure 16 were obtained using sample from the same batch of silver birch wood as had been used in wire-mesh experiments by Fraga et al.[115] Comparing with Table 5, we note that similar *peak* tar yields were observed in the wire-mesh and fluidized-bed reactors. As freeboard residence times were increased, Figure 16 clearly shows that the temperature of the maximum receded from a little above 450 to nearly 425 °C. The trend is consistent with what we expect from intensified secondary tar cracking reactions at longer residence times.

It may also be noted that in the wire-mesh reactor tar/oil yields held steady (within experimental scatter) with increasing temperature, after reaching peak values (Table 5). In other words, the yields did *not* decline in the way observed in the fluidized-bed reactor data of Figure 16. This is because the tars/oils are removed rapidly from the shallow reaction zone of the wire-mesh reactor before higher temperatures are reached. In this way, tar yields in the wire mesh reactor reflect the temperatures experienced by the solid samples. Tars released in wire-mesh reactors do not experience temperatures much above their own temperature of evaporation and tar/oil degradation is minimized. The similarities and differences between biomass pyrolysis data from the two reactors are qualitatively similar to data on coal pyrolysis from the same pair of reactors.[59]

Experiments in the fluidized-bed reactor were also useful in showing how, for any given sample, the position of the tar yield maximum provides an indication of the relative thermal stability (or reactivity) of the evolving tar/oil vapors. The analogous maximum for low-rank bituminous Linby coal was observed at the higher temperatures of 590−600 °C, compared to 425−450 °C for silver birch wood. The peak for Çan lignite (Turkey) was intermediate between the coal and the biomass maxima at about 530 °C.[60] The other observation arising from Figure 16 is the rapidity with which biomass-derived tars/oils are destroyed in the reactor freeboard with increasing temperatures and residence time. At 900 °C, tar/oil yields were reduced to near extinction. The speed of the decline underlines the thermally sensitive nature of biomass tars/oils; they appear far more susceptible to thermal cracking compared to tars from coal pyrolysis experiments.[60]

In pilot- and commercial-scale processing of biomass, the condensable content of fuel gases from bubbling fluidized beds tends to cause problems, sufficiently severe for catalytic methods to have been attempted for destroying the tars/oils.[130] As signaled earlier, however, no extractable material was found in any of the bed solids streams from the British Coal ABGC gasification pilot fluidized bed (200 kg h^{-1}). During operation with coal, sewage sludge, and their mixtures, tar destruction appeared complete in the presence of steam at around 950 °C and freeboard residence times of about ~1 s. Clearly, however, use of steam as well as maintaining higher temperatures in the bed and the freeboard entail energy and money costs. They make it difficult to arrive at economically viable biomass gasification processes.

3.2.3.2. Composition of Biomass Tars/Oils. Biomass tars/oils turn out to be extremely complex mixtures. Pioneering GC-MS analyses by Evans and Milne[131,132] and more recently by

dx.doi.org/10.1021/cr400194p | *Chem. Rev.* 2014, 114, 1547−1607

Branca et al.[133] have shown that biomass pyrolysis tars/oils contain very large numbers of chemical components, significant proportions of which are oxygenated compounds. However, GC-MS is only able to analyze molecules that are able to pass through the chromatographic column. Applications of GC-MS to pyrolysis tars from sugar cane bagasse and eucalyptus[134] suggest that more than 90% of these samples do not pass through GC columns due to low volatility and do not show up in GC-MS analysis. The foregoing does not invalidate findings by GC-MS but aims to point out that this type of analysis is subject to a mass limit, typically about 300 u for aromatic compounds and somewhat over 500 u for aliphatic compounds. Taking the cited works as guides, it appears increasingly difficult to identify oxygenated compounds by GC-MS above the 210 u level (acetosyringone [m/z 196], syringol acetone [m/z 210][133]) with upper limits achieved in the vicinity of 300 u.[131,132] In addition, GC-MS is not suitable for analyzing heat-sensitive molecules and there are problems due to coelution of oxygenates with pure hydrocarbons which further hinder identification in complex mixtures.[282,283]

Above the GC-MS range, individual compound identification becomes difficult. Analytical methods and techniques developed for characterizing fossil-fuel-derived materials, which cannot be observed by GC-MS have been recently reviewed in this journal.[135] Applications of these methods to the heavier fractions of both coal and biomass derived tars/oils will be discussed in section 4 of this review.

3.3. Synergistic Effects between Dissimilar Components of Solid Fuels

In a recent review of challenges faced, while exploring ways to make biofuels from biomass pyrolysis, Mettler and co-workers[112] correctly observed that "...detailed models capable of describing the chemistry and transport in real-world reactors is unavailable".

In this section, we will review the pyrolytic behavior of cellulose and lignin embedded within naturally occurring biomass. Taken together, the evidence suggests that these components do not pyrolyze independently during the thermal breakdown of lignocellulosic biomass. Furthermore, the extent and nature of synergistic effects appear to depend on how these components are enmeshed in a particular plant material. As a result, we have less than a full understanding of observed product trends and how they relate to plant structure at the macromolecular level. We are clearly some way short of formulating detailed chemical mechanisms required for quantitative predictions.

However, real-world reactors may equally well be modeled using fundamental experimental data from pyrolysis experiments on selected biomass samples combined with well-defined concepts of reactor design, such as extraparticle and bulk-phase heat and mass transfer and fluid flow. Where the complexity of pyrolytic processes has the last word is in having to account for the chemical reactivity of reactants and products during extraparticle chemical and physical processes. Those difficulties may not be insurmountable, however, provided experiments are designed with an eye to evaluating the effects of secondary reactions. The experiment described in Figure 15 represents one of many possible examples.

3.3.1. Synergistic Effects between Components of Lignocellulosic Biomass: A Brief Look. The major components in most lignocellulosic biomass are cellulose (~35−50% dry basis), hemicelluloses (~20−35%, dry basis), and lignins (10−25%, dry basis).[136−138] Some French and English oaks are reported to contain up to 30−35% lignins.[139] To these components must be added small proportions of extractables (resins, etc.) and small complements of mineral matter.[137,140,141]

3.3.1.1. On the Pyrolysis of Cellulose. Laevoglucosan (1,6-anhydro-β,D-glucopyranose) is the single-ring primary product that is liberated when covalent bonds holding together the linear polymer cellulose are cleaved. We already noted that high yields of laevoglucosan are possible when cellulose is pyrolyzed under conditions limiting thermal degradation of the primary products. Experimenting with pure cellulose piled into a metallic boat and pushed into a preheated tubular furnace, Shafizadeh et al. reported laevoglucosan yields as high as 50% despite ample opportunity for thermal degradation reactions.[117] In practice, it seems possible to obtain higher yields of laevoglucosan: tars recovered during later work in a fluidized-bed reactor operating at moderate temperatures yielded nearly 85% of the original cellulose mass as laevoglucosan.[129] Furthermore, when pure cellulose is pyrolyzed in a wire-mesh reactor (Figure 4), laevoglucosan is clearly identified by GC-MS as the major component detected in the tar/oil product.[114]

However, Shafizadeh's own work suggests that less than 3% laevoglucosan was found in the products when *wood* samples, normally containing up to ~50% cellulose, were pyrolyzed in the same metallic boats.[142] All subsequent work has confirmed the low levels of occurrence of laevoglucosan in tars/oils from pyrolysis of composite lignocellulosic materials, notwithstanding the high (35−50%) proportions of cellulose present in the original samples. Working with a wire-mesh reactor under conditions minimizing extraparticle secondary reactions, Fraga et al.[115] reported that no laevoglucosan could be detected by GC-MS in tars/oils from sugar cane bagasse. Only trace concentrations of laevoglucosan were identified in the tar/oil product from silver birch pyrolysis. The evidence points to *intraparticle* synergistic effects between components of lignocellulosic biomass during pyrolysis, providing a clear indication that these components do not pyrolyze independently.

3.3.1.2. On the Pyrolysis of Lignin. Another manifestation of synergistic effects between components of lignocellulosic biomass is provided by a comparison of char yields from pyrolysis of pure (prepared) lignin samples and from naturally occurring lignocellulosic biomass. Tables 5 and 6 show that, with rapid heating coupled to effective volatile removal from the reaction zone, finely ground (106−152 μm) silver birch wood and sugar cane bagasse particles gave less than 1−3% char residue when pyrolyzed between 600 and 900 °C.[114,115]

Meanwhile, Table 7 shows that a Kraft lignin gave far higher (>30%) char yields under similar experimental conditions. The estimated lignin content the of sugar cane bagasse sample was about 21% and that of the silver birch about 27%. On the basis of the cellulose, the lignin, and other biomass components pyrolyzing independently, we would have expected higher char yields from these two biomass samples. Conversely, the pure lignin data in Table 7 showed far greater char residues than would have been anticipated, judging by the char yields from the lignocellulosic biomass samples and their estimated original proportions of lignin.

The chemical structures and compositions of "pure" lignins vary between plant species and also change with the method of isolation.[143] Strictly, we have no evidence suggesting that the structures and composition of particular prepared lignin

dx.doi.org/10.1021/cr400194p | Chem. Rev. 2014, 114, 1547−1607

samples correspond closely to the properties of the lignins in original plant material. What we *can* do, however, is to survey results from a broad selection of lignin pyrolysis experiments to draw some qualitative conclusions. Table 9 presents data from a wide but not exhaustive survey of pyrolysis experiments performed using pure lignin samples isolated by a variety of chemical preparation methods from a wide range of plant materials.

In this context, a meaningful comparison of results requires selecting (pyrolysis) experimental designs, which more closely reflect the fundamental behavior of the samples. As explained earlier, data from wire-mesh- and fluidized-bed-type reactors would serve these aims rather better than most other reactor configurations in use. Nevertheless, data from other experimental designs have been included in Table 9 to get a broader perspective. As will be observed, the appeal of thermogravimetric balances for characterizing the pyrolytic behavior of biomass seems as undeniable as the manifest shortcomings of this type of equipment. It has been explained elsewhere that the inherent inaccuracies of TGA systems are accentuated by differentiating the data to derive pyrolysis kinetics.[61]

The data in Table 9 show that the high char yields recorded during experiments with the Holmen Lignin specimen in Table 7 were not an unusual or idiosyncratic result. Compared to pure prepared lignins therefore, naturally occurring lignocellulosic biomass clearly shows a char yield deficit when compared to char yields we might have anticipated from the (hypothetical) independent pyrolysis of individual biomass components. Thus, the course of pure lignin pyrolysis and the course of lignin pyrolysis reactions in naturally occurring plant material appear to take entirely different pathways. One possible explanation for this char yield deficit is the highly oxidizing environment of naturally occurring biomass, with cellulose and other oxygenated species, (e.g., hemicelluloses), pyrolyzing in close proximity to the lignin matrix.

Meanwhile, there is evidence showing that product distributions from different macerals during pyrolysis of coal particles appear to be additive. The apparent lack of synergistic effects presents an intriguing contrast to the more complex behavior of pyrolyzing biomass.

3.3.2. Synergistic Effects between Pyrolyzing Coal Macerals? This section summarizes tar and char yield data from pyrolysis of different macerals present in coal particles. It shows that the magnitude of possible synergistic effects between individual coal macerals separated from two middle-rank coals was within the experimental uncertainty of the tar and char yield determinations (also cf. Chapter 3 of ref 62).[65,57]

Table 10 presents the petrographic analyses of Linby and Point of Ayr (U.K.) coals and their separated maceral concentrates used in the study. As the separated maceral concentrate samples were not pure, the data were combined with tar and total volatile yields from the samples, provided in refs 62, 65, and 57. It was then possible to back-calculate the would-be tar and total volatile yields corresponding to the pure macerals of these coals.[153] Table 11 presents the theoretical yields calculated for the pure macerals of these two coals. Total volatile yields in these determinations are thought to be accurate to within ±1%, while tar yields are thought to be within ±2%.

Compared to atmospheric-pressure pyrolysis, greater tar yields were observed under vacuum in the case of whole coals and of vitrinite and liptinite concentrates. However, inertinite concentrates gave smaller increases in tar yield on application of vacuum, and the total volatile yields actually *decreased*. The latter result appears counterintuitive; repeated experiments with the present samples produced similar results and did not help clarify reasons for this observation. Similar observations on an inertinite concentrate derived from Treeton-Barnsley coal (U.K.) have been reported in a previous study.[153]

Combined with the maceral compositions of each coal (Table 9), the tar and volatile yields reported in Table 11 allow calculation of yields from the corresponding whole coals, assuming a weighted sum of pyrolysis yields from individual pure macerals. The calculation may be likened to reconstituting the pyrolysis yields of whole coals from those of individual maceral components present in each coal.

Table 12 compares actual *experimental* pyrolysis yields measured using ordinary Linby and Point of Ayr coal samples (from Table 8) with those of the *calculated* (reconstituted) yields for the same samples given in Table 11. Clearly, the *calculated* yields assume additivity, i.e., that the individual components pyrolyzed independently. This is the premise we found we could *not* assume in the case of the biomass samples.

For both vacuum and atmospheric-pressure data, the level of agreement in Table 12 between calculated and experimental values was well within experimental repeatability. In view of the stated experimental uncertainly in the pyrolysis experiments themselves and the undefined but usually larger errors in petrographic analyses, the level of agreement was even a little surprising. In any case, the results indicate the absence of measurable, experimentally significant synergistic effects between different macerals during pyrolysis of coals. It could thus be safely concluded that to a first approximation no synergistic effects could be observed between maceral concentrate samples from two low- to middle-rank coals, Linby and Point of Ayr coals, during pyrolysis experiments.

3.3.3. Synergistic Effects between Components of Lignocellulosic Biomass: A Closer Look. Pure or nearly pure maceral particles tend to have dimensions of several micrometers or less.[154,155] The results presented in Table 12 bring to mind questions about whether synergistic effects would be observed during pyrolysis of composite particles constituted from mixtures of fine powders of cellulose and lignin. The cellulose sample was pure, binder-free microgranular cellulose powder for TLC (Whatman; Part No. 4061-050), and the lignin sample was a Kraft lignin (Holmen AB, Sweden).

Cellulose and lignin powders were mixed in selected proportions, ranging from 100% cellulose to 100% lignin in four 25% steps. The mixed powders were compressed into pellets of about 1 cm diameter and several millimeters thick. Pellets were then crushed and the 106−152 μm size fraction sieved for use in pyrolysis experiments. Figure 17 presents total volatile yields from pyrolysis of the composite particles and compares them with hypothetical yields (straight lines) *calculated* by assuming that the two components pyrolyzed independently. As usual, char yields may be calculated from subtracting the value for total volatiles from 100%.

These data revealed a complex picture. Both rapid (1000 °C s^{-1}) and slow (1 °C s^{-1}) heating of composite particles gave lower total volatile yields (higher char yields) compared to the case assuming no synergistic effects. The data thus clearly showed what could be termed synergistic effects between powdered cellulose and lignin particles during pyrolysis of the composite particles.

However, the data in Figure 17 also showed that significantly *higher* total volatile release (*lower* char yields) were found when

dx.doi.org/10.1021/cr400194p | *Chem. Rev.* 2014, 114, 1547−1607

Table 9. Selection of Pyrolysis Char Yields from Lignins Prepared with Diverse Methods and Pyrolyzed in Diverse Types of Apparatus

authors (year)	lignin prep method	pyrolysis method	sample size	heating rate	char yield data (temp °C, char %)		comments
Iatridis and Gavalas[144] (1979)	Kraft lignin from Douglas fir	early version of captive sample technique (wire-mesh reactor)	200 mg	200−400 (approx) °C s^{-1}	400	~76−78	large sample (200 mg) may have contributed to increase char yield (est. < 5%)
					500	~56	
					600	~43	
					750	~35	
Chan and Krieger[145] (1981)	pinewood Kraft lignin	volume heating by dielectric-loss microwave heating	1.5 × 1.5 cm pellet	20 °C s^{-1} (est.)	650−750 (est.)	33%	pellet size might contribute to some char formation (est. < 5%)
Nunn et al.[146] (1985)	milled wood lignin from sweet gum hardwood	heated grid (wire-mesh) reactor	≤100 μm thick flakes	1000 °C s^{-1}	307	96.9	result at 1077 °C seems low, compared with result at 527 °C; most weight loss expected below 600−650 °C
					527	50	
					1077	14.5	
Caballero et al.[147] (1996)	eucalyptus wood Kraft lignin	Pyroprobe instrument	powder	nominal 20 000 °C s^{-1}	450	44[a]	sample stacking may have increased char yield by est. several percent
					700	35[a]	
					900	33[a]	
Ferdous et al.[148] (2002)	Alcell and Kraft lignins	thermogravimetric balance (TGA)	10 mg of powder	5−15 °C min^{-1}	800 Alcell	35	lowest char yields observed during heating at 15 °C min^{-1} to 800 °C
					800 Kraft	43	
		fixed-bed reactor		5−15 °C min^{-1}	800 Alcell	38−42[a]	secondary char formation in TGA and fixed-bed reactor; result to be treated as qualitative[61]
					800 Kraft	45−50[a]	
Wang et al.[149] (2009)	MWL[b] from Manchurian ash and Mongolian pine	thermogravimetric balance (TGA)	not available	1 °C s^{-1}	37% and 26%	secondary char formation in TGA and fixed-bed reactor; result to be treated as qualitative[61]	
De Wild et al.[150] (2009)	(1) Alcell organosolv process from mixture of hardwoods; (2) GRANIT precipitation after pulping nonwoody plants	thermogravimetric balance (TGA)	powder	5 °C min^{-1}	Alcell, 500	Alcell, ~48[a]	secondary char formation in TGA and fixed-bed reactor; result to be treated as qualitative[61]
					GRANIT, 500	GRANIT, ~43[a]	
		preheated fluidized bed	1−3 mm pellets	rapid >1000 °C s^{-1}	Allcell, 400	Allcell, 35	higher char yields in TGA compared to fluidized bed likely due to secondary char formation in TGA
					GRANIT, 400	GRANIT, 30	
Beis et al.[151] (2010)	Indulin AT Lignoboost were Kraft lignins; Acetocell	thermogravimetric balance (TGA)	10 mg of <425	5 °C min^{-1}	peak temp 5 °C min^{-1}	900 °C	higher char yields in TGA compared to fluidized bed likely due to secondary char formation in TGA; final char yields in TGA similar for different heating rates; Acetocell char yield in fluidized bed seems inordinately high

dx.doi.org/10.1021/cr400194p | Chem. Rev. 2014, 114, 1547−1607

Table 9. continued

authors (year)	lignin prep method	pyrolysis method	sample size	heating rate	char yield data (temp °C, char %)		comments
	lignin from an organosolv process		μm particles		Indulin AT	42[a]	
					Lignoboost	38[a]	
					Acetocell	42[a]	
		fluidized bed, all experiments at 550 °C	100 g of <425 μm particles	rapid >1000 °C s^{-1}	550 °C		
					Indulin AT	41	
					Lignoboost	29	
					Acetocell	63	

[a]Estimated from graphical data in the publication. [b]MWL: milled wood lignin; cf., e.g., Guerra and Filpponen.[152]

Table 10. Petrographic Analyses of Separated Linby and Point of Ayr Maceral Concentrates[a]

	vitrinites % v/v[b]	liptinites % v/v[b]	inertinites % v/v[b]
Linby (whole) coal	73	15	12
Linby vitrinite concentrate	85	6	9
Linby liptinite concentrate	16	70	14
Linby inertinite concentrate	35	4	61
Point of Ayr (whole) coal	84	6	10
Point of Ayr vitrinite concentrate	91	5	4
Point of Ayr liptinite concentrate	30	61	9
Point of Ayr inertinite concentrate	17	3	80

[a]Reproduced with permission from ref 57. Copyright 1993 Elsevier. [b]Dry, mineral matter free.

Table 11. Calculated Theoretical Tar and Total Volatile Yields for Pyrolysis of Linby and Point of Ayr Coal-Derived Pure Macerals at Atmospheric Pressure and under Vacuum[a]

	atmospheric pressure		vacuum	
sample	tar yields (w/w %, daf sample)	total volatiles (w/w %, daf sample)	tar yields (w/w %, daf sample)	total volatiles (w/w %, daf sample)
Linby				
vitrinites	28.2	44.0	35.6	46.4
liptinites	59.1	75.1	69.7	78.5
inertinites	23.1	39.3	26.7	35.9
Point of Ayr				
vitrinites	22.5	38.8	29.0	40.7
liptinites	64.2	78.4	86.5	95.4
inertinites	12.9	27.9	14.0	24.6

[a]Heating rate of 1000 °C s^{-1} to 700 °C with 30 s holding (atmospheric pressure) and 5 s (vacuum). (Reproduced with permission from ref 57. Copyright 1993 Elsevier).

Table 12. Comparison of Experimental and Calculated Tar and Total Volatile Yields for Pyrolysis of Linby and Point of Ayr Whole Coals[a]

	atmospheric pressure		vacuum	
	tar yields (w/w %, daf sample)	total volatiles (w/w %, daf sample)	tar yields (w/w %, daf sample)	total volatiles (w/w %, daf sample)
Linby whole coal				
calculated	32.2	48.1	39.6	50.0
experimental	30.7	46.6	37.9	49.7
Point of Ayr whole coal				
calculated	24.0	40.1	30.9	42.3
experimental	26.1	42.4	33.1	41.8

[a]Operation at atmospheric pressure and under vacuum. Calculated results are based on the assumption of additivity of yields from individual pure macerals. Heating at 1000 °C s^{-1} to 700 °C with holding 30 (atmospheric pressure) or 5 s (vacuum). (Reproduced with permission from ref 57. Copyright 1993 Elsevier.)

silver birch and sugar cane bagasse pyrolysis results were plotted on the basis of their estimated lignin contents (plotted on the *x* axis as 100% minus lignin content). Thus, samples prepared by mixing cellulose and lignin powders gave a different trend (*more char* than the hypothetical case assuming the absence of synergistic effects) compared to natural lignocellulosic biomass samples, which gave *less* char than the

dx.doi.org/10.1021/cr400194p | *Chem. Rev.* 2014, 114, 1547−1607

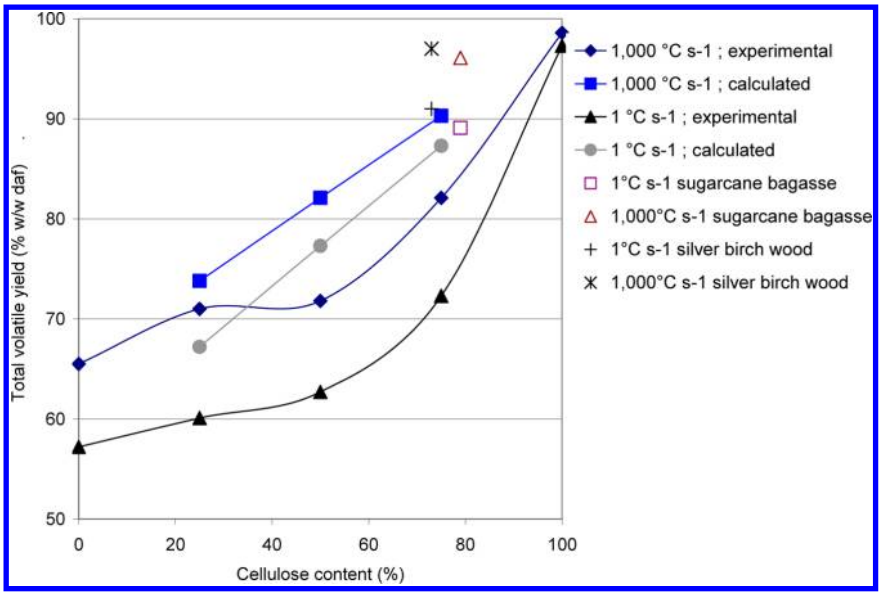

Figure 17. Theoretical and experimental yields of total volatiles as a function of cellulose content and heating rate at 600 °C and 30 s hold time. (Adapted from ref 114, p 161).

hypothetical straight line. This result is informative. It shows that the manner in which cellulose and lignin are associated within sample particles profoundly affects product distributions during pyrolysis.

In trying to arrive at an explanation of cellulose and lignin-related synergistic effects during pyrolysis of naturally occurring lignocellulosic biomass, several related factors need to be considered, probably in conjunction: (i) Intimate intermeshing of biomass components and the resulting physical impediments to the free evaporation of potentially volatile products during thermal breakdown. (ii) Decomposition of cellulose at lower temperatures compared to lignin, releasing thermally sensitive laevoglucosan within the heated lignin matrix. This is coupled to secondary intraparticle chemical reactions between products from different pyrolyzing components. (iii) Differences in the reactivities of tars/oils from the different components.

Let us briefly examine these elements within a likely pyrolytic sequence, ignoring for the time being the role of hemicelluloses, mineral matter and extractable resins, for which we do not have purpose-designed data.

(i) Intermeshing of Biomass Components. Mettler and co-workers attempted a detailed description of the intermeshing of biopolymers at the macromolecular level. The constitution of elementary lignocellulose is described, followed by the constitution of wood cells, which, in turn, make up woody microstructures and eventually wood fibers.[112] We thus expect that within naturally occurring structures, cellulose and lignin come into more intimate contact than in the composite particles, prepared from powders as described above. It would also be reasonable to expect that the tightly packed arrays of biopolymers that make up naturally occurring biomass are likely to serve as barriers to the quick evaporation and release of what in effect are thermally sensitive pyrolysis products.

(ii) Different Breakdown Temperature Ranges of Biomass Components. Comparison with coal pyrolysis suggests the intervention of yet another complicating factor. One major difference between coal and biomass pyrolysis arises from the different temperature intervals that must be reached before major components within lignocellulosic biomass begin to breakdown thermally. Table 13 presents a qualitative case for much of the cellulose pyrolyzing at lower temperatures than the lignin component it would have been intermeshed with.

Table 13. Comparing the Pyrolysis Temperatures of Cellulose and Lignin[a]

temp, °C	heating rate, °C s^{-1}	cellulose total volatiles, % w/w daf	lignin total volatiles, % w/w daf
400	1	88.2	44.7
	1000	90.4	50.6
600	1	97.3	57.2
	1000	98.6	65.5
900	1	98.4	58.7
	1000	99.4	68.3

[a]Carrier gas helium. Holding time at peak temperature: 30 s.[114]

There is supporting evidence showing the early thermal breakdown of cellulose from the fluidized-bed reactor, where cellulose was found to release nearly 70% tar at the relatively low temperature of 300 °C.[60] The corresponding tar yield from silver birch was about 40%.[60] Char yields from cellulose and silver birch wood at 300 °C were 20% and 44%, respectively.

TGA-derived slow (10 °C min^{-1}) pyrolysis data have shown that pure cellulose begins losing weight rapidly near 320 °C; this seems far too high compared to the fluidized bed results quoted earlier. Nevertheless, according to the same report, weight loss was completed by 400 °C.[156] Although the *onset* temperature for pyrolysis of the lignin sample appeared at some 10−20 °C lower, in this work, nearly 70% of the lignin remained in solid form at 400 °C, when the cellulose mass was already reduced to several percent of char-like solid. The study also showed the xylan sample (used as hemicellulose) began losing weight around 200 °C but maintaining nearly 40% of its original weight at 400 °C. The eventual solid residue from this sample was over 20%.

Clearly, the data sets are not complete. However, combining the latter results with Table 13, it may be concluded that much of the cellulose appears to decompose at temperatures where the other major components still present pyrolyzing solid masses. In looking for leads to explain synergistic effects

dx.doi.org/10.1021/cr400194p | Chem. Rev. 2014, 114, 1547−1607

between biomass components during pyrolysis, the thermal sensitivity of laevoglucosan provides a powerful clue. With a sublimation temperature of 115 °C and an onset of decomposition temperature of around 300 °C, volatilization of laevoglucosan at typical cellulose pyrolysis temperatures would be as rapid as its subsequent thermal degradation, particularly if trapped within charring lignin-like microstructures.

It is also likely that volatiles released during the early onset of hemicelluloses would have some impact on the incipient thermal breakdown of neighboring structural elements made up of cellulose and lignin. Within the fine structure, pyrolysis products are likely to interact both physically and chemically with enmeshing lignin and other structures. As secondary reactions of laevoglucosan (and hemicellulose-derived volatiles) within the confined space lead to thermal degradation, it might be expected that the resulting highly oxygenated environment would enhance reactions with lignin and contribute to the lignin char deficit referred to above.

(iii) Order of Relative Tar Reactivities. The fluidized-bed reactor experiments described above (Figure 15; also cf. ref 60) allow discussing the relative order of reactivity of tars/oils to thermal cracking and thermal degradation.

Figure 18 presents tar yields from pyrolysis of Linby coal at the shortest and longest freeboard residence times practicable

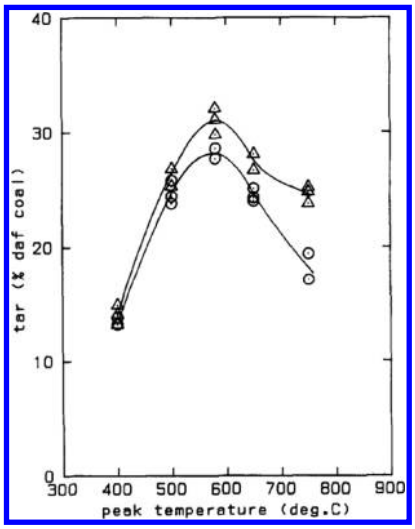

Figure 18. Fluidized-bed pyrolysis tar yields as a function of temperature for two different freeboard residence times: (Δ) 0.8 and (○) 4.5 s Linby (U.K.) coal. (Reproduced with permission from ref 59. Copyright 1990 Elsevier.)

in the fluidized-bed reactor shown in Figure 15. While the shapes of the curves are similar to those for silver birch wood (Figure 16), the data show far greater proportions of tar survival at higher temperatures by Linby coal tars. Tar yields showed a maximum around ~580−590 °C. For a lignite, the analogous maximum was observed at ~530 °C (not shown),[60] while for cellulose itself and for silver birch (Figure 16) the tar yield maxima occurred between 425 and 450 °C. The full set of data may be found in ref 60. Comparing Figures 16 and 18 clearly shows the significant differences between the temperature intervals within which tars from different substrates show reactivity to thermal cracking.

The differences between the pyrolysis onset temperatures of different biomass components (reviewed above) and the differences in the thermal stabilities of tars/oils from biomass components must be viewed as factors concurrently operating during thermal breakdown of lignocellulosic biomass. Once again, the data set is not complete but the demonstrated thermal sensitivity of cellulose tars/oils provides a measure of support for the explanation provided for the absence (or near absence) of laevoglucosan in the product mix from lignocellulosic biomass. Within this framework, the lignin char deficit discussed above is likely to be linked to reactive and highly oxygenated molecular fragments being generated by prior thermal breakdown of thermally more labile biomass components.

Some corroboration for the view that the reactive environment in the vicinity of lignin structures might alter the course of lignin pyrolysis is found in results from the differential scanning calorimetry (DSC) of cellulose and of the set of samples described in Tables 5−7. When compared with the thermograms of pure cellulose and pure lignin, the thermograms from silver birch wood and sugar cane bagasse showed evidence for cellulose decomposition but the peak observed when lignin was pyrolyzed on its own was not observed.[114] While this does not constitute definitive evidence, the indications are that the chemistry of lignin thermal breakdown is comprehensively altered in the chemical environment created by the presence of more labile and more highly oxygenated species pyrolyzing in close proximity.

3.3.3.1. Synergistic Effects: Factors Other than Cellulose−Lignin Interactions. Thus far we used laevoglucosan survival/destruction and lignin char yield deficits as yardsticks to gauge departures from linear additivity during pyrolysis of biomass. The behavior during pyrolysis of hemicelluloses, mineral matter, and extractables could not be analyzed in similar detail due to a relative dearth of clear evidence and purposely designed experiments. Several recent studies, however, have provided useful pointers.

Using an entrained flow reactor, Couhert et al.[157] focused on measuring pyrolysis gas yields from five naturally occurring biomass specimens. Gas yields from several samples of cellulose, xylan (representing hemicelluloses), and three prepared samples of lignin were also determined. An attempt was made to predict gas yields from naturally occurring biomass by calculating weighted sums of gas yields using the measurements on the isolated biomass components and their estimated contents in the natural biomass specimens. After concluding that "...such a simple approach was not successful", these researchers looked at the influence of mineral matter and suggested it as a possible cause for the discrepancies. However, their brief review of work on the subject concluded that "...conclusions are different depending on the authors and on the experimental conditions..." with discrepancies often being explained in terms of "...possible interactions between the components and the likely effect of mineral matter".

The reactivity enhancing effects of mineral matter had previously been inferred from results of a study on the copyrolysis of biomass with coal.[158] Vassilev et al. recently reviewed the compositions of mineral matter and extractables (termed extractives) in naturally occurring biomass.[137,140,141] Clearly, gaps in our knowledge about the chemical compositions of biomass materials are constantly being filled. What seems needed is the development of experiments deliberately conceived to elucidate the roles of specific biomass components during pyrolysis.

dx.doi.org/10.1021/cr400194p | Chem. Rev. 2014, 114, 1547−1607

3.3.3.2. Implications for Modeling Pyrolysis Reactions. Experiments with pelletized mixtures of cellulose and lignin powders were found to give trends that were the reverse of how naturally occurring biomass samples seem to behave. The attempt to understand synergistic effects observed during pyrolysis of lignocellulosic biomass led us to examine several additional connected phenomena: the intimate level of contact within matrices of natural biopolymers, the different thermal breakdown temperatures of different biomass component, and the differences between the thermal sensitivities of their evolving tars. We have also raised, but have not been able to answer, questions regarding the role of hemicelluloses, mineral matter, and extractables during pyrolysis.

These structural complexities go some way toward scoping the level of detail that would need to be included in ab initio models describing the chemistry of the thermal breakdown of lignocellulosic biomass. Given these complexities of synergistic interactions and their probable dependence on the detailed structures of particular plant species, attempting to work with ab initio mathematical models (simulations) of the chemistry of biomass pyrolysis in a manner that would follow "...analogously from the problems of cellulose..."[112] does not seem realistic. It seems we are some distance away from fully understanding the role of variables that determine observed trends. Quantitative predictions of the chemistry of pyrolytic processes may well be some distance away.

Although mathematical modeling of pyrolysis reactors is also deemed to be outside the scope of this review, these observations are not meant to signal the existence of barriers to mathematical modeling of larger scale reactors. Instead of attempting to develop ab initio mathematical models of the detailed thermal breakdown chemistry of solid fuels, however, it seems quite possible to develop primary pyrolysis product-distribution databases for selected samples from carefully conceived bench-scale experiments that would feed data into the design and simulation of larger, e.g., pilot- and plant-sized reactors. These considerations explain the emphasis in the present review on devising experiments (i) able to tease out the fundamental thermal breakdown patterns of solid fuel particles during pyrolysis and (ii) able to track the sequence of reactions that the released volatile products undergo in terms of secondary extraparticle reactions.

Meanwhile, there are many commercially available mathematical models on the market that reportedly provide excellent fits to data and claim ability to predict the pyrolytic behavior of (some) solid fuels. For clarity, it seems useful to point out, however, that such models usually require input from the type of experiments and data described in this review. What is aimed at in this review is to help clarify and explain the mechanisms and progress of the successive stages of pyrolytic processes. With these objectives in mind, mathematical models involving fitting data, usually by means of adjustable parameters, have been left outside the scope of the present discussion.

3.4. Upgrading Biomass Pyrolysis Tars/Oils

Generating alternative energy vectors from biomass is an environmentally desirable objective. With care, we may be able to produce liquid fuels with greater energy content than has been expended to produce the fuel in the first place. We would aim to utilize feedstocks *not* meant for food and seek *not* to replace food production on productive land with energy crops. Agricultural, forestry, and municipal wastes match these conditions without difficulty. We would also aim to pollute less in transporting feedstocks and producing and utilizing the biomass-derived fuels compared to their fossil-derived alternatives. These constraints present severe challenges for some of the technologies currently in place for producing renewable transport fuels from biomass. It is imperative, however, to improve or replace technologies where they fall short if the exercise is not to prove ultimately self-defeating. The experimental process routes discussed below must also be evaluated against these criteria before being presented as viable alternatives to society at large.

Numerous technologies proposed for fast pyrolysis of biomass[159,160] and the associated drying and grinding operations[161,162] have been reviewed in detail. It is also widely known and the data already presented in this review (mostly in section 3.2) clearly show that between 50% and 70% of solid biomass may be converted to liquid-phase products by pyrolysis. The long-time unanswered question is what to do with this liquid, apart from direct combustion, which is a reasonable alternative if we are unable to make transport fuels or other higher value products. Before reviewing biomass liquids upgrading, it would be useful to briefly look at the state of the art in coal liquid upgrading efforts.

3.4.3. Catalytic Upgrading of Coal-Derived Liquids. Early catalytic upgrading work on extracts from coal liquefaction has been reviewed by Mochida and Sakanishi.[163,164] Well into the 1990s, much of the Japanese effort at pilot-plant level was focused on low-rank coals, because PNA ring system sizes in extracts from these coals were smaller. The enduring challenge in upgrading bituminous coal extracts is to formulate catalytic reaction pathways that would tend to crack larger PNA ring systems rather than to hydrogenate them. More recently, the new pilot- and demonstration-scale CTL plants in China have stimulated research to improve catalyst formulations for upgrading coal-derived liquids.[165] Modified formulations of well-known catalysts such as Ni–Mo and W–Ni on alumina have been tested on low-temperature coal tars.[166]

One interesting development involves renewed focus on mesoporous catalyst supports capable of handling higher molecular mass coal extract molecules. Lei et al. evaluated the performance of Ni–W catalysts supported on ordered mesoporous silica supports such as MCM-41 and SBA-15.[167] The observed improvements due to larger than usual pore size distributions are consistent with earlier work by Song et al.[168−170] The latter had reported that conversion of asphaltenes and preasphaltenes and heteroatom removal by $NiMo/Al_2O_3$ catalysts were improved by increasing the average pore size of catalyst supports to between 300 and 800 Å. These observations were interpreted in terms of larger pore size distributions effectively increasing contact surface area by facilitating diffusion of larger molecular mass materials into the porous structure.

3.4.4. Catalytic Upgrading of Biomass-Derived Liquids. As will be discussed in section 4, the structural make up of biomass pyrolysis tars/oils contains smaller fused aromatic ring systems compared to coal-derived tars and extracts. Potentially this represents a significant advantage. However, biomass pyrolysis liquids are usually difficult to handle and process. They are corrosive. Gum formation and separation into aqueous and organic phases during storage introduces complications in pumping and eventual utilization. Furthermore, the viscosity of the organic phase tends to increase with storage time. Problems are also encountered

dx.doi.org/10.1021/cr400194p | *Chem. Rev.* 2014, 114, 1547−1607

during ignition in engines due to the low volatility of the fuel and the low calorific values associated with the high oxygen contents (up to 50%).[171,172] Direct combustion of pyrolysis tar/oil vapors prior to condensation provides a viable low-value route for disposal.

The more widespread use of biomass pyrolysis liquids requires making higher grade fuels or chemical feedstocks at acceptable cost. Partial deoxygenation would raise the density and calorific value of the feedstock. Combined experience to date suggests, however, that favored reaction pathways tend toward high rates of catalyst coking and fouling coupled with light gas formation, including large proportions of CO and CO_2 formation. It may also prove useful to revisit the commercial attractions of lighter chemical feedstocks, once the driving force behind the "destructive distillation of wood".

Early work on the catalytic upgrading of pyrolysis tars/oils has been reviewed by Pindoria et al.,[173] Furimsky,[174] and more recently Corma et al,[175] Sanna and Andrésen,[176] and Huber et al.[177] This section aims to briefly trace the contours of problematic areas in the catalytic upgrading of biomass tars/oils without seeking to present an exhaustive review of work in this field.

3.4.4.1. Catalytic Hydrotreatment of Biomass Pyrolysis Liquids. Many of the catalysts used in upgrading biomass pyrolysis tars/oils to low oxygen fuels (~1%) have been borrowed from the petrochemicals industry. These include the use of presulfided NiMo and CoMo catalysts on alumina supports, zeolites (e.g., H-ZSM5), and activated alumina.[178] Other catalysts studied include vanadium nitride and Pt or Ru on carbon or silica−alumina supports.[177,179]

Baker and Elliott[180,181] reported on coke formation leading to reactor blockages during hydrotreatment of biomass pyrolysis oils in a pilot-scale fixed-bed up-flow reactor (250−450 °C; 136 bar H_2 pressure). Coke formation could be reduced by prior hydrogenation at lower temperatures (270 °C) followed by hydrotreatment at 400 °C. Both stages were operated in the presence of $CoMo/Al_2O_3$ and $NiMo/Al_2O_3$ catalysts. Using the two-step procedure was successful in reducing hydrogen consumption but generated large amounts of CO_2. Meanwhile, the oxygen content of the final product was reduced from nearly 17% to between 2% and 3%.

Processing tars/oils diluted with hydrogen donors and other solvents has been attempted, with the aim of limiting extents of coking. Operating an atmospheric-pressure continuous fixed-bed down-flow microreactor at 370−440 °C, Sharma et al.[182−184] experimented with upgrading crude tall oils over an H-ZSM5 zeolite catalyst. The oils were mixed with methanol or tetralin. Conversions to hydrocarbons and water were on the order of 80−90 wt %. In the presence of tetralin and steam, conversion to gasoline range aromatic hydrocarbons in the liquid product was reported to be between 52 and 57 wt % of the amount charged (results are given tetralin free). Coke formation levels were between 6 and 12 wt %, with 2−7.6 wt % gas make. Using the same reactor system, Katikaneni et al.[185] tested a set of aluminophosphate catalysts of different acidities and pore size distributions. Compared to H-ZSM5, lower conversions of bio-oils to hydrocarbons were observed during hydrotreatment of a wood pyrolysis tar/oil (330−410 °C) and a vegetable oil (375−550 °C).

In a similar application, Adjaye and co-workers[186] investigated the catalytic upgrading of bio-oils from the liquefaction of aspen poplar wood in a continuous downflow, fixed-bed microreactor (250−520 °C, under atmospheric-pressure argon). The organic fractions of the bio-oils and tetralin were pumped continuously over the fixed bed of H-ZSM5 catalyst. Light distillate product initially increased with increasing temperature and leveled off at 390 °C. The aromatic content of the products was reported to increase from 45 wt % at 250 °C to a maximum of 65 wt % at 370 °C. At 450 °C, coke deposition on catalyst surfaces was found to increase to about 15 wt % of the feed (results are given tetralin free).

The wide ranges of molecular masses and molecular structures in biomass pyrolysis tars/oils present additional challenges to process development. Corma et al. worked on developing extra-large-pore zeolites for "bridging the gap between micro and mesoporous structures".[187] Model compound studies have shown that increasing the availability of acid sites may lead to higher conversions of some classes of compounds while enhancing the coking of others. Fractionation of tars/oils into narrower bands of material may alleviate some of these problems. One promising development involves adding water to enhance separation of the raw tar/oil into an aqueous and an organic phase and to treat the two phases separately.[177]

Another approach arises from recognizing that freshly condensed biomass tars/oils are reactive and begin to repolymerize almost immediately upon condensation. The direct upgrading of pyrolysis *vapors* over zeolite catalysts *prior to condensation* has been investigated at atmospheric pressure by numerous researchers.[188−192] Evans and Milne[193] experimented with cracking birch wood pyrolysis vapors over a ZSM5 catalyst by cofeeding with methanol and helium. Much of the oxygen from the tar/oil was rejected as water, CO, and CO_2 (24.9, 20.1, and 17.1 wt %, respectively). Char yields were on the order of 15 wt %. At a catalyst bed temperature of 500 °C, about 10% coke formation was observed. Total organic yields were 18 ± 4 wt %, of which 6.5 wt % were monocyclic aromatics, 6.8 wt % alkenes, and 1.2 wt % furans.

Rejai et al.[194] used a similar reactor system to pyrolyze samples of hardwood and RDF (refuse-derived fuel made into briquettes) in mixtures of helium and steam. The effect of operating temperature, space velocity, and steam to biomass ratio were investigated. Higher yields of hydrocarbons were reported at high space velocities and low steam to biomass ratios.

Diebold et al.[195] studied the catalytic deoxygenation and cracking of "biocrude" vapors to hydrocarbons. A fixed-bed reactor containing 100 g of H-ZSM5 catalyst was used. The catalyst stage was fed by a 1−3% slipstream of pyrolysis vapors from a rapid heating vortex reactor (625 °C), fed at 15 kg h^{-1} with southern pinewood or RDF. At steady state (520 °C), coke formation on the catalyst from pinewood pyrolysis vapors was 9.4 wt % of the feed. The product slate included about 9 wt % C5+ gasoline range compounds, 25.2 wt % water, 23.5% CO and CO_2, 4.7 wt % CH_4 and C_2-C_4 compounds, 13.2 wt % tar, and 15.1% pyrolysis char.

Pindoria et al.[173] described a two-stage high-pressure (10−40 bar H_2) fixed-bed reactor. Eucalyptus wood particles were hydropyrolyzed in the first stage by heating at 10 °C s^{-1} up to 500 °C. Evolving volatiles were swept directly into a Zeolite H-ZSM-5 catalyst bed operating at *lower* temperatures fixed between 300 and 400 °C. The aim of using high-pressure hydrogen was to maximize tar/oil yield and quality in the first stage and suppress coke formation in the catalytic stage. Fresh zeolite catalyst trapped more than 40% of the product from the hydropyrolysis stage. However, TGA-derived evidence indicated that the occluded material was not deposited as carbon

dx.doi.org/10.1021/cr400194p | Chem. Rev. 2014, 114, 1547−1607

but as volatiles trapped within the zeolite matrix. Reuse of the catalyst resulted in little more uptake of volatiles. However, extended use of the catalyst did not result in increased yields of light liquid products but in the increased production of light volatiles. The H-ZSM5 catalyst appeared to act more as an active cracking catalyst than as a promoter of hydrogenation or deoxygenation of the liquids produced in the hydropyrolysis stage. Characterization of the liquids collected at the exit of the reactor by size exclusion chromatography (SEC) and UV-fluorescence spectrometry indicated that structural changes in the liquid products were relatively minor despite the significant reduction in the yields of liquids under these process conditions. It was concluded that available reaction routes did not allow specific deoxygenation pathways to predominate without disintegrating parent molecules to light volatiles.

Very low char yields have also been recorded in highly reducing environments. During the straightforward liquefaction of Kraft lignin in the presence of excess tetralin (4:1 tetralin:Kraft lignin) at 400 °C, Connors et al.[196] reported initial char yields of nearly 10%, gradually declining to 3.4% after 10 h of exposure. However, with longer exposure, nearly one-half the original sample appears to have converted to water, gases, and volatile hydrocarbons. The sum of acetone and ether-soluble liquefaction product was reported to have reached a high of ∼75% in the first 15 min and to have gradually declined to less than 30% during the subsequent 10 h of exposure. The authors suggested that "...The observed material loss must obviously be ascribed to the formation of water, gases and volatile hydrocarbons..." Nevertheless, the Connors et al.[196] experiments suggest that some form of mild thermochemical treatment, possibly in a dense medium, may provide the appropriate choice of reaction conditions for breaking down the relatively small PNA ring systems of lignins without excessive wastage of feedstock or hydrogen. In this context, it may prove useful to examine the potential byproduct value of the "...gases and volatile hydrocarbons..." in evaluating overall project feasibility. By comparison, pyrolyzing lignins suggests itself as a relatively blunt instrument.

3.4.4.2. Catalytic Pyrolysis of Biomass. A potentially interesting application involves pyrolysis of biomass in fluidized beds where part (or all) of the bed material consists of catalysts. Ideally, the process would aim to effect stepwise deoxygenation of tar/oil molecules for making more stable, higher calorific value liquid fuels or feedstocks. More recent efforts seem focused on routes to make transport fuels, without ascribing much potential commercial value to byproduct light oxygenates, e.g., aldehydes, ketones, etc.

Numerous molecular sieve catalysts and some based on naturally occurring minerals have been tested with the aim of circumventing the familiar problems of liquids product loss to excessive water, gas, and coke formation. We note that the latter is distinct from pyrolysis−char formation during the biomass pyrolysis process taking place in the same reactor and is mainly associated with coking of tars/oils on catalyst surfaces. A review by Lappas et al.[197] suggested using circulating fluidized bed systems to maintain catalyst activity by burning off coke deposits (and presumably also pyrolysis chars) in the second chamber.

Pyrolyzing wood sawdust in a bed containing HZSM-5 zeolite-based catalysts was reported to have given high yields of single-ring aromatics and olefins: less than 15% aromatics and 10% olefins. Nearly 70% of the carbon from the feedstock appears to have presented as coke (∼ 30%) or CO and CO_2, with CH_4 making up the balance of the last 5%.[198]

Much of the published data clearly show the amount of initial oil/tar to be independent of the bed material,[199] which may be understood in terms of the initial pyrolysis step not being affected by the nature of the solids. However, some authors appear to have labored under the assumption that pyrolysis of the biomass was being catalyzed by the minerals. This is difficult to visualize since pyrolysis takes place *within* fuel particles and biomass to catalyst contact would only be a surface to surface phenomenon. Despite the conceptual difficulties and poor product distribution from many of the reported experiments (cf. Sanna and Andrésen[176] for a brief review), possible use of catalytic pyrolysis for effecting more measured structural changes in the biomass pyrolysis tars/oils remains an attractive avenue of inquiry.

In a study that seems to force, if not break, the mold, Sanna and Andrésen[176] found that at relatively low pyrolysis temperatures (430−460 °C) "...approximately 70−74 % of the starting energy remains in the bio-oil..." Two magnesium iron silicate minerals (activated serpentine and olivine) were used as catalysts to relatively good effect, as apparent loss of feedstock to coke was reported to be on the order of 5%. If confirmed, the 40% *reduction* in the oxygen content, while retaining much of the product as a liquid may be considered a pointer for further study, probably by operating at somewhat lower reactor temperatures. The somewhat speculative departure in this particular study, from traditional catalysts adopted/adapted from the petroleum industry, serves as a reminder that progress in processing biomass tars/oils may well pass through novel catalysts and novel catalytic process routes.

3.4.4.3. Upgrading Biomass Pyrolysis Liquids: Brief Conclusions. Taken together, these reports indicate that significant carbon fouling and coke formation are common to many of the processes intended for upgrading biomass-derived tars/oils. In the case of NiMo and CoMo catalysts, coking seems to persist despite application of expensive high-pressure hydrogen. While the use of ZSM-5-based zeolite catalysts has tended to improve conversion of tars/oils to limited extents, high rates of gas formation and rapid catalyst deactivation remain as major challenges.[200−203] It has proved difficult, furthermore, to find a way of breaking down large tar/oil molecules in measured steps, which would allow making more of the lighter liquid fractions and middle-distillate quality products needed for preparing transport-grade fuels or fuel additives. Instead, large molecular mass tar/oil molecules appear to rapidly disintegrate, mostly giving water, carbon oxides, methane, and char. Results from various hydrotreatment or other upgrading schemes suggest this disintegration might be a thermodynamically favored reaction pathway for the highly oxygenated and labile structures of biomass tar/oil molecules. As in the work of Sanna and Andrésen,[176] it may yet prove useful, however, to investigate combinations of less intense reaction conditions coupled to the use of hitherto untried catalysts or catalytic processing schemes. The latter do not seem much in evidence, perhaps because commercial demand for process routes specifically designed for upgrading biomass pyrolysis liquids has hitherto been limited.

dx.doi.org/10.1021/cr400194p | *Chem. Rev.* 2014, 114, 1547−1607

4. TRACKING THE COURSE OF THERMAL BREAKDOWN: ANALYTICAL TOOLS AND THEIR LIMITATIONS

The preceding two sections have described experiments designed for tracking the course of thermal breakdown reactions in coals and lignocellulosic biomass. Data from electron spin resonance spectroscopy was found helpful in defining the contours of chemical changes taking place during the onset of thermal breakdown. Analysis of the thermochemical reactions of coal and biomass was helped by working with different types of samples, by altering key reaction parameters (e.g., temperature, heating rate), as well as by designing and working with reactors with distinct configurations.

Apart from the information gleaned through ESR spectroscopy, however, much of the information collected thus far has relied primarily on the yields of tars, extracts, and chars measured during particular experiments. The approach has proved simple but effective. For instance, comparing char yields has made it possible to observe that the pyrolysis chemistry of pure (prepared) lignins follows entirely different reaction pathways from naturally occurring lignin, embedded in the composite matrices of naturally occurring lignocellulosic biomass.

Section 4 of this review will seek to explore ways of broadening the investigation of thermal breakdown through characterizing liquid products from these processes.

4.1. Characterizing the Liquid Products of Thermal Breakdown

Relatively small proportions of tars/oils released during pyrolysis of coal and lignocellulosic biomass are amenable to analysis by GC or GC-MS. The rest are higher boiling range, complex mixtures with broad ranges of molecular masses and structural features. In such mixtures, it is rarely useful to attempt to identify or isolate individual chemical species. Instead, it is more informative to characterize distillation cuts or sample fractions separated using some of the methods mentioned below and described in several recent reviews.[62,135,204,205]

Analytical tools available for characterizing fractions boiling above the GC or GC-MS range provide information that is a good deal less detailed and precise. Moreover, no single analytical technique in the toolkit is able to offer unambiguous, definitive information on molecular mass distributions of sample liquids or is able to provide clear structural information on its own. Recent advances in heavy hydrocarbon characterization have required collating and comparing evidence from several independent analytical methods.[62,135,205,206]

In what follows, section 4.2 will describe the manner in which some of the more familiar analytical methods have been adapted for examining the evolution of thermal breakdown processes. Section 4.3 will evaluate the constraints on the depth and scope of these characterizations in terms of the limitations of available analytical methods. More recent developments in estimating molecular mass distributions and exploring structural features of heavy hydrocarbon liquids will be outlined in section 4.4 followed by a brief review of potential growth areas in this type of analytical work (section 4.5).

4.2. Tracking Thermal Breakdown: Testing Some Well-Known Methods to Their Limits

This section outlines how examining liquid product structures and compositions with some of the more familiar analytical techniques has helped explore aspects of thermochemical reaction mechanisms. The capabilities and limitations of these techniques will be assessed by comparing with the information needed for studying thermal breakdown processes more closely.

4.2.1. Comparing Structures of Sequentially Extracted Fractions during Coal Liquefaction. The configuration of the flowing-solvent liquefaction reactor (section 2.4.2) enables dissolved coal products to be continuously removed from the reaction zone. The effluent product stream is rapidly quenched to suppress extraparticle secondary reactions of liquefaction products. Clearly, this product stream may be collected either as a total product mix (mixed cup) or as a time series of sequentially extracted fractions released by the sample. In the latter case, the product "cuts" can easily be related to consecutive intervals of the time−temperature ramp as well as to intervals during steady holding at the peak experimental temperature within the reactor.[54] The sequential product collection method allows examining the time−temperature resolved structures of successive coal extract cuts. The behavior of Point of Ayr and Linby coals (Table 4) was examined using tetralin and quinoline.[54,55] The discussion below summarizes findings from the extraction of Point of Ayr coal in tetralin.

4.2.1.1. Characterizing Successive Extract Fractions by SEC. Development of SEC for characterizing heavy hydrocarbon liquids has been described in several papers[207−210] and discussed in depth in a recent review.[135] Figure 19 presents

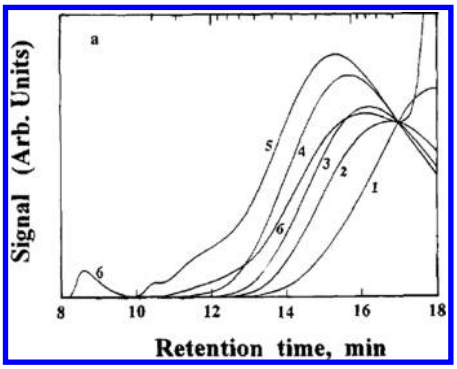

Figure 19. SEC-derived molecular mass distributions (UV detector) of Point of Ayr coal tetralin solubilization total fraction products. Heating at 5 °C s^{-1} to 450 °C, 400 s holding at peak temperature: (1) fraction 1 (0−70 s); (2) fraction 2 (70−80 s); (3) fraction 3 (80−90 s); (4) fraction 4 (90−100 s); (5) fraction 5 (100−140 s); (6) fraction 6 (140−190 s). (Reproduced with permission from ref 54. Copyright 1994 American Chemical Society.)

SEC chromatograms of successive extract fractions collected during liquefaction in tetralin of a sample of Point of Ayr (U.K.) coal. The data show a clear trend toward progressively shorter elution times (greater molecular masses) with increasing temperature and, once peak temperature is reached, increasing time at temperature.

In terms of thermal breakdown reactions, the steady broadening of molecular mass distributions with increasing intensity of the liquefaction process is consistent with observations made in section 2.1. As conditions (temperature, time at temperature) intensify, greater numbers of covalent bonds are cleaved, releasing larger molecules from the reacting solid matrix.

When analyzing liquefaction products prepared under laboratory conditions it is desirable to distinguish between coal-derived products and those from the chemical reactions (polymerization, adduction) of the vehicle solvent. In SEC,

dx.doi.org/10.1021/cr400194p | Chem. Rev. 2014, 114, 1547−1607

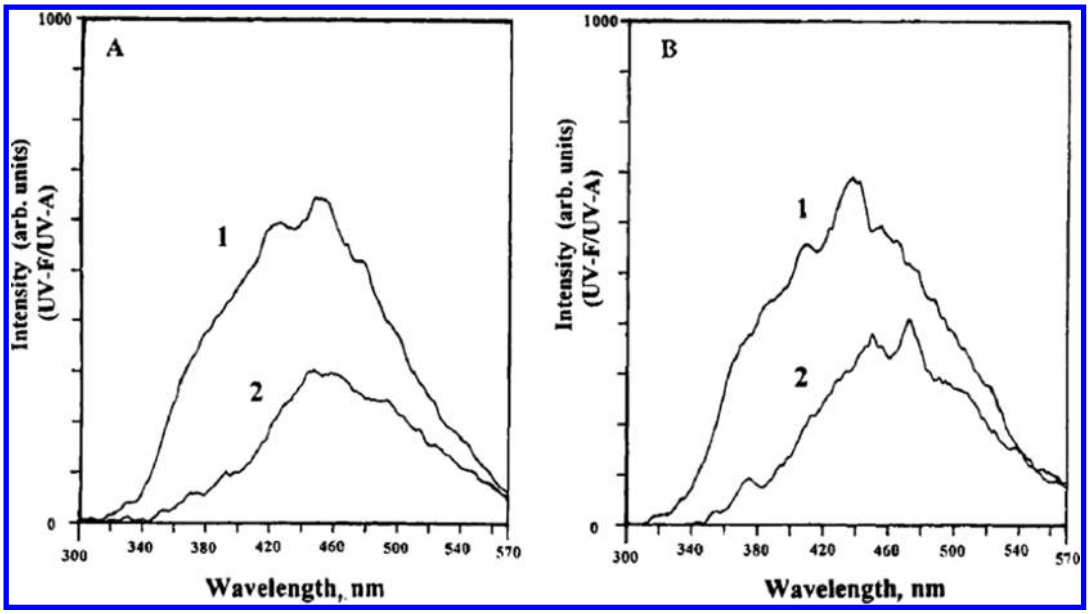

Figure 20. Online emission spectra, with excitation at 254 nm, of two successive SEC elution time cuts from (a) fraction 2 and (b) fraction 3 prepared in tetralin. In each case, trace 1 corresponds to the 16.8−17.0 min cut and trace 2 to the 15.3−15.5 min cut. (Reproduced with permission from ref 54. Copyright 1994 American Chemical Society.)

tetralin-derived products appear at longer elution times and may be blanked out, enabling a comparison of the larger molecular mass fractions of the extracts.

4.2.1.2. UV-Fluorescence Spectroscopy of the Fractions. Product fractions from these experiments were examined by UV-fluorescence spectroscopy.[135] The technique is not without its difficulties, as the spectra do not allow precise interpretations in terms of the occurrence of individual structural features. This is because of overlaps between characteristic emission bands of distinct molecular structures. UV-fluorescence spectra tend to shift to longer wavelengths with increasing sizes of conjugated aromatic ring systems and present lower fluorescence intensities. The method is useful, therefore, in *comparing* complex sample mixtures. Furthermore, correlations have been reported between the positions of spectral peaks and average molecular masses of coal tar pitch fractions,[211] suggesting that for pitch-like materials increasing molecular masses suggest the presence of increasing ring system sizes. These findings were found useful in interpreting the UV-fluorescence spectra of tars from a rank-ordered set of coal samples, pyrolyzed in a wire-mesh reactor.[212] An attempt at correlating peak wavelengths with NMR-derived average numbers of fused rings in PNA ring systems will be presented in Table 20.

Figure 20 shows online emission spectra (excited at 254 nm) of two successive SEC elution time cuts (15.3−15.5 and 16.8−17.0 min) from product fractions 2 and 3 (cf. Table 14) collected during liquefaction in tetralin.[54] In these figures, the intensity (y axis) is the ratio of the emission intensity for excitation at 254 nm to the average unit *absorbance* of the fluid element as a whole, simultaneously determined by the UV-absorption detector of the SEC system. The latter detector was also set at 254 nm. This method of plotting the data serves to eliminate the effect of changing solute concentrations as a function of retention time on UV-fluorescence emission intensities.[54]

When plotted in this way, the emission intensities tend to track changes in the quantum yields of the samples. The procedure has the advantage of comparing structural features of

Table 14. Temperature Intervals Corresponding to Time-Resolved Product Fractions[a]

fraction no.	time interval (s)	temp interval (°C)
1	0−70	ambient−350
2	70−80	350−400
3	80−90	400−450
4	90−100	450
5	100−140	450
6	140−190	450
7	190−490	450
8	490−	450−ambient

[a]Samples were heated at 5 °C s^{-1} to 450 °C and held for 400 s interval; a tetralin flow of 0.9 mL s^{-1} was maintained at 70 bar.[54]

different molecular mass (i.e., different SEC retention time) fractions of the same sample.[54] As explained in the original publication, this procedure has the additional advantage of avoiding interference from dimers and related adducts originating from reactions of the vehicle tetralin. The data showed smaller quantum yields for increasingly larger molecular mass material as well as shifts in the maxima to longer wavelengths with decreasing retention time (i.e., increasing molecular masses). Qualitatively similar results have been obtained with an analogous set of extracts prepared in quinoline.[54]

The observations that with increasing molecular mass (i) quantum yields decreased and (ii) spectral maxima shifted to longer wavelengths point to the increasing incidence of larger PNA ring systems with increasing molecular mass. Thus, successive stages of the extraction were characterized by progressively larger PNA ring systems and increasingly larger molecular masses as reaction intensities and extents of reaction increased.[54]

It appears, meanwhile, that thermal breakdown and extraction during the liquefaction process did *not* take place in the manner of peeling successive layers of an onion. After about 85% extraction, the coal particle size distribution

dx.doi.org/10.1021/cr400194p | *Chem. Rev.* 2014, 114, 1547−1607

remained more or less unchanged. However, particle densities had clearly altered with particles revealing distributions of cavities when split open.[213]

4.2.1.3. FT-IR Spectroscopy. FT-IR spectra of sequential fractions prepared in tetralin were acquired using KBr discs and compared to that of the original coal (not shown). As the extraction process advanced, concentrations of aliphatic and aromatic hydrogen and carbonyl/carboxyl groups in the extracts were found to have increased while the occurrence of alkyl−alkyl and alkyl−aryl ether bonds progressively declined. These findings are consistent with the expectation of splitting alkyl and ether bridges within the coal structure during the early stages of the liquefaction process, probably below or near 350 °C. In addition, decreasing extents of aromatic substitution and increasing polarity of products could be inferred from the data, as the temperature and extents of reaction increased.

4.2.1.4. Summary. Using detection by both UV-fluorescence and UV-absorption on SEC column effluent fractions proved useful. Successive extract fractions released from Point of Ayr coal in both tetralin and quinoline showed broadening molecular mass distributions with increasing intensity of reaction conditions, i.e., with increasing temperature and time. Overall, the thermal breakdown process in the presence of both tetralin and quinoline tended to release progressively larger and more aromatic molecular fragments into the liquid phase as a function of increasing temperature and time at temperature. Data from FT-IR spectroscopy helped to confirm what was already known about splitting alkyl and ether bridges within the coal structure during the early stages of the thermal breakdown process. The findings suggest that fractions released from coal during the early stages of the liquefaction process might require less severe catalytic hydroprocessing. Similar observations were made in the course of a parallel study of another middle-rank U.K. coal (Linby).[55]

Some of the problems encountered during this particular study were instrumental in shedding light on the solubility limitations of the solvent tetrahydrofuran and the upper mass limits detectable by UV-fluorescence spectroscopy

4.2.1.5. Limits of Solvent Power: Using Tetrahydrofuran as Eluent. Tetrahydrofuran (THF) has been the solvent and eluent of choice in much early work on characterization of complex liquids by size exclusion chromatography.[214−216] During routine use, the guard column of an SEC system operated with THF as eluent was observed to give increasingly large pressure drops.[217] The guard column was flushed through with the stronger solvent NMP (1-methyl-2-pyrrolydinone), producing a dark brown liquid. After flushing with NMP, the pressure drop across the guard column was reduced to levels observed for a new (unused) column. When the washings dissolved in NMP were characterized in an SEC system using NMP as eluent, intense signal was encountered at very short elution times, suggesting the presence of high-mass materials. Examination of these washings by UV-fluorescence showed a low-intensity signal at long wavelengths. The low fluorescence of these heavily colored washings indicated the presence of large polynuclear aromatic ring systems.

A wider range of observations relating to the insufficient solvent power of THF and evidence for adsorptive interactions between analyte molecules and column packing have been presented in a recent review.[135] On this evidence, when examining some of the heavier samples (e.g., pitch), THF is unable to break up interactions between analyte and column packing; furthermore, its solvent power seems low, allowing partial loss of sample through precipitation within the SEC column.

These difficulties are compounded by the reactivity of pure THF, which tends to polymerize on contact with air during storage. Polymerization products contaminate the solvent. Furthermore, they represent a safety hazard due to their potentially explosive character. This is normally countered by mixing proprietary polymeric additives in with the THF to block polymerization reactions during storage. No information is normally given regarding the composition of these additives. During analytic runs, there is therefore little chance of distinguishing between SEC signal from the stabilizer and heavier parts of the sample. The case for abandoning the use of THF as a solvent and as an eluent in the SEC and other general characterization work was compelling. Even so, occasional use of THF is being encountered in relatively recent analytical work.[218−221]

In the SEC of coal-derived materials the issue can be simply resolved by changing the eluent to NMP. It appears to completely dissolve most coal-derived samples including coal tar pitches. However, NMP is not a good solvent for aliphatic materials and only partially dissolves petroleum-derived heavy fractions: not more than about 50% of some petroleum asphaltenes dissolve in NMP.[135] In work done to address the problem, mixtures of NMP and chloroform in proportions of 5:1 or 6:1 have been found to completely dissolve both petroleum- and coal-derived heavy fractions.[208,210]

4.2.1.6. High-Mass Limits of UV-Fluorescence Spectrometry. UV-fluorescence and UV-absorption spectrometry have been compared as detection methods for size exclusion chromatography (SEC).[54,55] Original studies were associated with characterizing products from the sequential liquefaction experiments, as outlined above. Comparing the signal from the two methods showed that the presence of material eluting at relatively short retention times (higher mass material) clearly observed by UV-absorption could *not* be observed by the UV-fluorescence detector placed in tandem. At longer elution times, signals from the two detectors were similar.

The initial observations were made using THF as eluent. Several further attempts were made using 1-methyl-2-pyrrolidinone (NMP) as eluent to test high-mass detection ability by UV-fluorescence spectrometry. The responses from UV-absorption and UV-fluorescence detectors were compared at equal retention times using the same SEC system.[227,222,223] The samples examined included asphaltenes from heavy petroleum residues and three fractions of a coal tar pitch obtained by solvent solubility separation.

Figure 21 shows that only the chromatogram of the lightest fraction of the coal tar pitch (acetone-soluble fraction) gave close agreement between the two detection systems. In examining the heavier (acetone-insoluble−pyridine-soluble and pyridine-insoluble) fractions of the pitch, the UV-absorption detector showed an *early eluting* peak that corresponded to material excluded from column porosity in addition to a retained peak. However, the UV-fluorescence detector showed little sensitivity to material eluting under the excluded peak and clearly observed by the UV-absorption detector. Thus, the UV-fluorescence detector proved less effective than UV-absorption in detecting the material eluting at the shorter elution time edge of the retained peak. It only responded to material eluting at fairly long times. Comparing the signal from the two instruments by means of a calibration using polystyrene (PS) and polymethylmethacrylate (PMMA)

dx.doi.org/10.1021/cr400194p | *Chem. Rev.* 2014, 114, 1547−1607

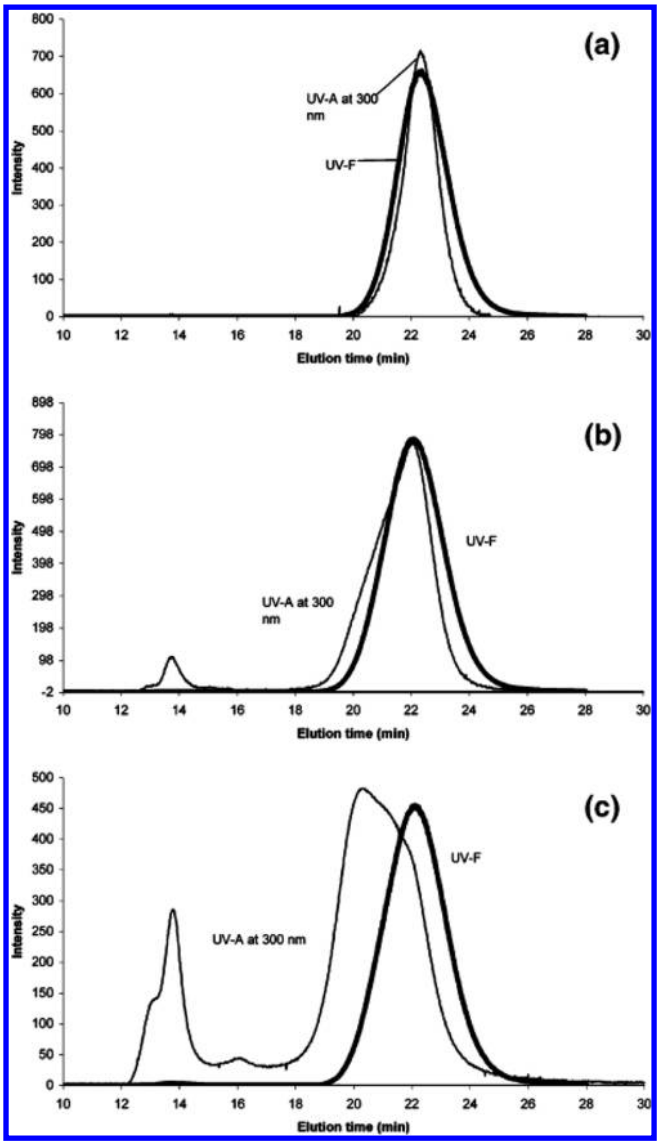

Figure 21. Size exclusion chromatography (SEC) chromatograms with simultaneous detection by UV-A at 300 nm and UV-F of (a) acetone solubles of pitch, (b) acetone-insoluble–pyridine-soluble fraction of the pitch, and (c) pyridine insolubles of a coal tar pitch. Mixed A SEC column with NMP eluent. (Reproduced with permission from ref 227. Copyright 2005 American Chemical Society.)

molecular mass standards, detection by UV-fluorescence seemed particularly ineffective for molecular masses much above 2500 u.[135,227]

These data clearly show that highly aromatic molecules in coal-, biomass-, and petroleum-derived materials with masses much greater than ~2500 u (as determined by SEC and LD-MS) do not fluoresce.[135,227,224,225] Reports based on fluorescence depolarization methods have correctly reported not being able to observe masses greater than ~2500 u.[226] To the extent that these materials could not be detected by fluorescence-based methods, the reported observations highlight the high-mass limits of the technique.

4.2.2. Products of Thermal Breakdown: Need to Fractionate. This subsection focuses on highlighting the necessity for fractionation in order to study samples of high-mass complex hydrocarbon mixtures in greater detail.

Testing the capabilities of analytical techniques used for tracking the course of thermal breakdown reactions required the use of a standard sample for comparing results across instruments over a relatively long time. Coal tar pitch is the >450 °C boiling distillation residue from coal tars collected during the coke-making process. The particular pitch sample mentioned in this section was chosen as a laboratory standard at Imperial College London due to its chemical stability and availability as a large homogeneous sample. It has been studied extensively[227−235] and the work reviewed.[62,135,205,206]

Figure 22 presents size exclusion chromatograms of the whole coal tar pitch and of its solubility fractions, separated as

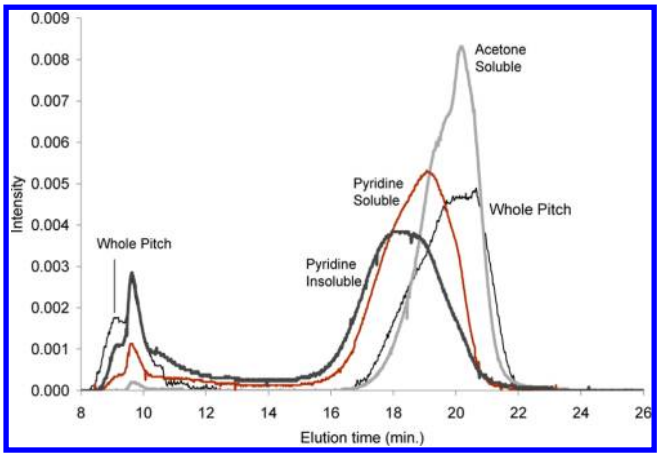

Figure 22. Area-normalized SEC chromatograms of the whole pitch[237] and its acetone-soluble, acetone-insoluble–pyridine-soluble, and pyridine-insoluble fractions.[205] Mixed D column, NMP as eluent, detection by UV absorption at 300 nm. Molecular size (mass) decreases with increasing elution time. (Reproduced with permission from refs 205and 237. Copyright 2007 and 2004 American Chemical Society (for the pitch fractions) and Elsevier (for the whole pitch), respectively.)

(i) acetone solubles, (ii) the pyridine-soluble part of the acetone insolubles, and (iii) the pyridine-insoluble fraction of the pitch. SEC chromatograms of the three solubility fractions were found to shift toward higher masses (shorter elution times) in the order from acetone solubles to pyridine insolubles (Figure 22).[207,227,229,236] According to the PS-PMMA calibrations of the SEC column, the acetone-soluble fraction contained masses up to ~800 u, the acetone-insoluble–pyridine-soluble fraction to at least 2500 u and the pyridine insolubles to at least 5000 u.[207,227,229] It was also found that the retained portion (i.e., later eluting peak) of the SEC chromatogram of the whole pitch showed signal in the same elution time interval as the chromatogram of the more abundant acetone-soluble fraction. The mass balance of the solvent separation of the pitch was PAS 46 wt %, PPS 24%, and PPI 30 wt %.[229]

This example illustrates how seeking to characterize in a single analytical step the whole of a widely polydispersed sample tends to show mostly the properties of the more abundant material within the sample mixture or, indeed, the fraction that is more amenable to analysis by the particular technique. Fractionation tends to side step these difficulties by preventing the more abundant materials from masking signal from the rest of the sample. Characterization of such fractions in isolation tends to lend access to more detailed information about structural features and molecular mass distributions of

dx.doi.org/10.1021/cr400194p | Chem. Rev. 2014, 114, 1547−1607

complex samples.[135] Useful methods of fractionation include separation by solvent solubility,[238] planar[224,239−241] and column[225,238,242] chromatography, preparative size exclusion chromatography (SEC),[235,277] and, less commonly, ultrafiltration.[231,62,135] Selection of fractionation methods depends on numerous factors. These methods have been compared and discussed in detail in a recent review published in this journal.[135]

Figure 23 shows that the whole pitch sample gave a UV-fluorescence spectrum that was nearly identical to that of the

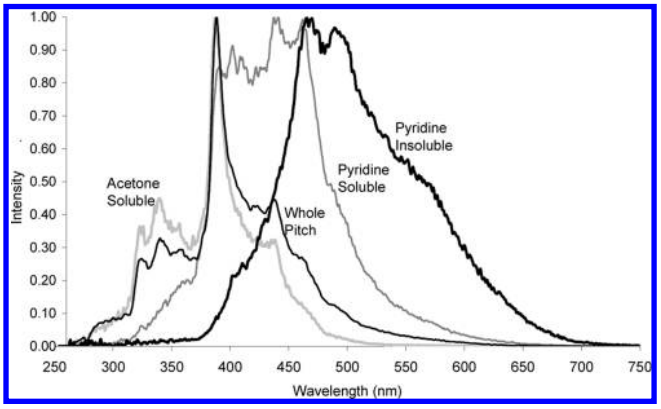

Figure 23. Peak-normalized synchronous mode UV-F spectra of the whole pitch, and its acetone-soluble, acetone-insoluble−pyridine-soluble, and pyridine-insoluble fractions in NMP solvent.[135,234] (Reproduced with permission from ref 234. Copyright 2005 John Wiley & Sons, Ltd.)

acetone-soluble fraction. Once again, these spectra show how the higher mass acetone-insoluble and pyridine-insoluble fractions are masked by the more abundant acetone-soluble fraction. The masking effect of the more abundant fraction in the whole sample was more obvious in the UV-fluorescence spectra of the pitch and its fractions compared to the SEC data in Figure 22.[135,229] These data collectively provide a powerful argument for the necessity of fractionation prior to the characterization of complex samples. Similar problems are encountered when petroleum-derived samples are characterized by UV-fluorescence spectroscopy. For example, nearly one-half the asphaltene sample extracted from a Maya (Mexican) crude oil was found not to contribute discernible signal to the UV-fluorescence spectrum of the bulk asphaltene sample.[243] Once fractionated, the peaks of the UV-fluorescence spectra were clearly observed to red shift toward longer wavelengths (bathochromic shifts) with diminishing ease of solubility of the fractions, ranging from acetone solubles to pyridine insolubles.

There is considerable agreement in the literature that increasing sizes of aromatic chromophores lead to shifts of UV-absorbance and UV-fluorescence spectra to longer wavelengths.[244−247] As already signaled, Zander and Haenel correlated bathochromic shifts in spectral peaks with increasing average molecular masses of pitch fractions.[211]

4.2.2.1. Analysis of Pitch Fractions by Mass Spectrometry. Figure 24 presents LD-MS spectra from the same solubility fractions described above. As discussed in detail below (section 4.3), the results from LD-MS can change depending on the instrument operating parameters. Nevertheless, molecular mass distributions obtained for pitch fractions by MALDI-MS and LD-MS consistently showed shifts toward broader mass

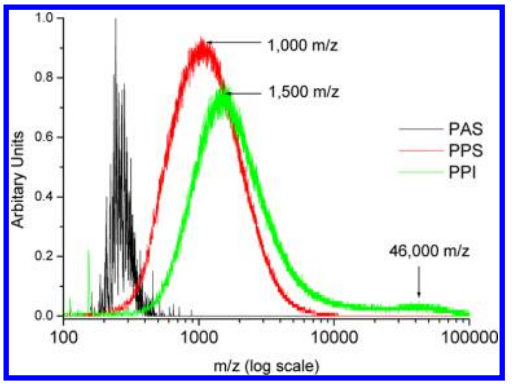

Figure 24. Laser desorption mass spectra from the pitch solubility fractions using a laser power of 10% of maximum and a high-mass accelerator voltage of 10 kV for the acetone-soluble fraction of the pitch (black) and 30% (8 kV) for the acetone-insoluble−pyridine-soluble (red) and pyridine-insoluble (green) fractions of the pitch (previously unpublished).

distributions with diminishing solubility from acetone solubles through to pyridine insolubles.[135] This is consistent with results from SEC shown above.

Pyrolysis-GC-MS has also been used to probe the structural properties of the pitch solubility fractions. In this instance, the pitch was separated by sequentially dissolving in heptane and toluene.[228] In these tests, fractions from separation by planar chromatography[224] have been used as well as those separated by solvent solubility. Planar chromatography was used to produce (i) acetonitrile mobile, (ii) acetonitrile-immobile−pyridine-mobile, and (iii) pyridine-immobile−NMP-mobile fractions.[224]

Only the lightest fractions of the pitch separated by either method (i.e., toluene solubles and acetonitrile mobiles[62,135,224]) gave significant amounts of detectable compounds in pyrolysis-GC-MS. These two lighter fractions showed similar distributions of aromatic and alkylaromatic compounds by pyrolysis-GC-MS, as indeed they had done by GC-MS analysis. Compounds identified by the two techniques ranged from benzene to methylbenzofluoranthene (m/z 266).[224,228]

The GC-MS total ion chromatograms for the pitch solubility fractions produced using heptane and toluene are shown in Figure 25.[228] In pyrolysis-GC-MS, the two heaviest fractions, i.e., the pyridine-mobile and NMP-mobile fractions from planar chromatography, both gave sparse signal from mostly alkene and alkane fragments with some low-intensity signal for PNA compounds. Likewise, only low-intensity signal was observed from the heptane-insoluble/toluene-soluble fraction. No signal other than a trace of toluene left over from the separation was observed in the toluene-insoluble fraction. These results show the difficulty of fragmenting the large PNA ring systems present in the heavier fractions during the pyrolysis step of the pyrolysis-GC-MS procedure. Taken together with data from size exclusion chromatography (UV-absorption detection) and static mode synchronous UV-fluorescence spectroscopy, these observations strongly suggest the presence of large, polynuclear aromatic ring systems with molecular masses well above 500 u within the heavier pitch fractions.[224,228,248]

Additional structural information was clearly needed, however, to get a little further forward in evaluating changes in the structural features of the set of samples.

4.2.2.2. NMR Characterization of the Pitch Fractions. Solution-state ^{1}H and ^{13}C NMR as well as solid-state ^{13}C NMR

dx.doi.org/10.1021/cr400194p | Chem. Rev. 2014, 114, 1547−1607

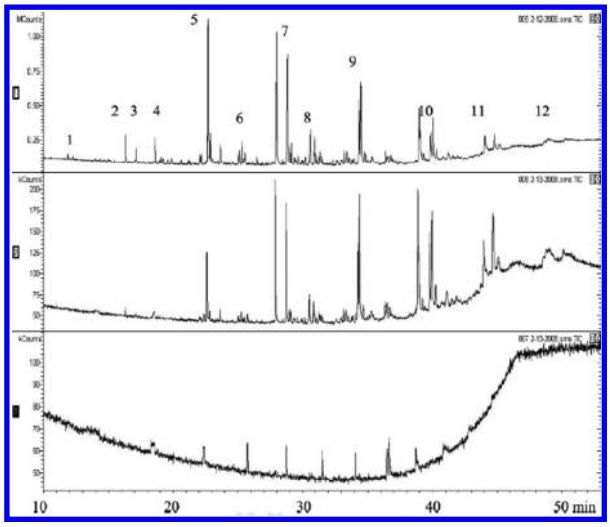

Figure 25. GC-MS chromatograms of PHS, heptane-soluble (top), PTS, toluene-soluble (middle), and PTI, toluene-insoluble (bottom) fractions. Peak identities and masses (m/z) are (1) methyl naphthalenes (142), (2) acenaphthene (154), (3) dibenzofuran (168), (4) fluorene (166), (5) phenanthrene and anthracene (178), (6) methylphenanthrenes (192) and cyclopentenophenanthrene (190), (7) fluoranthene and pyrene (202), (8) methylpyrene isomers (216), (9) chrysene isomers (228), (10) benzopyrene isomers (252), (11) benzo[*ghi*]perylene isomers (276), (12) dibenzopyrene isomers (302). (Reproduced with permission from ref 228. Copyright 2009 John Wiley & Sons, Ltd.)

methods have been used to examine the fractions of coal tar pitch separated by solvent solubility,[229] as well as fractions from planar[224] and column chromatographic separations.[225] For solution-state analysis, deuterated pyridine and NMP (pyridine-d_5 and NMP-d_9) were used as NMR solvents.[224,229]

In trying to obtain quantitative structural information, solid-state ^{13}C NMR spectra were acquired using single-pulse excitation (SPE) spectra,[225,229] alongside ^{13}C-CPMAS TOSS and NQS TOSS spectra.[224,225,229] Results from the SPE runs are summarized in Table 15 for the whole-pitch and column

Table 15. Solid-State ^{13}C NMR (75 MHz) Data for Pitch and Column Chromatography Fractions and SPE Spectra Smoothed at 5 and 100 Hz and Quantified Against TTMS[a]

sample	aliphatic/aromatic	%C detected[b]	aromaticity
whole pitch	0.040−0.043	43−46	96
acetonitrile mobile	0.072−0.084	60−91	92−93
pyridine mobile	0.080−0.086	47−50	92−93
NMP mobile	0.036−0.043	92	70−73

[a]Reproduced with permission from ref 225. Copyright 2003 Elsevier. [b] %C refers to the amount of carbon detected in the sample by NMR relative to amount of carbon in the sample as determined by ultimate analysis.

chromatography fractions from sequential use of acetonitrile, pyridine, and NMP.[225] SPE results from a separate study are shown in Table 16 for the whole pitch and its (i) acetone-soluble (PAS), (ii) acetone-insoluble−pyridine-soluble (PPS), and (iii) pyridine-insoluble (PPI) fractions.[229]

These results show some of the difficulties encountered in attempting to extract quantitative structural information from this set of complex samples, even when using such a powerful technique. First, significant proportions of the carbons present

Table 16. Solid-State ^{13}C NMR (75 MHz) Data for Pitch and Solubility Fraction and SPE Spectra Smoothed at 100 Hz and Quantified Against TTMS (relative standard deviation > ±10%)[229]

sample	aliphatic/aromatic	%C detected[a]	aromaticity
pitch	0.025	44	97
PAS	0.051	71	95
PPS	0.038	46	96
PPI	0.032	73	97

[a]%C refers to the amount of carbon detected in the sample by NMR relative to amount of carbon in the sample as determined by ultimate analysis.

could not be observed, either due to the long relaxation times required for quaternary aromatic carbon atoms imbedded in large molecules or due to the presence of paramagnetic sites.[224,225,229] Furthermore, the aliphatic peak areas of the spectra (not shown) overlapped with spinning side bands in the spectra for (i) the whole pitch, (ii) the pyridine-soluble-acetone-insoluble, and (iii) the pyridine-insoluble fractions to a much greater extent compared to the acetone-soluble fraction of the pitch.[229] Significant scatter was observed between 3 repeat analyses, where the relative standard deviation was > ±10% for all samples. Experimental scatter was lowest for the acetone-soluble fraction.[229]

The size (area) of the spinning side bands can in fact be reduced by working at lower field strengths. At 25 MHz, they amount to about 7% of the aromatic peak area.[249] However, using lower field strengths reduces the resolution of the spectra. In examining the various pitch fractions, the resolution was found to be insufficient to make a detailed analysis based on chemical shift classifications.[135,230] Due to this limitation, the differences observed between the samples by CPMASTOSS and NQSTOSS could not be used to make reliable estimates of structural parameters.[229]

It may be noted that a common assumption used to obtain detailed information on aromatic structures is that all molecules are fully pericondensed as suggested by Solum et al.[250] In the case of pitch-derived samples, however, this was unlikely to be an appropriate premise.[230,251] Overall, solid-state ^{13}C NMR could not be used reliably to discern the relatively small changes in aromaticity between different pitch fractions, which were being sought.

Solution-state ^{1}H and ^{13}C NMR spectra did not contribute to our understanding of structural differences between the set of pitch-derived samples. As NMP does not interfere with signal in the aromatic part of the spectrum, it was used as NMR solvent to examine the aromatic parts of the spectra. In separate experiments, pyridine, which is purely aromatic, was used as solvent for examining the aliphatic part of the spectra. However the results were poor, in part, due to the presence of unknown contaminants in the solvent (used as received), compounded by less than total sample solubility in pyridine.[224,225,229]

4.2.2.3. FT-IR Spectroscopy of the Pitch Fractions. Reviews of the instrumentation and tables of correspondences between IR frequencies and structures in carbonaceous materials are widely available.[96−98,252−258]

The coal tar pitch and its fractions separated by solvent solubility and column chromatography were examined by three infrared (IR) methods: (i) absorption using KBr disks,[62] (ii) attenuated total reflection (ATR) with a diamond cell,[62] and (iii) diffuse reflectance with a diamond cell.[229] Of the three

dx.doi.org/10.1021/cr400194p | *Chem. Rev.* 2014, 114, 1547−1607

Table 17. Number-Average Molecular Mass (M_n) Estimates for Coal Tar Pitch Solubility Fractions from LD-MS,[234,235] PD-MS,[233] SEC UV-A,[227,228,232] and SEC UV-F[227]

technique	LD-MS				PD-MS	SEC Mixed A column				
detection mode	reflector	linear	linear HM[a]	linear HM[a]	n/a	UV-A			UV-F[d]	
M_n integration method[227]	1	1	1	2	1	1[b]	1[c]	2[c]	1	2
acetone-sol.	290	290	n/a	n/a		300	230	280	155	175
acetone-insol.− pyridine-sol.	430	930	1100	1600	725	400	320	610	175	235
pyridine-insol. fraction	900	1800	3000	12 800	620	570	360	870	175	240

[a]HM, refers to a high-mass method[234,235] where the LD-MS operating parameters were selected to improve detection of high-mass ions at the expense of lower mass ions. [b]Results obtained from a UV-A detector, 350 nm, using NMP as eluent. [c]Results obtained from a UV-A detector, 300 nm, using NMP as eluent. [d]Results obtained from a UV-F detector, excitation at 350 nm and emission at 450 nm, using NMP as eluent.

Table 18. Approximate High-Mass Limits Observed by Various Methods for a Coal Tar Pitch and Its Solubility Fractions (from acetone and pyridine or heptane and toluene solvent pairs)[a]

method	whole pitch	acetone sol. (heptane sol.)	acetone-insol.−pyridine-sol. (heptane-insol.−toluene sol.)	pyridine insol. (toluene insol.)	similar coal extract/tar[b]
GC-MS	~300[262]	(302)[228]	(302)[228 c]	no signal[248] (no signal)[228]	326[263−265]
HT-GC-MS	~350[229]	~350[229]	~350[229 c]	no signal[229]	400[266,267]
HPLC-ESI-MS		414[d]	*f*	*f*	400[268]
probe-MS	600[262]	<700[229]	<700[229]	no signal[229,248]	700[269]
LC-MS					900[263−265]
FT-ICR-ESI MS		(<400)[228]	(<900)[228]	*f*	1000[228,270,271]
field desorption MS					1000[265]
field ionization MS					1100[265]
fast atom bombardment					<2000[265,272]
^{252}Cf plasma desorption			<4000[233]	<4000[233]	<4000[233]
MALDI- or LD-MS	>5000[229]	>2500[229] (~2500)[228]	>4000[229] (~3000)[228]	>10 000[229] (~10 000)[228]	>10 000[231,273,274]
VPO				no signal[62]	<10 000[62,227,275,276]
SEC with NMP[e]	>250[207,229]	>800[207,229,233] (1100)[228]	>2500[207,229] (2700)[228]	>5000[207,229] (9300)[228]	~10 000[207,229,235]

[a]No signal refers to the sample containing no molecules within the range of the technique, i.e., it contains only larger molecules. [b]Similar coal extract/tar refers to coal liquefaction extracts or pyrolysis tar/oil products; these data were included to cover gaps in measurements on the coal tar pitch and its fractions. [c]Weak signal, probably trace of material from a lighter fraction due to incomplete separation. [d]Acetonitrile-soluble fraction of the coal tar pitch.[233] [e]SEC performed using a Mixed A column (Polymer laboratories, U.K.) with UV-A detection at 300 nm. [f]Sample not suitable for analysis by the technique (i.e., not soluble in the solvent required).

methods, diffuse reflectance gave the highest resolution for this set of samples; relatively poor resolution was found during absorption measurements using the KBr disk. Nevertheless, the observed results for the set of pitch-derived samples, from the three methods were internally consistent. As expected, close agreement was observed between spectra of the whole pitch and that of the acetone solubles, i.e., the more abundant fraction with a relatively narrow molecular mass range (not shown).

One definitive structural difference that could be observed by FT-IR between the fractions was the total absence of signal from out-of-plane bending vibrations of aromatic substituents (between 900 and 700 cm^{-1}) in the spectrum of the pyridine-insoluble fraction. Loss of these frequencies suggests there were few substituent groups, probably due to the presence of large fused PNA ring systems; any existing substituent groups would appear to be sterically hindered.[259−261] Loss of signal in this region was consistent with the presence of increasingly larger PNA fused-ring systems[259] in the order PAS < PPS < PPI. The evidence also showed a trend of decreasing relative concentrations of aromatic carbon−carbon bonds and of increasing aliphatic C−H bonds in the order PPI > PPS > PAS.

4.2.2.4. Overview of Results from Characterization of Coal Tar Pitch Fractions. Examples in this subsection were selected to show the necessity of adopting fractionation as a routine first step in characterizing complex liquids from thermal breakdown and indeed most complex liquid mixtures containing material above the GC and GC-MS range.

When characterized by SEC and LD-MS, the more soluble pitch fractions showed narrower molecular mass distributions and the less soluble fractions showed broader mass distributions. Increasing molecular mass ranges from about 400 to above 3000 u could be identified. However, in LD-MS, the numerical high-mass limits appeared to depend on selection of experimental parameters. Improvements to LD-MS and MALDI-MS allowing assignment of more reliable numerical mass ranges will be discussed in section 4.4.

Taken together, data from UV-absorption, UV-fluorescence, and FT-IR provided evidence pointing toward progressively larger sizes of PNA ring systems correlating with decreasing sample solubility and increasing molecular mass.

Samples from the heavier fractions obtained by solvent separation (heptane-insoluble−toluene-soluble and toluene-insoluble) and the less mobile fractions in planar chromatography (acetonitrile-immobile−pyridine-mobile and pyridine-

dx.doi.org/10.1021/cr400194p | Chem. Rev. 2014, 114, 1547−1607

immobile−NMP-mobile fractions) could not be fragmented by pyrolysis-GC-MS to give molecular material able to pass through the GC column. This observation is consistent with the predominance in the heavier fractions of large PNA ring systems, which do not fragment through thermal treatment.

Analysis of the set of samples by solid-state SPE ^{13}C NMR methods showed poor carbon sampling and interference from spinning side bands. Poor spectral resolution was observed in ^{1}H and ^{13}C NMR solution-state work, where NMP and pyridine were used as solvents. The latter difficulties were attributed to trace contaminants in the solvents and poor solubility of the heaviest sample in pyridine. NMR work afforded little further structural insight for important properties such as PNA ring system sizes or the proportion of alkyl and alicyclic content in the different environments provided by the range of samples.

The emerging picture was one where the order of increasing molecular masses identified by SEC and LD-MS (PAS < PPS < PPI) was closely matched by increasing sizes of PNA ring systems, but available tools do not allow sizes of PNA ring systems or proportions of alicyclic (hydroaromatic) carbon contents to be estimated reliably. Developments in NMR spectroscopy based work, partly addressing these gaps, will be discussed in section 4.4.

4.3. Molecular Masses and Structures of Complex Mixtures: Analytical Issues

In this section, we evaluate some of the constraints imposed on the scope of the characterization effort by the limitations of the analytical techniques that have been used.

4.3.1. Molecular Masses of Complex Mixtures: Taking Stock. The variability observed between estimates of average molecular masses and between high-mass limits of complex polydispersed liquids have been recently assessed.[135] Results appear to vary, both between and within particular techniques. Many of the estimates, furthermore, appear bounded by the upper mass limits of the instruments themselves, and do not reflect the properties of the samples being characterized.

Table 17 presents estimates of number-average molecular mass (M_n) for the coal tar pitch and its acetone/pyridine solubility fractions discussed in section 4.2.2. Table 18 presents the high-mass limits of a wider range of coal tar pitch-derived samples separated by acetone/pyridine or, in parentheses, heptane/toluene solubility.

We already touched upon the limitations of GC and GC-MS methods. As discussed in section 4.3.3, sample volatility issues appear to limit detection of high-mass materials in probe MS and soft ionization techniques such as FIMS (field ionization mass spectrometry) and FAB (fast atom bombardment).[135]

Better agreement has been found between LD-MS and SEC with NMP used as eluent. Compared to other techniques, these two have shown higher molecular mass distributions and higher upper mass limits.[207,228,231,274,235,241,277] As already signaled, however, numerical results from LD-MS are dependent on selection of instrumental parameters. Meanwhile, there is also strong evidence suggesting that both LD-MS and MALDI-MS suffer from selective sampling issues, which would tend to limit the observation of higher mass material.[62,135,205,206]

4.3.2. Use of SEC in Evaluating Thermal Breakdown Products.[62,135,173,205,278] The case studies in section 4.2 show that SEC can be a powerful tool for *comparing* molecular mass distributions of thermal breakdown products. SEC has also been applied to examine a range of samples from biomass pyrolysis tars/oils,[173] biomass hydropyrolysis tars/oils,[279] biomass-coal cogasification tars,[111] and essential oils (oxygenates).[280]

In terms of arriving at actual molecular mass estimates, it is first necessary to examine whether SEC column elution times are dependent on the chemical structures of the analytes. To this end, the elution behavior of several sets of molecular mass standards with entirely different chemical compositions have been matched against each other. The work was done using two columns packed with polystyrene/polydivinylbenzene copolymer (Polymer Laboratories, U.K.), labeled as Mixed A (10 μm particles) and Mixed D (5 μm particles).[207]

The calibration curves prepared using polystyrene (PS) and polymethylmethacrylate (PMMA) molecular mass standards were found to be statistically indistinguishable. A set of polysaccharides (PSAC) standards and other oxygenates eluted earlier than predicted by the PS/PMMA calibrations. To a first approximation, deviations between the PSAC and the PS-PMMA lines have been treated as an upper limit to errors arising from structure-dependent variations in this SEC system. Below 15 000 u (by PS-PMMA), molecular masses of oxygenated samples could be estimated to within a factor of 2−2.5. In the worst case, the estimate would lie between 6000 and 15 000 u. Other structural features than oxygenates gave rise to far smaller deviations.[207]

When the level of agreement between the PS/PMMA calibration of SEC and MALDI ass spectrometry was evaluated, good agreement was observed up to about m/z 3000 between SEC and MALDI[235] and LD-MS.[277] The techniques are independent, suggesting that up to this limit SEC may be safely considered as a quantitative tool. As observed with the calibration curves, the accuracy of the SEC measurement appears subject to greater uncertainty with increasing molecular mass.[207,277]

In later work, the eluent composition was changed from pure NMP to 6:1 and 5:1 v/v NMP−chloroform mixtures. The new eluent mixture appears capable of totally dissolving all the coal tar pitch fractions as well as petroleum asphaltenes, which only partially dissolve in pure NMP. This change significantly reduced the difference in elution times between the oxygenated PSAC standards and the PS-PMMA calibration.[208,210] The new eluent mixture has been applied to characterization of crude oils and crude-oil-derived fractions separated by a number of methods.[229]

In order to assess the capacity of SEC to estimate molecular masses, the reasons for the bimodal distributions observed for many of the samples need to be explored. There is agreement that while the second (longer elution time) peak of the distribution corresponds to signal from material resolved by column porosity, the early eluting peak corresponds to signal from material excluded by column porosity. For the present purposes, the discussion above appears sufficient to establish the utility of findings corresponding to the second, longer eluting peak of the distribution. However, at short elution times (i.e., in the excluded region) the PS-PMMA calibration appears to give extremely large molecular masses. For example, when pitch samples were examined by SEC, the PS-PMMA calibration indicated the presence of material which eluted very early (12−16 min in the excluded region) corresponding to mass values far above 100 000 u.

When this material was collected from the outlet of the SEC system (12−16 min) and examined by LD-MS,[277] the mass range showed a peak maximum at about 3000 m/z with signal

dx.doi.org/10.1021/cr400194p | Chem. Rev. 2014, 114, 1547−1607

tailing off toward 10 000 m/z or a little higher. Two clear observations could be made: (i) When determined by LD-MS, the mass distribution of this early eluting material extended to greater values than material eluting at 16−25 min in the retained region; so the trend was internally consistent. However, (ii) the molecular mass distribution found by LD-MS was far narrower than that predicted by the SEC PS-PMMA calibration.[135,205,207,231,277]

As outlined elsewhere[135,207] (and ref 62, cf. p 277), one likely explanation involves possible changes from 2-dimensional to 3-dimensional conformations of molecules above the mass threshold defined by the leading edge of the resolved (longer eluting) second peak. It was noted that a sample of mixed C60 and C70 fullerenes eluted near the exclusion limit of the column, which indicates >100 000 u.[207] In view of their known molecular masses of 720 and 840 u respectively, these materials behaved as the two major outliers with respect to all calibration curves described above.

Clearly, size exclusion chromatography depends on a broad correlation between molecular mass and molecular size. With diameters of ∼1 nm, the shapes of the fullerenes make them the only species in the range of compounds tested, with as great a discrepancy between molecular mass and molecular size. When a set of colloidal silica samples (Nissan Chemical Industries Ltd., Houston, TX) of diameters 22, 12, and 9 nm were used to test the relationship between actual particle diameters and elution time they displayed on the same calibration line as the fullerene samples and a set of soot samples.[207] This particle-indexed calibration line was quite independent of particle density or molecular mass but directly related to physical size. Furthermore, it was quite distinct from the PS-PMMA calibration line. It showed the direct relationship between elution times and the sizes of fully 3-dimensional objects in these SEC columns.

On their own these findings do not constitute proof that the material showing signal under the excluded peak of SEC chromatograms necessarily corresponds to 3-dimensional conformations of larger mass molecules. However, the argument seems worth pursuing in future work. Another possible explanation for differences between SEC and LD-MS mass estimates for the material appearing in the excluded zone is that the mass limit for laser desorption of larger mass molecules may have been reached. The issue has been discussed elsewhere without reaching a definite conclusion.[135]

As an aside, the proposition that fuel-derived high-mass materials are composed of aggregates has been examined in a recent review[135] and will not be discussed here other than to note the absence of evidence for aggregation at the dilution levels used in SEC analyses. Certainly, repeated dilutions of the samples have produced no changes in elution behavior. Meanwhile, Wiehe[281] pointed out that resid asphaltenes do not volatilize out of cokers operated at about 500 °C or distill over during distillation, as would be expected if these fractions consisted of aggregates of smaller molecular species.

4.3.3. Use of LD-MS and MALDI-MS in Assessing Thermal Breakdown Products. As already signaled, high-mass limits reported by many mass-spectrometric techniques tend to reflect the detection limits of the instruments rather than indicate the characteristics of the samples. Table 19 presents the high-mass limits observed by various mass spectrometric methods during examination of products from thermal breakdown of coal and biomass pyrolysis and gasification tars, pitches, as well as petroleum-derived fractions including petroleum asphaltenes (refs 62, 135, 205, 206, 224, 225, 228−231, 233, 235, 241, and 243).

Table 19. Approximate High-Mass Limits of Various Mass Spectrometric Methods

technique	highest mass detected
heated probe-MS methods	<700 m/z
field desorption MS (FDMS)	<1000 m/z
field ionization MS (FIMS)	<1200 m/z
Fourier-transform ion cyclotron resonance MS (FT-ICR-MS)	<1500 m/z
fast atom bombardment (FAB)	<4000 m/z
^{252}Cf plasma desorption MS	<4000 m/z
MALDI-MS and LD-MS	≥10 000 m/z

The very high mass resolution of Fourier transform ion cyclotron resonance MS (FT-ICR-MS) has proved useful for deducing structural information for aromatic and heteroaromatic compounds in coal- and biomass-derived oil/tars up to $m/z \approx 1200$.[135,228,282,283] As discussed earlier, however, this instrument has not been found capable of providing information regarding average mass values or mass distributions due to selective sampling and solubility issues.[135,206,228] There appears to be a disjuncture between solvents compatible with ICR-MS (typically acetonitrile/methanol/toluene) and analysis of heavier coal- and biomass -derived fractions, which cannot be dissolved (and therefore cannot be analyzed) in these particular solvents.

The results summarized in Table 19 reflect the already stated observation that MALDI-MS and LD-MS give the highest mass estimates among available mass spectrometric techniques. The two techniques differ by addition of matrix to the sample in MALDI-MS to facilitate absorption of energy from the laser and its dispersion within the sample. While the procedure assists in acquiring more intense signal, MALDI-MS spectra are complicated by signal from matrix ions. As previously outlined, significant levels of agreement have been found between these two closely related techniques and size exclusion chromatography.[135,217,235,273,274,277,284−286] While the stated caveats about either technique cannot be ignored, the fact that SEC and LD-MS (and MALDI-MS) operate on distinct and independent principles provides a level of confidence in the broad agreement observed between the two techniques.

Another problem involving laser-desorption-based techniques is incomplete sampling due to the polydispersity of the sample and the structural variations within it. Different chemical structures in complex mixtures actually require different operating conditions for detection by LD-MS.[135,251] For instance, small aromatic molecules can be observed using low laser power levels, whereas larger, more complex molecules require greater laser power in order to desorb. There are also issues associated with molecular fragmentation under high laser powers required for observing other, usually larger, molecular species.[243,251] These factors tend to limit the structural and/or molecular mass ranges detected by the instrument during a single analytical run.

Formation of multimer and cluster ions through gas-phase reactions in the LD-MS sampling zone poses a contrasting challenge, probably giving rise to the artificial broadening of observed molecular mass distributions. The effect appears due to excessive gas-phase concentrations of sample molecules collecting in the sampling zone by a combination of "too much"

dx.doi.org/10.1021/cr400194p | Chem. Rev. 2014, 114, 1547−1607

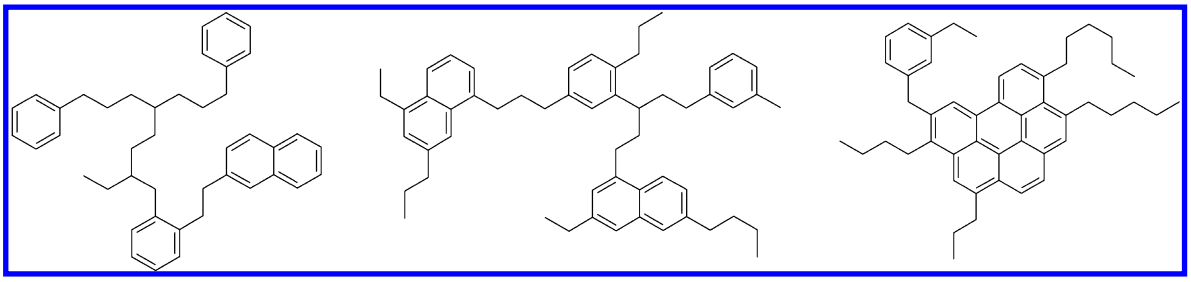

Figure 26. Pictorial examples of island-like (left), Archipelago-like (middle), and continental-like (right) structures.[251]

sample loaded onto the target, the polydispersity of the sample, and application of too much laser power.

When analyzing a polydispersed sample, the laser power required to observe the highest mass molecules can be high and lead to an excessively high concentration of the smaller molecules being generated in the sampling zone above the target. This is thought to trigger multimer ion and cluster ion formation, i.e., making larger molecular mass species not present in the original sample.[241] The effect is typically witnessed as detector overload. The solution recommended by the instrument manufacturer was to turn down the detector voltage to keep the ion count below 100 counts per laser shot. However, turning down the detector voltage does not necessarily prevent gas-phase reactions from occurring and can produce misleading results.[241]

4.3.4. Taking Stock: Molecular Masses and Molecular Structures in Complex Mixtures. *4.3.4.1. Molecular Masses.* Using the SEC calibrations referred to above, it seems reasonable to view molecular mass ranges inferred from the resolved (later eluting) second peak as broadly correct if not very precise. It seems necessary to clarify, however, the significance of the very high mass ranges indicated by SEC signal under the excluded (early eluting) peak. Indications from the elution times of fullerenes and silica particles suggest that investigating conformational changes of large molecules to mimic 3-dimensional structures may be worthwhile.

Meanwhile, improving the reliability of LD-MS and MALDI-MS requires new methods for discriminating more accurately between signal arising from the sample and that from multimer ions likely to form during application of the laser.

4.3.4.2. Detecting Structural Features. Given the mass distributions and chemical diversity of the materials released during thermal breakdown, the list of structural parameters about which it would be desirable to obtain more detailed information is extensive. To the extent that these parameters are determined as bulk properties, the complexity of the mixtures renders many of the average properties relatively meaningless. It is necessary, therefore, to fractionate before making the bulk measurements but also take some care in designing fractionation schemes that would make sense in terms of the types of structures being explored.

The structural information that is ideally required includes hydrogen and carbon aromaticities, the size and number of aromatic ring systems per average molecule, the types of covalent linkages between PNA ring systems, the types of carbon and hydrogen environments of aliphatic side chains of aromatic systems, hydroaromatic (alicyclic) content, and the types and occurrences of oxygen functionalities. Of these properties, the number of aromatic rings per average molecule can be quantified by combining data from quantitative solution-state ^{1}H and ^{13}C NMR spectroscopy provided the number-average molecular mass and the elemental carbon and hydrogen contents are known.[230,251,287,288]

In terms of thermal breakdown, large PNA ring systems do not readily break up under pyrolysis or liquefaction conditions. At higher temperatures (T > 900 °C) these species will graphitize but not fragment. Under hydrocracking conditions in liquid phase, they tend to per-hydrogenate rather than break up to form smaller aromatic units. Analyzing for PNA ring system sizes is where sample fractionation comes into its own by linking the distribution of fused-ring systems to distinct fractions.

Other relevant structural parameters can also be quantified, such as (i) the types of covalent linkages between aromatic ring systems, (ii) the frequency of types and occurrence of carbon and hydrogen environments involving aliphatic side chains of aromatic systems, and (iii) the number of naphthenic rings, which all require combining data from quantitative solution-state ^{1}H and ^{13}C NMR spectroscopy provided the number-average molecular mass and the elemental carbon and hydrogen contents are known.

Thus, improved average molecular mass estimates would be useful in obtaining more accurate quantitative information for the parameters outlined above. This information can then be used to better estimate the number and size of fused (conjugated) aromatic ring systems per average molecule as this parameter cannot be quantified directly by existing methods. The necessity for accurate average mass estimates, in turn, requires that SEC and methods based on laser-desorption mass spectrometry be further refined.

4.4. Analytical Method Development

The discussion in sections 4.2 and 4.3 aimed to trace the contours of available characterization methods in determining the properties of liquid products from the thermal breakdown of coal and biomass. The well-established methods of natural compound identification seem powerless in the face of the complexity of the mixtures from thermal breakdown, where no single chemical species occurs with very great frequency. Even after fractionation, we are constrained to look for average bulk properties, due to the large number of chemical species contained in these samples.

Despite the difficulties outlined, a level of confidence could be established for the mass estimates obtained thus far. Up to about 3000 u there was good agreement between SEC and LD-MS, although LD-MS-based estimates lacked precision. As already signaled, the mass limits indicated by LD-MS spectra of tar/oils in part depend on operator decision, such as sample loading on the target and selection of instrument parameters such as laser power, detector voltage, etc. Typically, spectra are observed to broaden as the laser power is ramped, which makes it difficult to distinguish between sample-derived ions and multimer and cluster ions.[241,243] Overall, the level of

dx.doi.org/10.1021/cr400194p | Chem. Rev. 2014, 114, 1547−1607

uncertainty was found to increase for fractions with molecular masses greater than about 3000−5000 u.

The average structural properties to look for in these mixtures are reasonably well understood. For instance, it would be desirable to map the types of covalent linkages between aromatic units in these large molecules. It would be helpful to estimate how these linkages relate to molecular architecture, i.e., whether the larger molecules are composed of island-, Archipelago-, or continental-like structures (cf. Figure 26).[251] The term island-like structures refers to molecules which typically contain small aromatic cores connected to one another by long aliphatic-, alicyclic-, and/or heteroatom-containing bridges. Archipelago-like structures refer to molecules with aromatic units linked by shorter bridges and with more alkyl side chains. Continental-like structures refer to a large PNA ring system as the core attached to smaller PNA groups and alkyl chains as pendent groups. It would also be fascinating to explore whether molecules eluting under the excluded peak assume planar (2-D) and worm-like or cage-like (3-D) structures; their shapes and conformations are largely unknown.

In the rest of this section, we will discuss elements of recent method development work that might help reveal a little more about the molecular mass and structural distributions of products of thermal breakdown.[62,135,204]

4.4.1. Method Development for Molecular Mass Distributions (LD-MS and SEC). The method explored for improving LD-MS measurements was to first fractionate the sample fraction by planar chromatography (PC). This was followed by LD-MS analysis of the separated fractions directly from the silica-coated surfaces of the chromatographic plates. Cut pieces of PC plates bearing the separated fractions were introduced directly into the spectrometer as the target. This aims to achieve two objectives: (i) the usual rationale for subfractionation of the sample to reduce masking of signal from the less abundant material by the more abundant material; (ii) reducing sample loading by thinly spreading the sample onto the PC plate. Reduced sample loading is thought to produce relatively low gas-phase sample concentrations at the ion extraction stage, thus reducing the probability of reactive collisions when the laser is fired. The technique was found to demonstrably suppress secondary multimer and cluster ion formation and improve the reproducibility of the spectra.[135,229,241,243] An example of the improvement in molecular mass estimates that are obtained by this approach is presented in section 4.4.4.

Clearly, fractionation by PC is not a quantitative procedure. It is not possible, therefore, to determine M_n estimates from these LD-MS data sets. Instead, that data is used to determine the mass ranges of individual fractions. In this way a single mass spectrum can be selected to calculate number- and weight-average molecular mass values.[243] In the case of uncertainty regarding the 'single' mass spectrum that best represents the entire sample, two or several spectra may be used to determine an upper and lower estimate for the M_n value. Data from the new method have proved more reproducible and appear internally more consistent. Examples of mass estimates from LD-MS and SEC, obtained using planar-chromatography-separated fractions of anthracene and creosote oils from coke oven tars, are given in section 4.4.4.

4.4.2. Method Development for Acquiring Molecular Structural Information (NMR and UV-F). NMP (1-methyl-2-pyrrolidinone) and to a somewhat lesser extent quinoline are capable of completely dissolving coal-derived liquids in the high concentrations required for NMR analysis.[229,230,289] In order to reduce errors and improve the quality of NMR data on both coal-[230] and petroleum-derived[251] samples, ^{1}H and ^{13}C high-resolution solution-state NMR methods were optimized and calibrated for use with undeuterated quinoline and undeuterated NMP as solvents.[135,229,230] The modifications made it possible to calculate average structural parameters (ASP) for *all* subfractions of the samples that were analyzed, including the heavy fractions.

4.4.2.1. Average Structural Parameters (ASPs) That Can Be Calculated without Using M_n. Some of the structural parameters can be derived as a ratio relative to the total amount of elemental carbon or hydrogen in the sample, which mitigates the need for the number-average molecular weight of the sample.[230,251] These include aromaticity, peri-condensed quaternary carbon, aromatic quaternary carbons with aliphatic substituents, protonated aromatic carbon, and the average lengths of alkyl side chains. However, some of the key parameters cannot be calculated in this way. These include cata-condensed quaternary carbon, aromatic quaternary carbons with aromatic substituents, the number of aromatic rings, and the number of naphthenic rings per average molecule.[230,251] Figure 27 depicts several quaternary aromatic carbon environments.

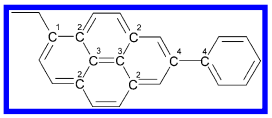

Figure 27. Quaternary aromatic carbon environments: (1) aromatic quaternary carbons with aliphatic substituents, (2) cata-condensed, (3) peri-condensed, and (4) aromatic quaternary carbons with aromatic substituents.

In section 2.4.3 the vital role of hydroaromatic (alicyclic) structures in coal thermal breakdown was highlighted. The hydroaromatic content is also used to assess fuel quality for petroleum-, coal-, and biomass-derived tars/oils.[62,290,291] Estimating hydroaromatic (alicyclic) distributions is done preferably by solution-state ^{13}C NMR. It can be determined quantitatively by ^{13}C NMR only for samples that contain solely mono- to triaromatics.[292] Low-resolution MS can also be calibrated to quantify hydroaromatic content for light coal oils.[293] A number of indirect methods also exist which include catalytic solvent dehydrogenation.[294−296] Recently, a 2-D HSQC solution-state NMR method has been reported that makes it possible to estimate the hydroaromatic content more quickly and easily than previously but, as for the ^{13}C NMR method, only for samples that contain mono- to triaromatics.

4.4.2.2. Average Structural Parameter (ASPs) Calculations That Require M_n. In addition to the *quality* of the NMR data, however, the success or otherwise of several average structural parameter (ASP) calculations is dependent on the accuracy of the M_n values available.[135,229,230,243,251] This is demonstrated in section 4.4.5 through a comparison of (i) ASP results obtained using M_n estimates derived before the optimized PC/LD-MS methods was developed with (ii) results obtained using the improved M_n estimates.

An approximate relationship has been observed between the wavelength of maximum fluorescence and the number of conjugated aromatic rings in PNA ring systems, as estimated from ASP calculations (Table 20).[135] However, many PNA compounds do not follow this trend due to their particular

dx.doi.org/10.1021/cr400194p | Chem. Rev. 2014, 114, 1547−1607

Table 20. Correlations between the Average Numbers of Rings in Polynuclear Aromatic Ring Systems (determined by NMR) and the Wavelengths of Maximum Fluorescence Intensity in the UV-Fluorescence Spectra[135]

wavelength of peak with maximum intensity	aromatic-ring equivalents	wavelength of peak with maximum intensity	aromatic-ring equivalents
270 nm	1 ring	390 nm	5 rings
300 nm	2 rings	420 nm	6 rings
330 nm	3 rings	450 nm	7 rings
360 nm	4 rings	≥480 nm	≥8 rings

structures (e.g., perlyene) and fluoresce at longer wavelengths than expected from their number of conjugated aromatic rings.

4.4.2.3. Characterization of Biomass Tars/Oils. Characterization of biomass fast pyrolysis tars/oil or liquefaction products often presents additional challenges to those already touched upon. Mohan et al.[160] provided a useful review of the most common methods used to examine biomass-derived tars/oils. For liquid-state NMR analysis, acetone-d_6 or dimethyl sulfoxide is often used as the solvent of choice, despite inherent problems arising from overlaps of solvent peaks with the sample spectrum.[297,298]There is no obvious way to avoid this problem due to the low solubility of biotars/oils in common NMR solvents. A thorough account of the issues can be found elsewhere.[297−299] In attempts to obtain more complete structural information the often used HSQC NMR method[298] provides information for carbon environments attached to hydrogen. Vital information on quaternary carbons *cannot* be obtained. In general, solid-state NMR methods provide more structural information on biomass-derived pitches, chars, and cokes than those from coal, due to a greater abundance of oxygen functionalities in the biomass-derived samples.[300,301] Nevertheless, many of the issues relating to quantification and observability have yet to be resolved.

4.4.3. Summary of Developments. Improved M_n-value estimates make it possible to obtain structural information from NMR spectroscopy through ASP calculations.[135] The importance of sample fractionation prior to analysis to reduce polydispersity and masking effects cannot be overstated. Results presented in section 4.4.4 demonstrate the necessity to fractionate by planar chromatography even relatively light samples of narrow polydispersity, such as anthracene oil and creosote oil, in order to reveal their full mass ranges.[241]

For more widely polydispersed materials such as pyrolysis tars/oils or coal tar pitch it is necessary to fractionate (by planar chromatography) products of a primary fractionation (e.g., by solubility) in order to obtain reliable information on molecular mass ranges and average values. When these data sets are combined with ASP calculations using results from NMR spectroscopy, detailed and more reliable information can be obtained, as shown in examples provided in section 4.4.5 and 4.4.6.[135]

4.4.4. Improved Mass Estimates for Anthracene and Creosote Oils. A potential advance in developing a more robust method for estimating molecular mass distributions and average mass values was tested during an LD-MS study of creosote oil (CO) and anthracene oil (AO-1) samples.[241] These were samples recovered from distillation of coke oven tars. CO has a nominal boiling point range of 200−300 °C and the AO-1 sample over 250−370 °C.[241]

LD-MS spectra recorded from analysis of the whole anthracene oil are presented in Figure 28, showing the variability of results depending on the instrumental parameters used. As explained in section 4.4.1,[241] in order to reduce the variability of the spectra and obtain more reliable results, the sample was subsequently fractionated by planar chromatog-

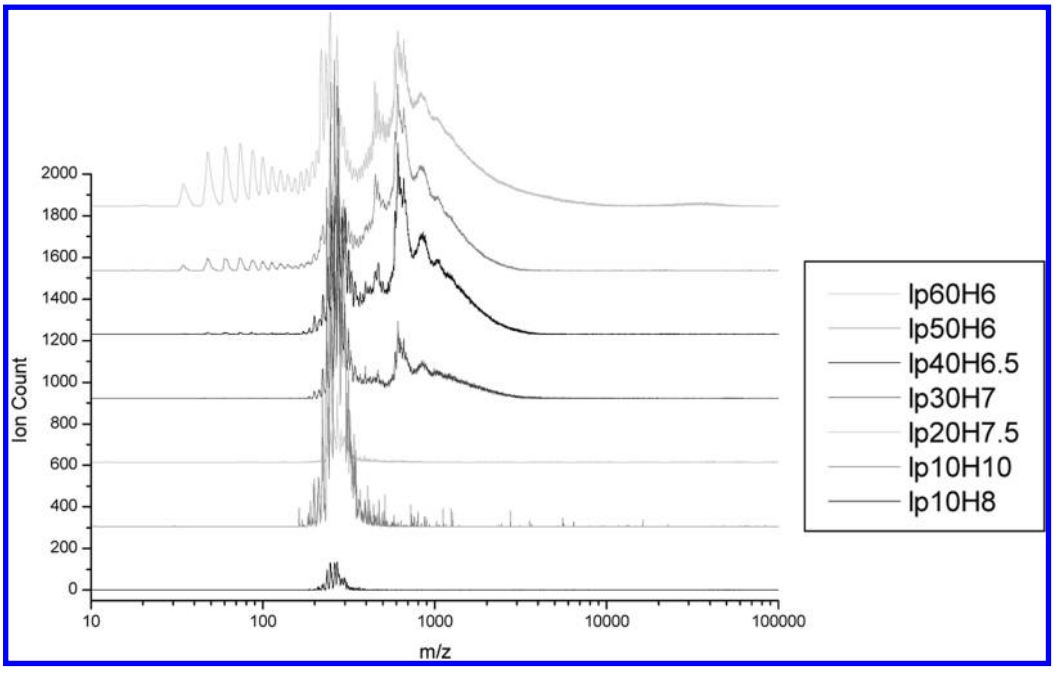

Figure 28. Effect of increasing laser power on LD-MS spectra of the neat AO-1. High-mass accelerator (H) voltage was reduced to keep the ion count below 100 units per shot. Linear mode, 600 ns delayed ion extraction time, laser power (% of max)/H (kV) from bottom to top: 10/8, 10/10, 20/7.5, 30/7, 40/6.5, 50/6, 60/6, and 70/5.5%/kV. Each mass spectrum is the sum of 10 scans. (Reproduced with permission from ref 241. Copyright 2008 American Chemical Society.)

dx.doi.org/10.1021/cr400194p | *Chem. Rev.* 2014, 114, 1547−1607

raphy followed by LD-MS analysis, performing laser desorption direct from the silica surface of the PC plate.

Figure 29 presents LD-MS spectra comparing the anthracene oil (AO-1) planar chromatography fractions 1, 4, and 5, where

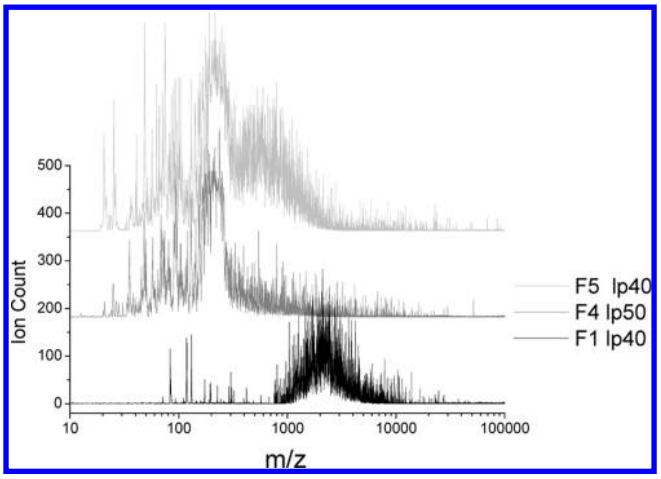

Figure 29. LD-MS spectra comparing the anthracene oil (AO-1) planar chromatography fractions 1, 4, and 5. Linear mode, no DIE, HMA 10 kV, and laser power 40−50% of max. Each mass spectrum is the sum of 10 scans. (Reproduced with permission from ref 241. Copyright 2008 American Chemical Society.)

mobility of samples on the plate *increased* from 1 to 5. Two points emerge when comparing the mass ranges observed from the PC fractions (Figure 29) with those from the whole sample (Figure 28). (i) Analyzing the whole sample gave ions ranging to m/z ~400 at low laser power and to ~3000 m/z as the laser power was ramped. (ii) PC fractions revealed ions to at least m/z 5000, and the mass distributions were largely independent of laser power.[241] It appears the range of masses observed in analysis of the whole sample was probably underestimated due to mass discrimination, which is common for highly polydispersed samples and leads to suppression of high-mass signal.[135,206,243,241] When the high-mass material was isolated from the rest of the anthracene oil sample (i.e., when PC fraction 1 was isolated), ions ranging to >5000 m/z could easily be detected by LD-MS (Figure 29).[241]

Analysis of the whole CO (creosote oil) sample by LD-MS using low laser power gave ions ranging up to m/z ~300, and as the laser power was ramped the spectra drifted up to ~1200, whereas its PC separated fractions showed ions to m/z ~1000. The difference between the higher mass estimates is relatively small and due to either (i) better ionization of the higher mass components during analysis of the whole sample due to lighter components acting as matrix or (ii) multimer ions being generated during analysis of the whole sample, leading to artificially high m/z ions being observed.[241] It was not possible to ascertain which of the two possibilities was correct. It was clear, however, that the sample contained molecular species with masses to at least m/z 1000.

With careful balancing of sample loading on the target, laser power, total ion current, and delayed ion extraction, it was thus possible to observe high-mass materials without generating multimer (i.e., artifact) ions. The key to suppressing multimer and cluster ion formation, however, appears to be the low target loading and consequent low gas-phase sample concentrations following the laser pulse. Meanwhile, simply diluting the sample solution before application to the standard LD-MS target, as a way of reducing sample loading on the target, did not prove useful.[241] This was found to cause mass discrimination for the CO and AO-1 samples leading to underestimation of their mass distributions. Using planar chromatography to prepare targets appears to be the best way (to date) to suppress multimer and cluster ion formation and reveal the high-mass materials unambiguously.[229,241,243]

These mass distribution determinations by LD-MS were found to be consistent with SEC analysis of the CO and AO

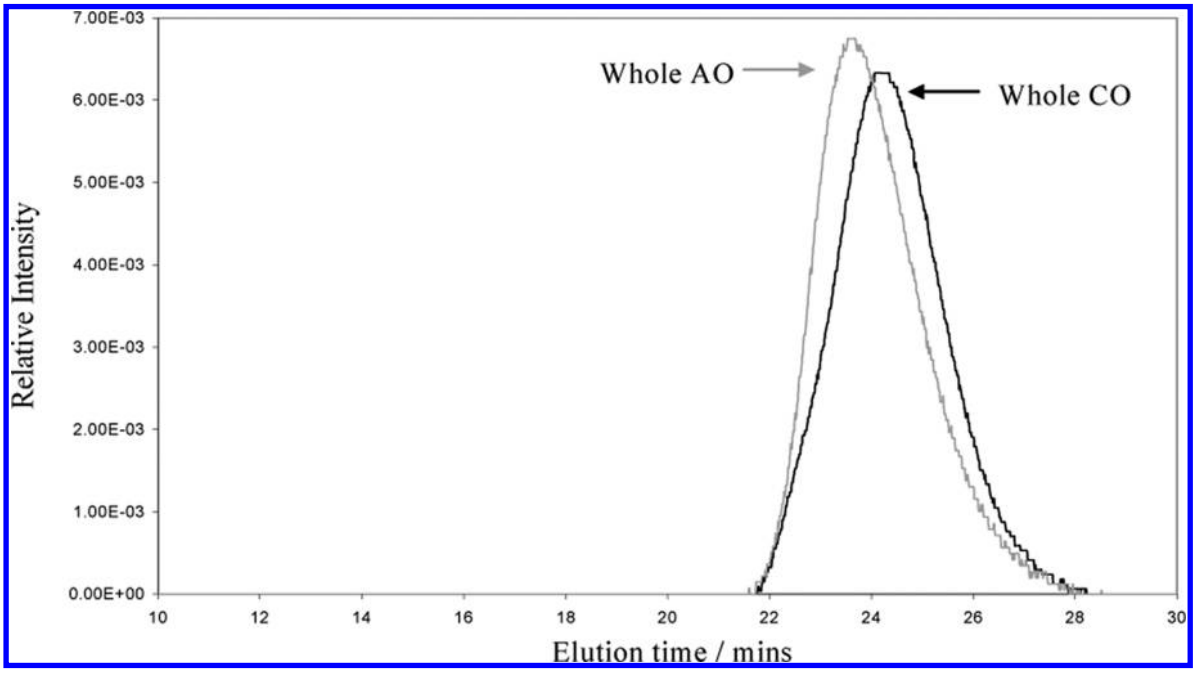

Figure 30. Area-normalized SEC chromatograms of the original whole creosote oil and anthracene oil. Detection was by UV-absorption at 300 nm; Mixed A column using NMP as eluent. (Reproduced with permission from ref 241. Copyright 2008 American Chemical Society.)

dx.doi.org/10.1021/cr400194p | *Chem. Rev.* 2014, 114, 1547−1607

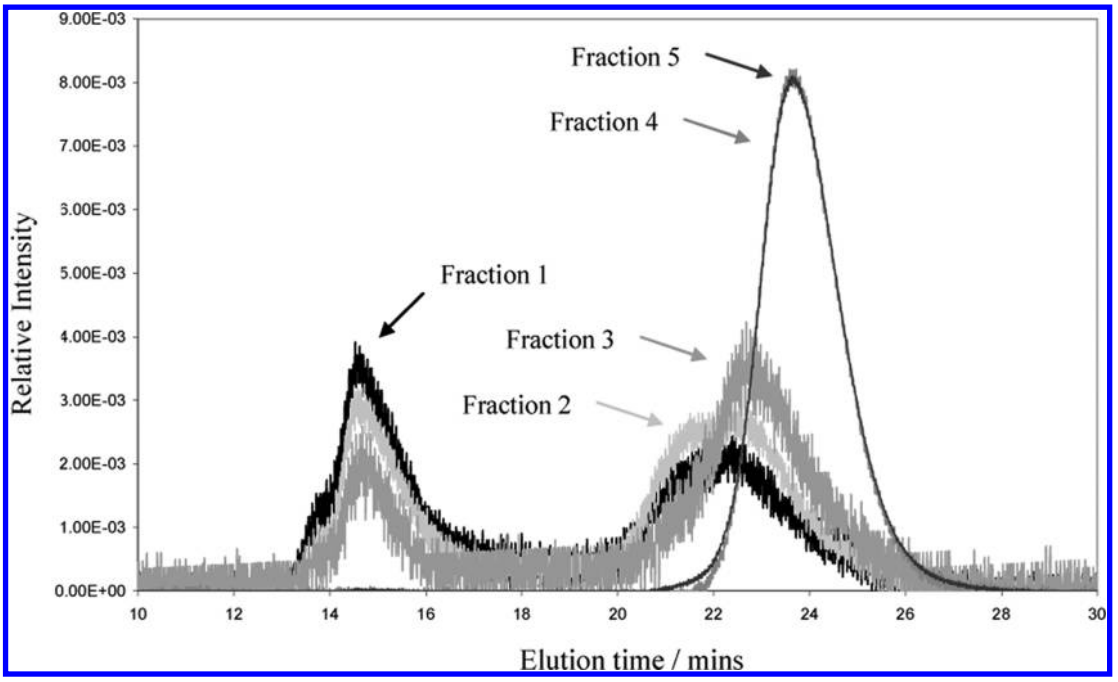

Figure 31. Area-normalized SEC chromatograms of anthracene oil fractions separated by planar chromatography. Detection by UV-absorbance at 300 nm. Mixed A column with NMP as eluent. (Reproduced with permission from ref 241. Copyright 2008 American Chemical Society.)

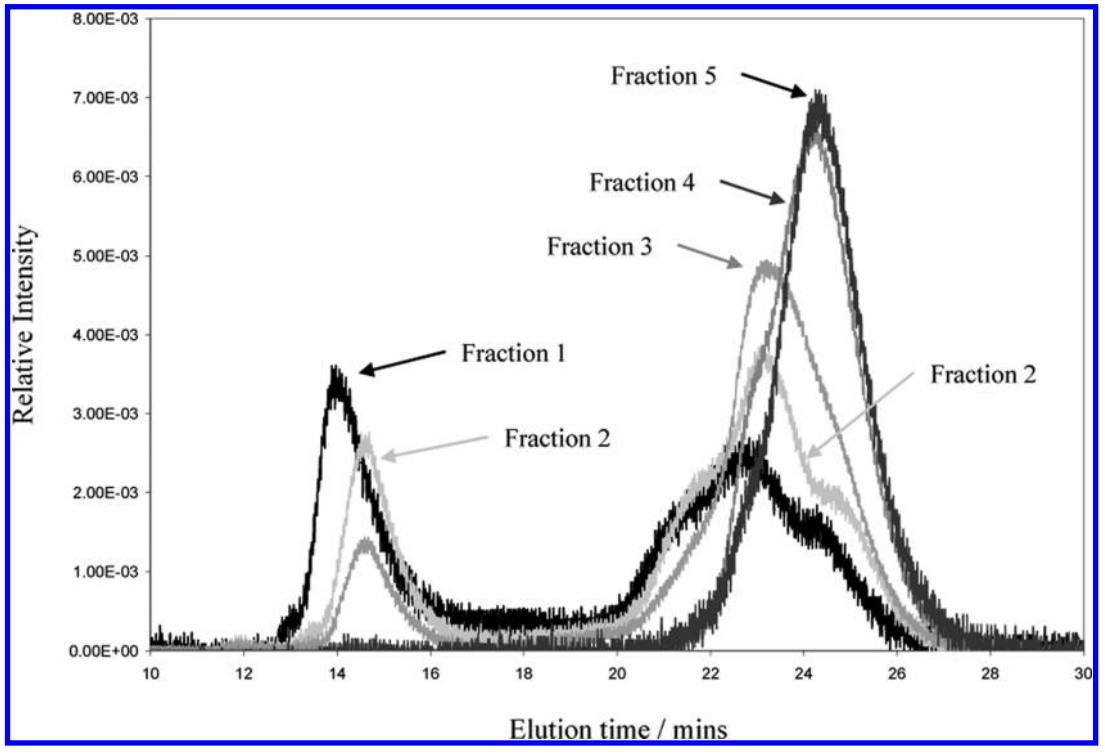

Figure 32. Area-normalized SEC chromatograms of creosote oil fractions separated by planar chromatography. Detection by UV-absorbance at 300 nm. Mixed A column with NMP as eluent. (Reproduced with permission from ref 241. Copyright 2008 American Chemical Society.)

samples.[241] SEC chromatograms obtained from the whole CO and AO samples are presented in Figure 30 and the PC fractions from CO and AO-1 in Figures 31 and 32, respectively. The mass estimates derived from LD-MS and SEC for the CO and AO samples are listed in Table 21, showing good agreement considering the two techniques work in entirely independent ways.[135] Furthermore, comparison of the SEC chromatogram from the whole AO and CO (Figure 30) with their PC fractions (Figures 31 and 32) again shows how analyzing the whole sample alone leads to limited information being obtained, even for these light distillate samples.[241]

Before moving on, the presence of high molecular mass aromatic molecules in light samples such as creosote and anthracene oils requires some explanation, even though the proportion of high-mass material in the CO and AO samples was rather small. These two samples are distillate cuts that

dx.doi.org/10.1021/cr400194p | Chem. Rev. 2014, 114, 1547−1607

Table 21. SEC- (300 nm) and LD-MS-Based Mass Estimates for the Creosote and Anthracene Oils and their PC Fractions[a]

			anthracene oil						creosote oil					
		unit	whole	F1	F2	F3	F4	F5	whole	F1	F2	F3	F4	F5
SEC	peak max	u	200	1500	550	400	200	200	100	350	300	270	100	100
	upper limit[b]	u	700	5000	5000	1900	700	700	700	5000	5000	2700	700	700
LD-MS	peak max	m/z	250−280	2200	n/a[e]	n/a	200	200	250−280	500	n/a	n/a	150	160
	upper limit[c]	m/z	900−2800	8000	n/a	n/a	500	1600	450−1100	1000	n/a	n/a	400	500
	tail[d]	m/z	1500−8000	>10k	n/a	n/a	10k	10k	1000−1200	2500	n/a	n/a	3000	2000

[a]Reproduced with permission from ref 241. Copyright 2008 American Chemical Society. [b]Upper limit for SEC refers to the forward edge of the retained peak; the time used is taken as +30 s from where the signal clearly deviates from the baseline. Excluded material which elutes before 18 min is not accounted for; therefore, mass values are underestimated.[241] [c]Upper limit for LD-MS refers to where there is clear ion intensity, assuming there are no multimer ions.[241] [d]Tail for LD-MS refers to noisy signal that tails off to high mass; it is unclear if this is real signal or artefact.[241] [e]n/a means it was not possible to obtained satisfactory LD-MS spectra because either the sample could not be ionized or it fragmented and/or due to low abundance.[241]

Table 22. Experimental Data Used in the ASP Calculations[a]

symbol	parameter	PAS	PPS	PPI
H_{Ar}	fraction of aromatic hydrogen	0.75	0.79	0.94
H_{α}	fraction of aliphatic hydrogen α to an aromatic ring	0.21	0.18	0.03
$H_{\beta} + H_{\gamma}$	fraction of aliphatic hydrogen β and γ to an aromatic ring	0.03	0.03	0.03
H_{Al}	fraction of aliphatic hydrogen	0.25	0.21	0.06
C_{Ar}	fraction of aromatic carbon	0.88	0.95	0.98
C_{Al}	fraction of aliphatic carbon	0.12	0.05	0.02
M_n	number-average mol wt	200−300	400−1600	900−12 800
%C	percent carbon from elemental analysis	91.7	92.3	93.1
%H	percent hydrogen from elemental analysis	4.9	3.9	2.8

[a]Reproduced with permission from ref 230. Copyright 2008 American Chemical Society. The term fractions in the first six rows indicates the fractions of total hydrogen or carbon. Row 7 presents number-average molecular mass in terms of u, i.e., atomic mass units. Last two rows present percentages of elemental carbon and hydrogen in the sample.

Table 23. Selected ASP Results Independent of M_n[a]

symbol	definition[a]	equation	PAS	PPS	PPI
n	number of carbons per alkyl side chain, including naphthenic groups	$(H_{\alpha} + H_{\beta} + H_{\gamma})/H_{\alpha}$	1.15	1.17	1.0−2.0
C_s	fraction of saturated carbons per molecule, including naphthenic	$C_{Al}{}^{a}$ C	0.12	0.05	0.02
C_n	fraction of naphthenic carbons per molecule	$(C_{Al}{-}CH_3)^{a}$ C	0.06	0.02	<0.01
C_{al}	fraction of straight chain alkyl carbons	$C_s - C_n$	0.06	0.03	0.02
$C_{ar\text{-}US}$	fraction of protonated aromatic carbon	$H_{Ar}{}^{a}$ H	0.48	0.40	0.34
$C_{ar\text{-}PC}$	fraction of peri-condensed carbon	$C_{ar1} - (H_{Ar}{}^{a}$ H)	0.15	0.24	0.30
$C_{ar\text{-}s}$	fraction of aromatic carbons substituted by saturated carbon	C_s/n	0.10	0.04	0.01−0.02
Φ	condensation index	$[(C_{Ar}{}^{a}$ C$) - C_{ar\text{-}P}]/(C_{Ar}{}^{a}$ C)	0.34	0.54	0.65

[a]Values are given as fractions of total carbon except 'n' which is derived as the number of carbons atoms. (Reproduced with permission from ref 230. Copyright 2008 American Chemical Society.) Definitions taken from ref 288. To derive these parameters independent of M_n, 'C' and 'H' were assigned a value of 1.0 instead of their original values as defined in Table 24 below.

should not have contained nonvolatile high-mass species. It is likely that the high-mass molecules found in these samples are due to carryover/entrainment of liquids (aerosols) and solids during distillation that was performed as part of an industrial process. It is also just possible that sample aging after recovery may also have played a role (cf. section 2.5.2).[111]

The agreement obtained between these two independent techniques singles out the combination of SEC and LD-MS measurements as a robust and reliable method.[135] Zubkova's recent review of fractionation methods for coal liquids has also suggested that combining planar chromatography with LD-MS- and SEC-based determinations appears as the most effective method currently available for estimating mass distributions.[204]

4.4.5. How M_n Values Can Influence Calculation of Structural Parameters: Coal Tar Pitch. The challenges of arriving at precise mass estimates raise questions regarding the sensitivity of average structural parameter (ASP) calculations to M_n values. Using data from the optimized NMR method[230] (section 4.4.2) and two sets of M_n estimates, ASP calculations were undertaken for the three pitch fractions discussed earlier (section 4.2.2).

Of the two sets to be compared, the first set[230] of data was the best available prior to development of the planar-chromatography-assisted LD-MS determinations.[229,243] We also note that heteroatom contents were not accounted for in these ASP calculations.[229] The differences in the results turned out to be minor for this coal tar pitch, as the abundance of heteroatoms was low.[135]

4.4.5.1. ASPs Calculated Using the First Set of M_n Data. The first set of M_n estimates for the three solubility fractions prepared from the coal tar pitch were given in Table 17. The acetone-soluble (PAS) fraction was estimated to have an M_n value of between 200 and 300 u. For the acetone-insoluble−pyridine-soluble (PPS) fraction, the range extended from ∼400

dx.doi.org/10.1021/cr400194p | Chem. Rev. 2014, 114, 1547−1607

Table 24. Selected ASP Results Dependent on M_n (based on ref 288)[a]

		PAS		PPS		PPI		
symbol	definitions							
M_n	number-average molecular weight estimate	200	300	400	1600	900	12 800	*6000*
m	number of aromatic nuclei	1.0	1.0	1.0	1.0	1.0	1.0	1.0
H	total number of hydrogen atoms per average molecule	9.7	14.6	15.5	61.9	25	356	*167*
C	total number of carbon atoms per average molecule	15.3	22.9	30.7	123.0	70	992	*465*
$C_{ar\text{-}AS}$	fraction of aromatic carbons substituted by aromatic groups	0.04	0.14	−0.02	0.12	−0.07 to −0.05	0.01−0.03	*0.00*
C_{Cata}[b]	fraction of cata-condensed carbon	0.10	0.00	0.27	0.14	0.33	0.31−0.33	*0.33*
R_A	number of aromatic rings per average molecule	1.5	2.2	5.2	20.9	14.7	209	*98*
R_N	number of naphthenic rings per average molecule	1.4	2.1	0.6	2.3	1.0	14.1	*6.6*

[a]Reproduced with permission from ref 230. Copyright 2008 American Chemical Society. [b]Where $C_{ar\text{-}AS}$ is negative, a value of zero was used in the calculations to find C_{Cata}.

to 1600 u and for the pyridine-insoluble (PPI) fraction from ∼900 to 12 800 u.[230] The complete data sets that are required to perform the ASP calculations are shown in Table 22. ASP results independent of M_n are shown in Table 23 and those dependent on M_n in Table 24. For brevity, not all results have been shown.[230,251,288] The amount of hydrogen and carbon detected by the optimized NMR method relative to the theoretical amounts (from ultimate analysis) for the samples and a mixture of model compounds are shown in Table 25.[230]

Table 25. Percentage of Hydrogen and Carbon Detected by Quantitative NMR Analysis Based on Theoretical Values for Total Amounts of Carbon or Hydrogen[a]

sample	percent of total H	percent of total C
model compounds	100 (±<2)	100 (±2)
PAS	98 (±<2)	92 (±3)
PPS	99 (±2)	87 (±5)
PPI	13[b] (±>10)	68[b] (±>10)

[a]Reproduced with permission from ref 230. Copyright 2008 American Chemical Society. [b]Very weak signal.

One of the key findings from the study was that when lower M_n estimates are used in the ASP calculations, the calculated value of $C_{ar\text{-}AS}$ (aromatic carbons substituted by aromatic groups, i.e., biphenyl-like, sigma C−C bonds as shown in Figure 27) for the PPS and PPI fractions turned out to be negative, cf. Table 24.[230] This suggested that the lower M_n estimates do not fit the data. The M_n values that gave zero values (signifying the beginning of the expected range) for the $C_{ar\text{-}AS}$ parameter are 450 and 6200 u for the PPS and PPI fractions, respectively.[230] Due to the relative insensitivity of the calculation to actual M_n values, the M_n values that allowed setting $C_{ar\text{-}AS}$ values to zero represented approximate (read useful) estimates rather than precise values for the correct M_n. For the PAS fraction, either M_n value led to plausible structural parameter values.[230]

4.4.5.2. Summary of ASP Results from the First Set of M_n Data. As signaled earlier in section 4.4.1, some of the parameters can be determined independently of M_n values (Table 23) while others cannot be determined in this way (Table 24).[230,243]

The aromaticity (independent of M_n) and the average-number of aromatic rings per polynuclear aromatic structure (dependent on M_n) were both found to decrease with *increasing* solubility of the pitch fractions (PPI > PPS > PAS).[230] Similarly, peri-condensed and all other quaternary carbon species were found to decrease with *increasing* solubility. Peri-condensed carbons were found to be about 30% for the PPI, 24% for the PPS, and 15% for the PAS. This strongly suggested the presence of larger polynuclear aromatic ring systems in the PPS and PPI fractions compared to the PAS fraction. Results from QUAT NMR experiments (which detects quaternary carbon atoms only) also confirmed the trend of decreasing proportions of peri-condensed carbon with increasing solubility: PPI > PPS > PAS.[230]

Taken together, the findings suggest that continental-type structures became more dominant as the solvent solubility of these coal-derived fractions diminished. The estimated average number of aromatic rings *per average molecule* ranged from 1 to 2 rings in the PAS fraction, 4 to 21 for the PPS, and 11 to 210 rings in the pyridine-insoluble fraction.[230] These ring numbers were directly related to the M_n assigned to the particular fraction in the ASP calculations.

It is noted that even when using the optimized NMR method, *quantitative* results are obtained only for the PAS fraction and the model compounds but not for the heavier PPS or PPI fractions. Table 25 shows that the amount of hydrogen (w/w) detected decreases from near 100% for PAS and PPS to only 13% for the pyridine-insoluble material. The amount of carbon (w/w) detected decreased from 92% for PAS to 87% for PPS and ∼70% for PPI. These findings have clear general implications for analysis of polydispersed samples by NMR without prior fractionation. If anything, they point to the necessity of working with finer fractionation cuts.

4.4.5.3. Summary of ASP Results from the Second Set of M_n Data. The parameters calculated for the PAS fraction were not greatly affected by the improved M_n values. ASP calculations for the PPS and PPI fractions were, however, more sensitive to the improved mass estimates.

For the PPS sample, the original ASPs were calculated for two M_n values (400 and 1600 u) due to the uncertainty in the estimates. The result from the planar-chromatography-assisted LD-MS method gave an estimate of 1650 u for the PPS sample.[229] Thus, the ASP results based on the previous upper M_n estimate (1600 u) could be considered as still valid.

Meanwhile, the estimated M_n values used in the previous set of ASP calculations for the PPI sample were 900 and 12 800 u as the lower and upper limits, respectively. One important finding from those ASP calculations was that a minimum value of ∼6000 u had to be assumed for M_n before the calculations could even be undertaken. In other words, if a value of M_n below 6000 u was used in the calculations, negative values were obtained for some of the parameters.

However, the M_n values calculated for the PPI sample from the PC-assisted LD-MS method were found to be much lower (2000−2500 u) than the 6000 u estimated from the ASP

dx.doi.org/10.1021/cr400194p | Chem. Rev. 2014, 114, 1547−1607

calculations. Therefore, if the new M_n values are used some negative ASP values are obtained. In the work done so far, the ASP results based on an M_n estimate of 6000 u would seem to best characterize the PPI sample (cf. Table 24).

Pyridine-insoluble fractions evidently present special challenges. What we can see from what in effect are partial analyses is that these fractions contain large fused PNA ring systems that do not seem to respond very much to LD-MS.[244,302] Furthermore, calculating M_n from the resolved part of an SEC chromatogram alone tends to underestimate the molecular mass by some margin, since so much of the sample shows signal in the excluded zone. Developing the analyses of these heaviest fractions appears as an area in need of a breakthrough.

These finding show that the upper limit of the LD-MS method for characterizing the PPI sample has effectively been reached. Similar observations have been made for other heavy coal- and petroleum-derived materials using these methods.[135]

4.4.5.4. Summary of ASP Calculations. The M_n for the PAS sample arrived at with the PC-assisted LD-MS method was determined to be about 550 u. On this basis, an average molecule was calculated to contain approximately four aromatic rings (R_A) and three naphthenic rings (R_N). The average molecule also contained less than 10% of the total carbon in cata-condensed environments. Fourteen percent of the total carbon was calculated to be aromatic carbon substituted with aromatic groups ($C_{ar\text{-}AS}$). About 15% of the carbon was found in peri-condensed and 48% in protonated aromatic carbon ($C_{ar\text{-}US}$) environments. The remainder of the carbon (12%) was in alkyl groups attached to aromatics.[229]

Using an M_n value of 1600 u for the PPS sample, the average molecule was found to contain about 21 aromatic rings (R_A) alongside an average of 2 naphthenic rings per molecule. C_{Cata} was ~14% of the total carbon; $C_{ar\text{-}AS} \approx 12\%$. Peri-condensed carbon accounted for ~20% and protonated aromatic carbon for about 40% of the total.[229]

For the PPI sample, where M_n was assumed to be 6000 u, the average molecule was found to contain about 100 aromatic rings (R_A) and an average of about seven naphthenic rings per molecule (R_N).[229] C_{Cata} was nearly ~33% of the total carbon, $C_{ar\text{-}AS} \approx 0\%$, while peri-condensed carbon accounted for ~30% and protonated aromatic carbon ~34%. Values effected by the uncertainty in M_n are $C_{ar\text{-}AS}$ (which becomes negative if a lower value is used), C_{Cata}, R_A, and R_N. On the basis of these ASP calculations, the LD-MS-derived M_n value was, therefore, underestimated for this sample. The apparent precision of the numerical results notwithstanding, results from ASP calculations for such complex samples need to be treated as rough guides to underlying trends, which provide qualitative information regarding changes in structure that are difficult to determine in any other way.

A more detailed account of the findings from the ASP calculations including discussions of the errors involved and limitations of the method for the coal tar pitch and its fractions has been given elsewhere.[229,230] The optimized ASP method was more recently applied to a set of petroleum-derived maltenes and asphaltenes.[251]

4.4.6. Improved Structural Information: Pitches Made by Polymerizing Anthracene Oil. Coal tar pitch has multiple uses and been in relatively short supply in Europe and North America due to changes in coke-making technology and contraction of the coke-making industry. Over 50% of world coke production now takes place in China.[6] Polymerization of lower boiling 250−370 °C anthracene oil[303] by means of an air-blowing process has been proposed as a way of making pitch-grade materials.[304−306]

Figure 33 presents a schematic diagram of the process involving successive cycles of (i) air blowing for partial

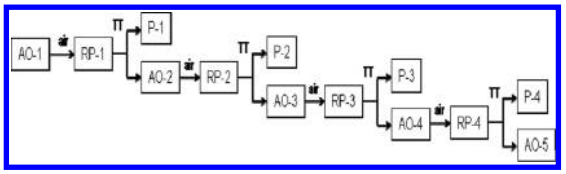

Figure 33. Schematic diagram showing the steps followed in the preparation of pitches from anthracene oil, where air refers to air blowing at temperature and TT refers to thermal treatment and distillation.[229]

oxidation (RP-1), (ii) thermal treatment for polymerization (TT), and (iii) distillation to separate the new pitch (P-1) from lighter distillate, AO-2. The cycle is repeated by partially oxidizing the distillate AO-2 and so on. In successive steps, AO-*n* is oxidized to reaction product (RP-*n*), which is then heat treated and distilled to separate the new pitch (P-*n*) from the lighter fraction (AO-*n*+1), where *n* is the cycle number.[99,229,307]

The reaction mechanisms of the process are broadly understood. Oxygen in the air-blowing phase is thought to produce peroxy structures and other oxygen functionalities (hydroxy groups, ketones, carboxylic anhydrides, etc.). Increasing the air-blowing temperature increases oxygen uptake and promotes cross-linking. The thermal treatment step is thought to disrupt oxygenates and cross-linked structures, creating reactive free radicals, leading to lower oxygen contents and greater levels of aromatic condensation compared to the parent air-blown fraction.[99,308,309]

A set of samples from this air-blowing process was studied using the optimized ASP method outlined above. The pitches discussed below, P-1 and P-4, come from the first and forth cycle of a single process which starts with AO-1 as feedstock. Pitch samples were subdivided into narrow bands of material through solvent separation into five fractions; solvents are listed in Table 26. Each of the solubility fractions was further subdivided using planar chromatography[229] to aid in estimation of M_n as described in section 4.4.1. M_n values determined for each solubility fraction of P-1 and P-4 by LD-MS are presented

Table 26. Main Experimental Values Used in the ASP Calculations (definitions given in Table 22)[229]

fraction	sample	H_{Ar}	C_{Ar}	M_n/u	%C	%H
heptane-sol.	P-1a	0.900	0.940	320	92.0	5.1
	P-4a	0.903	0.941	400	91.7	5.2
heptane-insol.−acetonitrile-sol.	P-1b	0.860	0.940	420	91.4	5.0
	P-4b	0.898	0.939	600	91.2	4.8
acetonitrile-insol.−toluene-sol.	P-1c	0.843	0.948	1100	92.3	4.3
	P-4c	0.842	0.936	1500	91.8	4.4
toluene-insol.−pyridine-sol.	P-1d	0.810	0.963	1600−2000	90.8	3.9
	P-4d	0.920	0.978	1800	90.3	3.9
pyridine-insol.	P-1e	0.625	0.943	2100−3600	91.1	3.5
	P-4e	0.728	0.958	1900−2900	90.9	3.6

dx.doi.org/10.1021/cr400194p | Chem. Rev. 2014, 114, 1547−1607

in Table 26. The fractionations revealed differences between the molecular masses and structural features of the pitches[229] that were not apparent from analysis of the whole samples.[307]

In some instances two mass spectra were acquired under different conditions to obtain a lower and an upper M_n estimate.[229] Solution-state NMR data were recorded[229] using the optimized method[230] described in section 4.4.2 to examine the solubility fractions of the pitches. As in the previous section, NMR data were combined with M_n estimates and elemental hydrogen and carbon values in ASP calculations based on the work of Dickinson[287] and Rongbao.[288] A more detailed account has been presented in ref 229.

Summary of Findings for the Air-Blowing Process. Subdivision of the anthracene oils into narrow bands using planar chromatography revealed changes in their mass distribution, detected by SEC and LD-MS, and in the relative sizes of conjugated aromatic ring systems, as observed by UV-fluorescence spectroscopy. Demonstrable evidence was found for the presence of high-mass species (1000−5000 u) that were *not* expected to be in the anthracene oil samples at all.[229,241] A clear trend of decreasing average mass and size of aromatic chromophores was found in the *anthracene oils* from the latter processing cycles (i.e., from AO-1 to AO-5). These results are consistent with earlier findings[307] and show that the largest molecules which also contain the largest sizes of conjugated PNA groups (in the AO samples) appear to be the most oxygen reactive species during the air-blowing process. In the AO's recovered after successive cycles, these species are therefore found to have been depleted more rapidly than others.

ASP calculations have helped detect differences between the structures of pitch in the early stages (P-1) and pitch structures in the later stages of the process (P-4). Larger molecular sizes and larger PNA ring systems were observed in the pitch samples recovered from the successive processing cycles, indicating that samples were getting progressively heavier with the increasing severity of the oxidative and thermal treatment steps.[229] In terms of findings from ASP calculations, changes were detected in the amounts of cata-condensed aromatic-carbon (C_{cata}) and aromatic carbon substituted with aromatic groups ($C_{ar\text{-}AS}$) between successive stages of the process (cf. Table 27).

Table 27. Selected ASP Results Dependent on M_n (based on ref 288)[a]

sample	M_n	m	$C_{ar\text{-}AS}$	C_{Cata}	R_A	R_N
P-1a	320	1	0.03	0.34	2.4	1.3
P-4a	400	1	0.13	0.20	3.0	1.4
P-1b	420	1	0.09	0.24	3.5	1.2
P-4b	600	1	0.13	0.23	4.9	2.6
P-1c	1100	1	0.07	0.30	12.4	2.4
P-4c	1500	1	0.13	0.21	15.9	4.5
P-1d	1600	1	0.00	0.39	21.5	0.00
P-1d	*2000*	*1*	*0.00*	*0.39*	*26.9*	*0.00*
P-4d	1800	1	0.06	0.33	22.1	1.2
P-1e	2100	1	0.00	0.50	34.1	0.00
P-1e	*3600*	*1*	*0.00*	*0.50*	*58.5*	*0.00*
P-4e	1900	1	0.00	0.42	28.7	0.00
P-4e	*2900*	*1*	*0.00*	*0.42*	*43.7*	*0.00*

[a]Values are given as average numbers of rings, except $C_{ar\text{-}AS}$ and C_{Cata} which are fractions (definitions are given in Table 25).[229]. Values in italics are for repeat calculations using a different M_n.

This information makes it possible to infer basic reaction mechanisms for distinct phases of the process.[229] Briefly, the pitch produced during the first cycle of the process (P-1) contained a greater proportion of its carbon in cata-condensed aromatic environments than the pitch from the fourth cycle. This suggests that average structures of the P-1 pitch evolved through condensation reactions and ring-closure reactions within AO-1, leading to increasing sizes of fused PNA ring systems.

Meanwhile, the pitch from the fourth cycle (P-4) showed the highest content of $C_{ar\text{-}AS}$, which suggests formation of covalent sigma bonds *between* fused-ring islands. This involves cross-linking reactions that form biphenyl-like aromatic−aromatic sigma bonds ($C_{ar\text{-}AS}$).[229] At the same time the P-4 sample contained molecules with the highest average molecule mass.

These findings suggest either a change in reaction pathways during passage from AO-1 to P-1 compared to AO-4 to P-4 or a progressive set of structural changes of successive reactants, where the reactant in each phase is different, which is what the UV-F and NMR results for successive AOs indicate.[99,229,241] An example of the different types of structures produced in formation of P-1 and P-4 is presented in Figures 34 and 35, respectively.

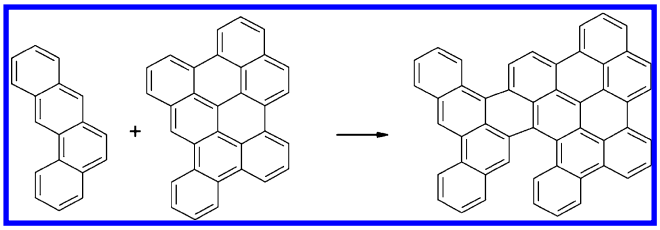

Figure 34. Simplified schematic example of the transformation of anthracene oil AO-1 into pitch P-1.[229]

Figures 34 and 35 are meant to show that P-1 samples contain molecules that are planar and that P-4 is more cross-linked, with its PNA ring systems possibly held in different planes to one another. These conclusions on structure from ASP calculations are consistent with the work of Menendez and co-workers on the pyrolysis behavior and ability of these pitches to generate mesophase and coke.[99,307]

Upon pyrolysis, both the pitches gave rise to mesophase formation.[303] The pitch produced in the first cycle (P-1) generated mesophase more readily. On further heating, this mesophase led to a coke with a fluid-domain optical texture that is indicative of large areas of fused aromatic ring systems in the form of pregraphitic structures. The pitch from the fourth cycle generated lower quantities of mesophase; on further heating, a less ordered coke was produced, containing smaller regions of fused aromatic ring systems that had a mosaic optical texture.[307] Figure 36 shows optical photomicrographs under polarized light of the cokes generated from heat treatment of the two pitches, P-1 and P-4, alongside pictorial examples of the different sizes of pregraphitic stacking units that lead to the observation of fluid domains and mosaic-like textures.[307]

4.4.6.2. Summary. Use of the optimized ASP methods has given detailed structural information for the complete range of samples from the AO-polymerization process from light oils to the pyridine-insoluble fraction of pitches. Detailed characterization of the pitch samples from different cycles of the process revealed changes in structure and mass. The basic reaction mechanisms inferred from these studies[229] correlate well with

dx.doi.org/10.1021/cr400194p | Chem. Rev. 2014, 114, 1547−1607

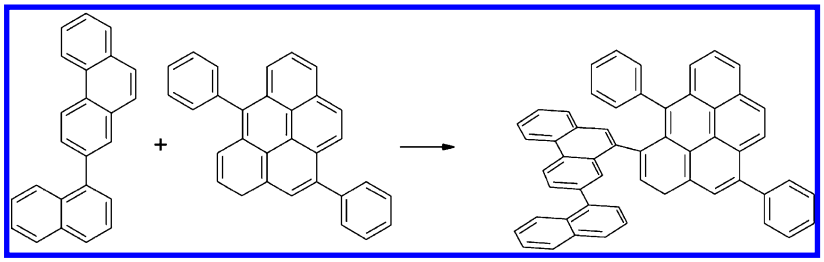

Figure 35. Simplified schematic example of the transformation of anthracene oil AO-4 into pitch P-4.[229]

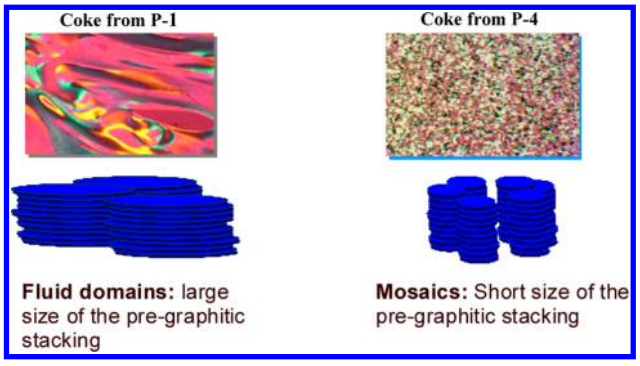

Figure 36. (Top) Optical microscopy images of the cokes produced from thermal treatment of P-1 and P-4. (Bottom) Pictorial examples of the different sizes of pregraphitic stacking units that lead to observation of fluid domains or mosaic structures. (Reproduced with permission from ref 307. Copyright 2008 American Chemical Society.)

independent studies[99,307] on the same samples. Similar conclusions were independently reached on the structural makeup of the pitches from different cycles of the process, which provides further validation of the multitechnique approach.

As a final example of the usefulness of the optimized ASP approach, the NMP-soluble and -insoluble fractions of an asphaltene from Maya crude oil were examined.[251] The results were surprising. NMP is a very strong solvent for aromatics and poor for aliphatics. Therefore, it was anticipated that the NMP-soluble fraction would be the more aromatic of the two samples. However, the results revealed that the aromaticity of the NMP-soluble fraction was lower than the NMP-insoluble fraction by ~4% (error < ±2%). The reason for the insolubility of this material in NMP was due to structural differences. It was found that the NMP-insoluble molecules contain large aromatic cores (continental structures) surrounded by long alkyl side chains, whereas the NMP-soluble molecules contain smaller sizes of PCA units *linked* by long alkyl chains (Archipelago structures).

4.5. Tracking Thermal Breakdown: Future Prospects for Analytical Work

The analytical framework presented in section 4 rests on the two pillars of molecular mass determinations and structural analysis. It is clearly legitimate and proper to debate whether this is an adequate framework. There have indeed been false dawns, but debating new courses of action can often lead to steep increases in analytical power.

Overall, the most important hurdles to overcome involve the ability to estimate the sizes of PNA systems and the alicyclic contents of molecules more precisely; there is also a need for new LD-MS-based methods or other techniques to observe masses higher than ~10 000 u.

Meanwhile, both pillars of the present framework offer potential avenues for improvement.

4.5.1. Molecular Masses. In SEC, a potentially useful line of investigation involves finding ways of assimilating signal under the excluded peak into our calculations. This line of work would likely entail exploring the role of molecular shapes and conformations for material with masses above the 1000−3000 u level. In developing LD-MS we need to investigate whether we have come up against the limits of the technique for the heavier fractions of fuel-derived complex mixtures. After all, polystyrene standard samples of up to 120k u have been identified by LD-MS and MALDI-MS (M. Millan; Imperial College; unpublished work). In analyzing the heaviest fractions, we need to explore whether the difficulties encountered are associated with the large sizes of PNA ring systems. We also need to investigate whether we have made full use of the possibilities offered through the use of diverse matrices in MALDI-MS. Exploring new matrices with the aim of ensuring more complete ionization of complex samples, in particular, to aid detection of the highest mass species and materials, which show excessive fragmentation, appears as a potentially useful line of research.

4.5.2. Structural Work. In furthering structural work, the deeper fractionation of complex samples may provide more information, although the procedure would eventually have to face practical difficulties involving too many subsamples that would need to be analyzed and how to combine the multiple streams of data.

There have been interesting emerging areas of study in the use of in-situ NMR measurements. Ben and Ragauskas reported on the in-situ NMR characterization of pyrolysis oil aging,[310] although the method used by these authors did not allow for detection of quaternary carbon environments. Dufour and Snape[311] recently reported the first in-situ ^{1}H NMR study during biomass pyrolysis in attempting to better understand the molecular mobility of hydrogen and the transient liquid/plastic phase (softening) that occurs. In a related study, high-temperature rheology was performed on the same sample set and the results correlated against the ^{1}H NMR data to explore the softening of biomass components during pyrolysis,[312] akin to the approach used to study the coke-making process and coal pyrolysis. Thus far work on only one biomass feedstock has been reported in addition to cellulose, xylan, and a prepared lignin.

In-situ NMR studies have the potential to provide vital information required to better understand the role of hydrogen and reveal at least some partial mechanistic information during thermal breakdown and aging of liquid products and during their further processing.

Fletcher et al.[313] recently reported some work aimed at building a generalized model for predicting the pyrolysis behavior of low-grade fuels (biomass and black liquor) based on structural information obtained from ^{13}C NMR analysis of

the feedstock. These authors highlighted the need for improved experimental data to improve and validate the model.

One major need is to find better NMR-compatible solvents that are stronger for dissolving high concentrations of sample and whose spectra do not overlap with sample. More generally, it is necessary to understand the limitations of particular analytical approaches, as well as their benefits, in order to select appropriate combinations of multitechnique approaches to obtain as complete information as possible, relevant to the aims of the research.

One useful line of work would involve comparing findings (i) from the optimized ASP method outlined in section 4.4 to characterize quaternary carbons,[230,251] (ii) with data from HSQC 2D NMR to obtain more detailed information on aromatic substituents and nonaromatic linkages (alkyl and oxygenated environments),[310] and (iii) that the multitechnique approaches aimed at quantifying oxygenates[283] would provide more complete structural information than has thus far been reported for the products of thermal breakdown. In structural work, it is also desirable to investigate how oxygenates influence UV-fluorescence spectra, particularly for large aromatic molecules (>500 u).

4.5.3. Method Development for Oxygenates. One of the observations from the examples provided in section 3 on biomass pyrolysis and the case studies (section 4.2) is the need for improved identification and quantification of oxygenated species in coal- and biomass-derived products of thermal breakdown. Improvements in this line of analysis would also be potentially relevant to the study of hydrodeoxygenation (HDO) processes for coal- and biomass-derived tars/oils.[282,283]

Progress has recently been made on this front for low-mass molecules (<300 u) using two-dimensional GC methods, using conventional GC−GC, or comprehensive GC × GC.[135,282,283] Work using GC-AED (atomic emission detector) has also improved detection of nitrogen- and sulfur-bearing compounds.[282] As an example of the intricacy of molecular structures in tar/oil samples, 250 oxygenates were identified using GC × GC, all of which belong to phenol and benzofuran moieties for a direct coal liquefaction distillate sample which contained <3 wt % elemental oxygen.[282,314]

A more recent study showed it was possible to quantify phenols (C6−C11) and alcohols (C4−C9) in naptha (IBP 200 °C) and gasoil (200−350 °C) cuts from a direct coal liquefaction distillate by GC × GC.[283] Carboxylic, ketone, and furan groups were identified but could not be quantified. It was necessary to use a multitechnique approach to obtain quantitative information on all oxygen functionalities: carboxylic acid (by FT-ICR-MS and ^{31}P NMR) and ketone groups (by UV−vis); however, furans could only be estimated by difference.[283]

A different multitechnique approach has been developed by Elliot and McCormick for examining oxygenates in light distillate fractions from hydrotreated biomass pyrolysis oils based on ^{13}C NMR, total acid number, and HPLC.[299] Boateng et al.[298] reported an interesting ^{13}C NMR and chemometric analysis approach which revealed a possible correlation between the findings from principle component analysis and higher heating values. For biomass-derived pitches, chars, and cokes, i.e., oxygenates in very large molecules, solid-state NMR can also provide valuable information.[300,301]

The quantitative information on oxygen functionalities gained from the multitechnique approaches described above, in particular in ref 283, is useful to aid the study of thermal breakdown and upgrading processes (HDO or air blowing) and their products. There remains a need however for further development to obtain quantitative information on oxygen functionalities in the heavier components in these materials (>500 u).

5. SUMMARY AND CONCLUSIONS

Experimental data and analytical tools used in formulating a conceptual model of thermal breakdown in middle-rank coals and lignocellulosic biomass have been reviewed. The aim was to investigate thermochemical reaction pathways as a function of reaction conditions and reactor design. In trying to explain eventual product distributions, evidence relating to covalent bond cleavage has been assessed in juxtaposition to observable patterns of retrogressive recombination reactions of reactive intermediates. Validation of reaction mechanisms inferred from this analysis has been sought in the modalities of liquid product formation and by examining the structures and compositions of the liquid products. Finally, an evaluation of analytical tools and methods available for characterizing these complex liquids and tracking thermal breakdown processes has been carried out.

Thermal Breakdown. Several questions provided the initial framework of the problem at hand: (1) At what temperature does thermal breakdown begin? (2) Are there similarities between the reaction pathways of pyrolysis and liquefaction? (3) When and how do these reaction pathways begin to *diverge*? Furthermore, (4) when and why are pyrolytic reactions sensitive to changes in heating rates? Finally, (5) what do these results tell us about the way retrogressive recombination reactions tend to work?

The underlying complication that distinguishes thermal breakdown from ordinary reaction schemes is the reactivity of its intermediate products. This makes the outcome of pyrolysis experiments sensitive to reactor and sample configuration. The review cites several examples of reactors which allow distinguishing between the pyrolytic behavior of the fuel and effects arising from the configuration of the experiment itself.

Initial Stages of Thermal Breakdown. For any given sample, however, covalent bond cleavage in carbonaceous materials is taken to be a function of temperature alone. Electron resonance spectroscopy (ESR) has been used to observe the onset of covalent bond cleavage, near 310 °C for a lignite, rising to 340 °C with increasing coal rank. When a particular sample is heated, we expect the initial stages of pyrolysis and liquefaction to present similar patterns of covalent bond cleavage.

In liquefaction, rapid release of extracts into the surrounding solvent was observed to take place above 350−375 °C. The temperature delay between the *onset* of covalent bond scission (310−340 °C) and more intense dissolution suggests that several covalent bonds must break before larger molecular mass materials can detach from the solid matrix.

During liquefaction at 400 °C, up to 40−50% of the coal mass can dissolve (depending on the coal) in the liquid medium. By contrast, at 400 °C weight loss during dry pyrolysis rarely exceeds several percent of the initial mass. The pathways of pyrolysis and liquefaction begin to diverge, therefore, during the accumulation phase of solvent extractables (tar precursors) within the particles. In liquefaction, the solvent serves to remove most of the extractables from the coal particles. During the early stages of (dry) pyrolysis in a gaseous medium, however, accumulated extractables remain inside the coal particles. The extractables content of particles (dry) heated to

dx.doi.org/10.1021/cr400194p | *Chem. Rev.* 2014, 114, 1547−1607

about 400 °C was found to be as high as 65−80% depending on the coal.

Clear relationships have been observed, furthermore, between the plasticity of coals at a given temperature and the extractable *content* of the coal particles.

Effect of Rapid Heating. There is clear evidence showing that middle-rank coals heated at rates faster that 500 °C s^{-1} to temperatures of 375 °C or above tend to (i) enhance the proportion of solvent extractables (tar precursors) released within coal particles, (ii) enhance the plasticity of the sample, and (iii) give rise to higher eventual tar yields when the samples are heated to 700 °C and beyond.

As covalent bond cleavage is primarily a function of temperature, given sufficient time at peak temperature for reactions to reach completion, we expect similar patterns of bond cleavage and similar amounts of potential extractables initially released within coal particles at any given temperature irrespective of the heating rate. The observed differences in extractable yields between fast and slow heating are thus explained in terms of more intense char-forming recombination reactions taking place during slow heating to 400 °C. However, these observations do not explain why fewer retrogressive reactions take place during rapid heating.

Explaining How High Heating Rates Work. Fast heating tends to telescope the sequence of pyrolytic events into a narrower time frame and shift the temperature scale of pyrolytic events to higher temperatures. For several coals tested, this upward shift ranged between 90 and 140 °C. It is thought that during rapid heating the internal release of hydrogen temporally overlaps more thoroughly with processes of covalent bond cleavage. The pyrolyzing mass may thus be able to assimilate internally released hydrogen more effectively and quench (cap) more of the reactive free radicals.

There are two likely sources for internally released hydrogen. During slow heating, low-level release of molecular hydrogen from pyrolyzing coals can be measured relatively easily from about 285−300 °C. During fast heating, released hydrogen would be more likely to remain in contact with the pyrolyzing coal mass.

Second, it is thought that internally released donatable hydrogen plays a role that is analogous to donor solvents (e.g., tetralin) during liquefaction in effectively blocking potentially char-forming free-radical recombination reactions. In coals, donatable hydrogen is thought to originate from the hydroaromatic component. Experimental data has been presented indicating direct links between hydroaromatic content and increasing tar and total volatile yields. In rapid heating, thermal activation of hydrogen-donor activity can overlap with covalent bond cleavage and block free-radical recombination reactions more effectively. More efficient hydrogen release to the pyrolyzing coal would thus explain the enhanced plasticity of weakly coking coals during rapid heating and the resulting increase in tar and total volatiles yields

The accumulated evidence indicates that weakly coking coals show greater sensitivity to increasing heating rates. Such coals tend to be marginally deficient in hydrogen. Meanwhile, good coking coals present high proportions of extractables (tar precursors) and show high levels of plasticity irrespective of the heating rate. The composition of such coals suggests they initially contain sufficiently high amounts of donatable hydrogen to ensure melting and usually also have relatively low contents of hydrogen-scavenging elements such as oxygen and sulfur.

Fast and Slow Free-Radical Recombination Reactions in Thermal Breakdown. *Rapid Recombination Reactions in Pyrolysis.* During slow heating (slower than 500 °C s^{-1}) more retrogressive char formation is observed to take place. The effect is observed more clearly in coals that are marginally deficient in hydrogen. It appears to be due to internally released hydrogen escaping before intense covalent bond-cleavage reaction temperatures are reached.

Slow Recombination Reactions in Pyrolysis. Extractables that survive heating to 400 °C within coal particles were found to be chemically stable for at least 120 s and possibly longer. Recombination reactions making fresh char were observed to proceed only slowly as the temperature was raised to 450 °C and beyond.

Rapid Recombination Reactions in Liquefaction. A flowing-solvent liquefaction reactor has been described, where dissolved extracts are continuously carried out of the reaction zone. The difference in conversion, in this reactor, between H-donor and nondonor solvents is thought to arise from the outcome of short-range interactions between freshly formed free radicals during the covalent bond-cleavage phase. In the absence of sufficient locally available hydrogen more frequent rapid char-forming recombination reactions result from such short-range interactions. In the presence of a hydrogen-donor solvent, such as tetralin, greater extract yields (about 10%) are obtained compared to liquefaction in a stronger solvent, which however is not a hydrogen donor (e.g., quinoline, anthracene).

Slow Recombination Reactions in Liquefaction. During liquefaction in non-H-donor solvents in batch reactors, initial rapid dissolution of coal-derived material results in rising concentrations of partially reactive products in close proximity, dissolved in the non-H-donor solvent. With increasing time at temperature during liquefaction in 1-methylnaphthalene already dissolved extracts were observed to form solids at 450 °C at a very slow rate (12−13% in 25 min).

Observations from carefully designed pyrolysis and liquefaction experiments have thus provided evidence for reactions of free radicals with broad ranges of reactivities.

Reference Points for Biomass Pyrolysis. There are compelling reasons for reviewing fundamental aspects of lignocellulosic biomass pyrolysis alongside thermal breakdown in middle-rank coals. Coal and biomass pyrolysis experiments present a level of similarity that is unusual among nominally distinct fields of research. In this review, the outline of biomass pyrolysis research has been presented in a manner that is inclusive of what may be learned from work on both coals and biomass.

Data on the pyrolytic behavior of cellulose and lignin embedded within naturally occurring biomass has been reviewed. Taken together, the evidence suggests that these components do not pyrolyze independently during thermal breakdown of lignocellulosic biomass. One important result was the observation that the pyrolysis chemistry of pure (prepared) lignins follows entirely different reaction pathways from naturally occurring lignin embedded in the composite matrices of naturally occurring lignocellulosic biomass.

Several layers of evidence have been reviewed showing the extent and nature of synergistic effects and how they depend on the manner in which the components are enmeshed in particular plant material or laboratory-made particles. The evidence shows the contribution to synergistic effects of different breakdown temperature ranges of distinct biomass components and of their distinct tar-cracking reactivities.

However, relatively few built experiments seem to have been designed to explore the equally complex roles of hemicelluloses, resins, and mineral matter on the overall pyrolytic process.

The evidence presented suggests we are yet some distance away from fully grasping the role of key factors that shape some of the observed trends. Attempting to work with ab initio mathematical models (simulations) of the chemistry of the pyrolysis of individual biomass components does not seem realistic.

It appears possible, nevertheless, to develop pyrolytic databases for samples of interest from carefully conceived bench-scale pyrolysis experiments that would feed data into the design and simulation of pilot- and plant-sized equipment. It seems necessary, however, to also devise experiments able to quantify the sequence of reactions of the released volatile products as they move through large reactors. Some examples have been provided in this review.

Upgrading Biomass Pyrolysis Tars/Oils. Between 50% and 70% of solid biomass may be converted to liquid-phase products by pyrolysis. The question is what to do with this liquid, apart from direct combustion or injection into modified diesel engines for power production. The latter provide reasonable alternatives in the absence of processes to make transport fuels or other higher value products.

In efforts to upgrade coal liquids, cracking large polynuclear aromatic ring systems through reaction pathways that would produce smaller and more useful aromatic molecules has remained as one of the major challenges. Due to smaller ring system sizes, this does not appear to be a problem in processing biomass pyrolysis tars/oils. A brief review of the literature on upgrading biomass liquids indicates, on the other hand, that significant carbon fouling and coke formation nevertheless remain common to many catalytic processes intended for upgrading biomass-derived tars/oils.

In the case of NiMo and CoMo catalysts, coking seems to persist despite application of expensive high-pressure hydrogen. ZSM-5 and similar zeolite catalysts have tended to improve conversions of tars/oils to limited extents, although high rates of gas formation and rapid catalyst deactivation remain as major challenges. More generally, it has proved difficult to devise reaction pathways for breaking down large tar/oil molecules in measured steps, which would allow making more of the middle-distillate quality products, needed for preparing transport-grade fuels or fuel additives. Instead, large tar/oil molecules tend to disintegrate, mostly giving water, carbon oxides, methane, and char. Results from a wide range of experiments suggest that this disintegration might be a thermodynamically favored route for the highly oxygenated, labile structures of biomass tars/oils. It may yet prove useful, however, to investigate combinations of less intense reaction conditions coupled to the use of hitherto untried catalysts or catalytic processing schemes. The latter have not seemed much in evidence, perhaps because commercial demand for catalysts specifically designed for upgrading biomass pyrolysis liquids has been limited.

Tracking the Course of Thermochemical Reactions. One way to broaden the scope of the investigation was by characterizing the liquid products of thermal breakdown.

Successive Extract Fractions Released from Coals. Molecular mass distributions and structural features of successive extract fractions released from coal particles in the flowing-solvent liquefaction reactor were examined. Size exclusion chromatography (SEC) as well as UV-fluorescence and FT-IR spectroscopy were used as primary tools in these characterizations. Overall, the thermal breakdown process tended to release progressively larger and more aromatic molecular fragments into the liquid phase as a function of increasing reactor temperature and time at temperature.

In the second example, results from characterization of a coal tar pitch were compared with those from the solvent-separated fractions of the same sample. When complex, polydispersed samples are characterized in a single analytical step, the whole sample tends to display the properties of the more abundant material within the sample mixture or show more of the fraction that is more amenable to analysis by the particular technique. Fractionation tends to side step these difficulties by preventing the more abundant materials from masking signal from the rest of the sample. Characterization of sample fractions in isolation tends to lend access to more detailed information about structural features and molecular mass distributions. The results provided a powerful argument for the necessity of fractionation prior to characterization of complex samples.

The two sets of selected experiments tested these well-known analytical methods to their limits in characterizing these complex liquids. Despite shortcomings in molecular mass determinations outlined in the main text, it was possible to conclude that the order of increasing molecular masses between individual fractions identified by size exclusion chromatography and LD-MS was closely matched by increasing sizes of PNA ring systems. However, available analytical tools did not allow PNA ring system sizes or the proportions of alicyclic (hydroaromatic) carbon contents to be estimated reliably. Moreover, solid-state ^{13}C NMR could not be used reliably to discern the relatively small changes in aromaticity between different pitch fractions, which were being sought.

Analytical Method Development. A review of analytical methods used for characterizing complex polydispersed heavy hydrocarbons was recently presented in this journal.[135] The two strands of recent advances in this area have involved refining LD-MS determinations of molecular mass distributions and in the improvement of solution-state NMR methods in estimating average structural parameters.

Molecular Mass Determinations. Samples were fractionated by planar chromatography. Cut pieces of the PC plates bearing the several dispersed fractions were then introduced into the spectrometer as the target. The procedure aimed to achieve two objectives: (i) to reduce masking of signal from the less abundant material by the more abundant material; (ii) to reduce sample loading by thinly spreading the sample onto the PC plate to produce low gas-phase sample concentrations at the ion extraction stage. The technique was found to suppress secondary cluster ion formation and improve the reproducibility of the spectra.

Overall, good agreement was observed up to about m/z 3000 between SEC and MALDI and LD-MS. The techniques are independent, suggesting that up to this limit SEC may be safely considered as a quantitative tool. As observed with the calibration curves, the accuracy of the SEC measurement appears subject to greater uncertainty with increasing molecular mass. The agreement obtained between these two independent techniques singled out the combination of SEC and LD-MS measurements as the most effective method currently available for estimating molecular mass distributions. The findings strongly suggested, however, that upper mass limits of the LD-MS method had effectively been reached for characterizing

dx.doi.org/10.1021/cr400194p | Chem. Rev. 2014, 114, 1547−1607

the pyridine-insoluble (i.e., heaviest) fraction of the pitch sample.

Structural Characterization of Thermal Breakdown Products. NMP and quinoline are capable of nearly completely dissolving coal-derived liquids in the high concentrations required for NMR analysis. In order to reduce errors and improve the quality of NMR spectra, high-resolution solution-state ^{1}H and ^{13}C NMR methods were optimized and calibrated. Undeuterated quinoline (to show the aliphatic zone) and NMP (to show the aromatic zone) were used as solvents. The modifications included the use of coaxial NMR tubes to isolate the lock solvent from the actual sample solution. The improved resolution of the spectra made it possible to calculate average structural parameters for all subfractions of the samples analyzed.

The parameters calculated for the pitch-acetone-soluble fraction were not greatly affected using the improved average molecular mass values. ASP calculations for the pitch-pyridine-soluble (but acetone-insoluble) and pyridine-insoluble fractions were more sensitive to the improved average molecular mass (M_n) estimates.

The M_n for the acetone-soluble pitch fraction arrived at with the PC-assisted LD-MS method was determined to be about 550 u. On this basis, an average molecule was calculated to contain approximately four aromatic rings (R_A) and three naphthenic rings (R_N). The average molecule also contained less than 10% of the total carbon in cata-condensed environments. Fourteen percent of the total carbon was calculated to be aromatic carbon substituted with aromatic groups ($C_{ar\text{-}AS}$). About 15% of the carbon was found in peri-condensed and 48% in protonated aromatic carbon ($C_{ar\text{-}US}$) environments. The remainder of the carbon (12%) was in alkyl groups attached to aromatics

Using an M_n value of 1600 u for the PPS sample, the average molecule was found to contain about 21 aromatic rings (R_A), alongside an average of 2 naphthenic rings per molecule. C_{Cata} was ~14% of the total carbon; $C_{ar\text{-}AS} \approx 12\%$. Peri-condensed carbon accounted for ~20% and protonated aromatic carbon for about 40% of the total.

For the PPI sample, where M_n was assumed to be 6000 u, the average molecule was found to contain about 100 aromatic rings (R_A) and an average of about seven naphthenic rings per molecule (R_N). C_{Cata} was nearly ~33% of the total carbon, $C_{ar\text{-}AS} \approx 0\%$, while peri-condensed carbon accounted for ~30% and protonated-aromatic carbon ~34%.

The apparent precision of the numerical results notwithstanding, results from ASP calculations for such complex samples need to be treated as rough guides to underlying trends, which provide qualitative information regarding changes in structure that are difficult to determine in any other way.

Use of this methodology was used to explain the structural differences between cokes made from two different types of pitch. ASP parameters calculated for a synthetic pitch made from polymerizing waste anthracene oil suggested the predominance of large planar molecules, representing continental-type fused-ring PNA ring systems. On heating, this pitch readily generated mesophase. On further heating, the mesophase led to a coke with a fluid-domain optical texture that was indicative of large areas of fused aromatic ring systems in the form of pregraphitic structures.

By contrast, polymerization of an anthracene oil residue, which appeared (by ASP calculations) to contain smaller fused-ring PNA ring systems, gave rise to a pitch, which ASP calculations suggested was more cross-linked and contained smaller island-type fused-ring structures. This second pitch generated lower quantities of mesophase. On further heating, a less ordered coke was produced containing smaller regions of fused aromatic ring systems that had a mosaic optical texture. ASP calculations based on more recent analytical procedures thus appeared to predict correct trends in pitch and coke formation.

AUTHOR INFORMATION

Corresponding Author

*E-mail: morgatr@gmail.com, morgantr@hawaii.edu.

Notes

The authors declare no competing financial interest.

Biographies

Trevor James Morgan received his Ph.D. degree from Imperial College London in 2008 under Professor R. Kandiyoti (Chemical Engineering Department). The subject was development and application of analytical chemistry methods to complex (heavy) coal and petroleum-derived materials. Prior to this he worked with the same research group for 8 years, providing research−technical support. After completing his Ph.D. degree he worked as a consultant to one of the major oil companies to develop analytical chemistry methods. This was followed by postdoctoral positions at Imperial College London with Professor R. Kandiyoti on the analytical chemical aspects of fuel conversion and with Professors D. Dugwell and J. Hewitt on deposition in crude oil heat exchangers. He moved to the European Commission−Joint Research Centre−Institute for Energy, the Netherlands, in 2009, where he was lead scientist on gasification of biomass and development of related analytical chemistry methods. Now he is working on gas pyrolysis and gasification of tropical biomass, agricultural by-products, and waste materials at the Hawaii Natural Energy Institute, University of Hawaii at Manoa, with Dr. Scott Turn. He will continue to pursue his interest in analytical methods related to thermochemical processes.

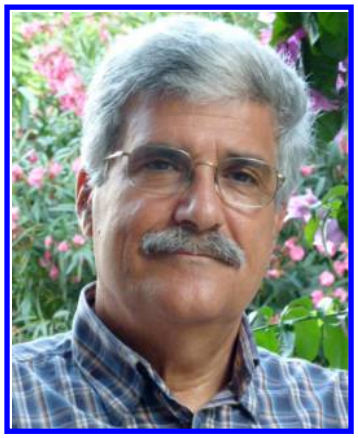

R. Kandiyoti received his B.S. degree in Chemical Engineering from Columbia University in New York (1965) and his Ph.D. degree from the University of London (Imperial College 1969). He served as faculty in the Chemical Engineering Departments of the Middle East Technical University (Ankara, Turkey, 1969−72) and Boğaziçi University (Istanbul, Turkey, 1974−80) before joining Imperial College London (1980), where he served as Lecturer, Senior Lecturer, Reader, and Professor of Chemical Engineering and as coordinator of the Energy Engineering Group. On retirement in September 2008, he was appointed as Distinguished Research Fellow in the same Department. He has worked in the general area of fuels and energy, where he has authored or coauthored over 350 publications on topics relating to experimental reactor design for thermochemical characterization of fossil fuels, biomass, and waste as well as on analytical methods for characterization of heavy hydrocarbon liquids and environmental aspects of power generation. His books include *Solid Fuels and Heavy Hydrocarbon Liquids: Thermal Characterization and Analysis*, *Fundamentals of Reaction Engineering*, and *Pipelines: Flowing oil and crude politics*.

REFERENCES

(1) *IEA Coal Information*; International Energy Agency: Paris, 2011, ISBN-978-92-64-10209-5; pp III.15− III. 23.
(2) *BP Statistical Review*; 2012; Coal Production http://www.bp.com/sectiongenericarticle800.do?categoryId=9037184&contentId=7068603.
(3) *Medium-Term Coal Market Report*; International Energy Agency: Paris, 2012; ISBN: 9789264177963 (PDF) ; 9789264177956 (print).
(4) *IEA Press Release*; Dec 17, 2012; http://www.iea.org/newsroomandevents/pressreleases/2012/december/name,34441,en.html.
(5) Haga, T.; Katoh, K.; Ibaraki, T. *Nippon Steel Technical Report No. 101*; Nov 2012; http://www.nssmc.com/en/tech/report/nsc/pdf/NSTR101-31_tech_review-5-2.pdf.
(6) Jones, A. *Global Steel Conference*, New Delhi, India; Jan 2011; http://cdn.steelonthenet.com/kb/files/world_coke_coking_coal_markets_2011.pdf.
(7) van der Horst, D.; Sinclair, P. In *Biomass and Bioenergy New Research*; Brenes, M.D., Ed.; Nova Science Publishers: Hauppauge, NY, 2006; Chapter 11, p 275.
(8) Babu, B. V. *Biofuels, Bioprod. Biorefin.* **2008**, *2*, 393.
(9) Bridgewater, A. V. *Biomass Bioenergy* **2012**, *38*, 68.
(10) Peterson, A. A.; Vogel, F.; Lachance, R. P.; Fröling, M.; Antal, M. J.; Tester, J. W. *Energy Environ. Sci.* **2008**, *1*, 32.
(11) Serio, M. A.; Kroo, E.; Wójtowicz, M. A. *Prepr. Pap.—Am. Chem. Soc., Div. Fuel Chem.* **2003**, *48*, 584.
(12) In *Chemistry of Coal Utilization*; Lowry, H. H., Ed.; John Wiley and Sons: New York, 1963; Supplementary Vol. *1*, Chapters 4, 9, 10, 11, pp 13−15.
(13) *Chemistry of Coal Utilization*; Elliott, M. A., Ed.; John Wiley and Sons: New York, 1981; Supplementary Vol. *2*, Chapters 6, 8, pp 11−18.
(14) Burke, F. P.; Brandes, S. D.; McCoy, D. C.; Winschel, R. A.; Gray, D.; Tomlinson, G. *Summary Report of the DoE Direct Liquefaction Process Development Campaign of the late 20th Century (DOE/PC 93054-94)*; July 2011, DOE Contract DE-AC22-94PC93054; http://www.osti.gov/bridge/servlets/purl/794281-khohbO/native/794281.pdf
(15) Geerdes, M.; Toxopeus, H.; Van Der Vliet, C. *Modern Blast Furnace Ironmaking*; Delft University Press: The Netherlands, 2009; ISBN 978-1-60750-040-7.
(16) Valia, H. S. *Steelworks*; http://www.steel.org/en/Making%20Steel/How%20Its%20Made/Processes/Processes%20Info/Coke%20Production%20For%20Blast%20Furnace%20Ironmaking.aspx.
(17) King, D. L.; de Klerk, A. *Synthetic Liquids Production and Refining*; ACS Symposium Series; American Chemical Society: Washington, DC, 2011; Chapter 1; http://pubs.acs.org/doi/pdf/10.1021/bk-2011-1084.ch001.
(18) Bunt, J. R.; Waanders, F. B. *Fuel* **2008**, *87*, 1751.
(19) Bunt, J. R.; Waanders, F. B. *Fuel* **2008**, *87*, 2374.
(20) Hindman, M. *World CTL Conference*, Beijing, April 13−15, 2010;http://www.exxonmobil.com/apps/refiningtechnologies/files/conference_2011.1204.MTG_World_CTL.pdf.
(21) Sills, R. *North American Gas Seminar*, Houston, TX, Mar 6, 2012; http://www.xtlinstitute.com/Issues_Affecting_XTL_Projects_Houston_March_2012.pdf.
(22) *2012 NETL CO_2 Capture Technology Meeting*, Pittsburgh, PA, July 9−12, 2012; http://www.netl.doe.gov/publications/proceedings/12/co2capture/presentations/1-Monday/Z%20Ye-Shenhua%20Group-Demonstration%20Project.pdf.
(23) van Krevelen, D. W. *Coal: Typology, Physics, Chemistry, Constitution*; Elsevier: Amsterdam, 1993; ISBN 0 444 89586 8.
(24) Mochida, I.; Moriguchi, Y.; Shimohara, T.; Korai, Y.; Fujitsu, H.; Takeshita, K. *Fuel* **1982**, *61*, 1014.
(25) Li, C.-Z. *Advances in the Science of Victorian Brown Coal*: Elsevier: Amsterdam, 2004; p 409.
(26) Harrison, J. S.; Kimber, G. M.; Gray, M. D. *Int. Conf. Coal Sci., Tokyo* **1989**, *II*, 655.
(27) Moore, S. A.; Jones, M. A.; Kimber, G. M. *Int. Conf. Coal Sci., Tokyo* **1989**, *II*, 663.
(28) Kimber, G. M. A history of UK coal liquefaction, *ETSU/DTI Report No. Coal R078*, UK Department of Trade and Industry: London, 1997.
(29) Yao, Z.-S.; Wei, X.-Y.; Lu, J.; Liu, F.-J.; Huang, Y.-G.; Xu, J. J.; Chen, F.-J.; Huang, Y.; Li, Y.; Lu, Y.; Zong, Z.-M. *Energy Fuels* **2010**, *24*, 1801.
(30) Stanislaus, A.; Cooper, B. H. *Catal. Rev. Sci. Eng.* **1994**, *36*, 75.
(31) http://www.chemicals-technology.com/projects/uop-biorefinery-demonstration-facility/, Sept 2012. Also, Rekoske, J. (UOP) Personal communication, Sept 2012.
(32) Rabou, L. P. L.; Zwart, R. W. R.; Vreugdenhil, B. J.; Bos, L. *Energy Fuels* **2009**, *23*, 6189.
(33) http://www.ensyn.com/wp-content/uploads/2011/04/EC-Corp-PPT-April-2011.pdf.
(34) http://www.btg-btl.com/index.php?r=faq#Question 8.
(35) Iribarren, D.; Peters, J. F.; Dufour, J. *Fuel* **2012**, *97* (0), 812.
(36) Paterson, N.; Elphick, S.; Dugwell, D. R.; Kandiyoti, R. *Energy Fuels* **2001**, *15*, 894.
(37) Paterson, N.; Zhuo, Y.; Dugwell, D. R.; Kandiyoti, R. *Energy Fuels* **2002**, *16*, 127.
(38) Zhuo, Y.; Paterson, N.; Avid, B.; Dugwell, D. R.; Kandiyoti, R. *Energy Fuels* **2002**, *16*, 742.
(39) Stach, E.; Mackowsky, M. T.; Teichmüller, M.; Taylor, G. H.; Chandra, D.; Teichmüller, R. *Stach's Textbook of Coal Petrology*; Gebrüder Borntraeger:Berlin, Stuttgart, 1982.

(40) Rouzaud, J. N. ; Oberlin, A., The characterization of coals and cokes by Transmission Electron Microscopy. In *Advanced methodologies in coal characterization*; Charcosset, H., Nickel-Pepin-Donat, B., Eds.; Elsevier: Amsterdam, 1990; Chapter 17, pp 311−355.
(41) Singer, L. S. *Proceedings of the Conference on Carbon, 1961*, 5th ed.; Pergamon Press: New York, 1963; p 37.
(42) Singer, L. S.; Lewis, I. C. *Carbon* **1978**, *16*, 417.
(43) Lewis, I. C.; Singer, L. S. In *Chemistry and Physics of Carbon*; Walker, P. L., Thrower, P. A., Eds.; Marcel Dekker: New York and Basel, 1981; Vol. *17*, p 1.
(44) Singer, L. S.; Lewis, I. C. *Appl. Spectrosc.* **1982**, *36*, 52.
(45) Fowler, T. G.; Bartle, K. D.; Kandiyoti, R. *Carbon* **1987**, *25*, 709.
(46) Fowler, T. G.; Bartle, K. D.; Kandiyoti, R. *Energy Fuels* **1989**, *3*, 515.
(47) Retcofsky, H. L.; Hough, M. R.; Maguire, M. M.; Clarkson, R. B. *Appl. Spectrosc.* **1982**, *36*, 187.
(48) Sprecher, R. F.; Retcofskv, H. L. *Fuel* **1983**, *62*, 473.
(49) Fowler, T. G.; Kandiyoti, R.; Bartle, K. D.; Taylor, N. *Proc. Int. Conf. Coal Sci.* **1987**, 617.
(50) Fowler, T. G.; Bartle, K. D.; Kandiyoti, R. *Fuel* **1988**, *67*, 173.
(51) Fowler, T. G.; Kandiyoti, R.; Bartle, K. D.; Taylor, N. *Proc. Int. Conf. Coal Sci.* **1987**, 617.
(52) Fowler, T. G.; Kandiyoti, R.; Bartle, K. D.; Snape, C. E. *Carbon* **1989**, *27*, 197.
(53) Xu, B.; Kandiyoti, R. *Energy Fuels* **1996**, *10*, 1115.
(54) Xu, B.; Madrali, E. S.; Wu, F.; Li, C.-Z.; Herod, A. A.; Kandiyoti, R. *Energy Fuels* **1994**, *8*, 1360.
(55) Li, C.-Z.; Wu, F.; Xu, B.; Kandiyoti, R. *Fuel* **1995**, *74*, 37.
(56) Gibbins, J. R.; Kandiyoti, R. *Fuel* **1989**, *68*, 895.
(57) Li, C.-Z.; Bartle, K. D.; Kandiyoti, R. *Fuel* **1993**, *72*, 1459.
(58) Griffiths, D. M. L.; Mainhood, J. S. R *Fuel* **1967**, *46*, 167.
(59) Gonenc, Z. S.; Gibbins, J. R.; Katheklakis, I. E.; Kandiyoti, R. *Fuel* **1990**, *69*, 383.
(60) Stiles, H. N.; Kandiyoti, R. *Fuel* **1989**, *68*, 275.
(61) Kandiyoti, R. *Fuel* **2002**, *81*, 975.
(62) Kandiyoti, R.; Herod, A. A.; Bartle, K. D. *Solid Fuels and Heavy Hydrocarbon Liquids: Thermal Characterization and Analysis*; Elsevier Science Publishers: Amsterdam, Oxford, London, New York, 2006; pp 38−40.
(63) Loison, R.; Chauvin, R. *Chim. Ind. Paris* **1964**, *91*, 269.
(64) Howard, J. B. In *Chemistry of Coal Utilization, Second Supplementary Volume*; Elliott, M. M., Ed.; Wiley: New York, 1981; p 665.
(65) Li, C.-Z.; Bartle, K. D.; Kandiyoti, R. *Fuel* **1993**, *72*, 3.
(66) Peralta, D.; Paterson, N.; Dugwell, D.; Kandiyoti, R. *Energy Fuels* **2005**, *19*, 532.
(67) Güell, A. J.; Kandiyoti, R. *Energy Fuels* **1993**, *7*, 943.
(68) Messenböck, R. C.; Dugwell, D. R.; Kandiyoti, R. *Energy Fuels* **1999**, *13*, 122.
(69) Gao, L.; Paterson, N.; Fennel, P.; Dugwell, D. R.; Kandiyoti, R. *Energy Fuels* **2008**, *22*, 2504.
(70) Wu, L.; Paterson, N.; Dugwell, D. R.; Kandiyoti, R. *Energy Fuels* **2007**, *21*, 2325.
(71) Brown, D. D.; Thomas, K. M. *Fuel* **1993**, *72*, 359.
(72) Gibbins-Matham, J. R.; Kandiyoti, R. *Energy Fuels* **1988**, *2*, 505.
(73) Vorres, K. S. *Energy Fuels* **1990**, *4*, 420.
(74) Habermehl, D.; Orywal, F.; Beyer, H. D. In *Chemistry of Coal Utilization, Second Supplementary Volume*; Elliott, M. M., Ed.; Wiley: New York, 1981; p 317.
(75) Song, C.; Nihomnatsu, T.; Nomura, M. *Ind. Eng. Chem. Res.* **1991**, *30*, 1526.
(76) Hamilton, L. H. *Fuel* **1980**, *59*, 112.
(77) Hamilton, L. H. *Fuel* **1981**, *60*, 909.
(78) Aramaki, T.; Arima, T.; Yamashita, Y.; Inaba, A. *Tetsu to Hagane* **1996**, *82*, 5.
(79) Friedel, R. A.; Shulz, J. L.; Sharkey, A. G. *Fuel* **1968**, *47*, 403.
(80) Kessler, T.; Friedel, R. A.; Sharkey, A. G. *Fuel* **1970**, *49*, 222.
(81) Howard, H. C. In *Chemistry of Coal Utilization*; Lowry, H. H., Ed.; John Wiley and Sons: New York, 1963; Supplementary Vol. *I*, p 342.
(82) Wender, I.; Heredy, L. A.; Neuworth, M. B.; Dryden, I. G. C. In *Chemistry of Coal Utilization*; Elliott, M. A., Ed.; John Wiley and Sons: New York, 1981; Supplementary Vol. *2*, p 479.
(83) Orchin, M.; Golumbic, C.; Anderson, J. E.; Storch, H. H. *Bulletin No. 505*; U.S. Bureau of Mines: Washington, DC, 1951.
(84) Dryden, I. G. C.; Pankhurst, K. S. *Fuel* **1955**, *34*, 363.
(85) Brown, H. R.; Waters, P. L. *Fuel* **1966**, *45*, 7.
(86) Brown, H. R.; Waters, P. L. *Fuel* **1966**, *45*, 41.
(87) Dryden, I. G. C.; Joy, W. K. *Fuel* **1961**, *40*, 473.
(88) Fong, W. S.; Khalil, Y. F.; Peters, W. A.; Howard, J. B. *Fuel* **1986**, *65*, 195.
(89) Fukuda, K.; Dugwell, D. R.; Herod, A. A.; Kandiyoti, R. *Energy Fuels* **2004**, *18*, 1140.
(90) Gray, V. R. *Fuel* **1988**, *67*, 1298.
(91) Wiser, W. *Fuel* **1968**, *47*, 475.
(92) Neavel, R. C. *Coal Science*; Academic Press: New York, 1981; p 1.
(93) Neuburg, H. J.; Kandiyoti, R.; O'Brien, R. J.; Fowler, T. G.; Bartle, K. D. *Fuel* **1987**, *66*, 486.
(94) Li, C.-Z.; Madrali, E. S.; Wu, F.; Xu, B.; Cai, H.-Y.; Güell, A. J.; Kandiyoti, R. *Fuel* **1994**, *73*, 851.
(95) Peover, M. E. *J. Chem. Soc.* **1960**, 5020.
(96) Reggel, L.; Wender, I.; Raymond, R. *Fuel* **1968**, *47*, 373.
(97) Reggel, L.; Wender, I.; Raymond, R. *Fuel* **1971**, *50*, 152.
(98) Reggel, L.; Wender, I.; Raymond, R. *Fuel* **1973**, *52*, 162.
(99) Álvarez, P.; Díez, N.; Blanco, C.; Santamaría, R.; Menéndez, R.; Granda, M. *Fuel* **2013**, *105*, 471.
(100) Gould, K. A.; Wiehe, I. A. *Energy Fuels* **2007**, *21*, 1199.
(101) Guo, A.; Wang, Z.; Zhang, H.; Zhang, X.; Wang, Z. *Energy Fuels* **2010**, *25*, 3093.
(102) Gibbins, J. R.; Kandiyoti, R. *Fuel Process. Technol.* **1990**, *24*, 237.
(103) Gibbins, J. R.; Kandiyoti, R. *Rev. Sci. Instrum.* **1991**, *62* (9), 2234.
(104) Gibbins, J. R.; Kandiyoti, R. *Fuel* **1991**, *70*, 909.
(105) Xu, B.; Dix, M.; Kandiyoti, R. *Rev. Sci. Instrum.* **1995**, *66* (7), 3966.
(106) Clarke, J. W.; Kimber, G. M.; Rantell, T. D.; Shipley, D. E. *ACS Symp. Ser.* **1980**, *139*, 111.
(107) Gibbins, J. R.; Kimber, G.; Gaines, A. F.; Kandiyoti, R. *Fuel* **1991**, *70*, 380.
(108) Begon, V.; Suelves, I.; Herod, A. A.; Dugwell, D. R.; Kandiyoti, R. *Fuel* **2000**, *79*, 1423.
(109) Somrang, Y. *Ph.D. Thesis*, Imperial College London: London, 2011.
(110) Czernik, S.; Johnson, D. K.; Black, S. *Biomass Bioenergy* **1994**, *7*, 187.
(111) George, A.; Lorente, E.; Berrueco, C.; Alvarez, P.; Millan, M.; Ungeheuer, J.; Andersen, L. K.; Morgan, T. J. *Energy Fuels* **2013**, *27* (7), 3786.
(112) Mettler, M. S.; Vlachos, D. G.; Dauenhauer, P. J. *Energy Environ. Sci.* **2012**, *5*, 7797.
(113) Solomon, P. R.; Serio, M. A.; Carangelo, R. M.; Markham, J. R. *Fuel* **1986**, *65*, 182.
(114) Fraga-Araujo, A. R. *Ph.D. Thesis*, University of London: London, 1990.
(115) Fraga, A. R.; Gaines, A. F.; Kandiyoti, R. *Fuel* **1991**, *70*, 803.
(116) Shafizadeh, F. *Adv. Carbohydr. Chem.* **1968**, *23*, 419.
(117) Shafizadeh, F.; Fu, Y. L. *Carbohydr. Res.* **1973**, *29*, 113.
(118) Antal, M. J.; Mochidzuki, K.; Paredes, L. S. *Ind. Eng. Chem. Res.* **2003**, *42*, 3690.
(119) Zaror, C. A.; Hutchings, I. S.; Pyle, D. L.; Stiles, H. N.; Kandiyoti, R. *Fuel* **1985**, *64*, 990.
(120) British Standard 1016, part 12; http://store.ihs.com/specsstore/controller?event=LINK_DOCDETAILS&getCurVer=false&docId=QGXUCAAAAAAAAAAA&mid=W097.

(121) Howard, J. B.; Anthony, D. B. *AIChE J.* **1976**, *22*, 625.
(122) Zhuo, Y.; Messenbock, R.; Collot, A.-G.; Paterson, N.; Dugwell, D. R.; Kandiyoti, R. *Fuel* **2000**, *79*, 793.
(123) Scott, S. C.; Piskorz, J. *Can. J. Chem. Eng.* **1982**, *60*, 666.
(124) Scott, S. C.; Piskorz, J. *Flash pyrolysis of biomass*; Ann Arbor Science Publisers: Ann Arbor, MI, 1982; Chapter 23.
(125) Scott, S. C.; Piskorz, J. *Can. J. Chem. Eng.* **1984**, *62*, 404.
(126) Scott, D. S.; Piskorz, J.; Radlein, D. *Ind. Eng. Chem. Process. Des. Dev.* **1985**, *24*, 581.
(127) Tyler, R. J. *Fuel* **1979**, *58*, 680.
(128) Tyler, R. J. *Fuel* **1980**, *59*, 218.
(129) Stiles, H. N. *Ph.D. Thesis*, University of London: London, 1986.
(130) Corella, J.; Toledo, J. M.; Padilla, R. *Ind. Eng. Chem. Res.* **2004**, *43*, 2433.
(131) Evans, R. J.; Milne, T. A. *Energy Fuels* **1987**, *1*, 123.
(132) Evans, R. J.; Milne, T. A. *Energy Fuels* **1987**, *1*, 311.
(133) Branca, C.; Giudicianni, P.; Blasi, C. D. *Ind. Eng. Chem. Res.* **2003**, *42*, 3190.
(134) Pindoria, R. V.; Lim, J.-Y.; Hawkes, J. E.; Lazaro, M.-J.; Herod, A. A.; Kandiyoti, R. *Fuel* **1997**, *76*, 1013.
(135) Herod, A. A.; Bartle, K. D.; Morgan, T. J.; Kandiyoti, R. *Chem. Rev.* **2012**, *112* (7), 3892.
(136) Hua-Jiang Huang, H.-J.; Ramaswamy, S.; Tschirner, U. W.; Ramarao, B. V. *Sep. Purif. Technol.* **2008**, *62*, 1.
(137) Vassilev, S. V.; Baxter, D.; Andersen, L. K.; Vassileva, C. G.; Morgan, T. J. *Fuel* **2012**, *94*, 1.
(138) Vassilev, S. V.; Baxter, D.; Andersen, L. K.; Vassileva, C. G. *Fuel* **2010**, *89*, 913.
(139) Gunther, C., Mosandl, A. The Composition of Oak and an Overview of its Influence on Maturation, 1986 (updated Aug 16, 2001); accessed Oct 16, 2012; http://homedistiller.org/oak.pdf.
(140) Vassilev, S. V.; Baxter, D.; Andersen, L. K.; Vassileva, C. G. *Fuel* **2013**, *105*, 40.
(141) Vassilev, S. V.; Baxter, D.; Andersen, L. K.; Vassileva, C. G. *Fuel* **2013**, *105*, 19.
(142) Shafizadeh, F. J. J. *Anal. Appl. Pyrol.* **1982**, *3*, 283.
(143) Li, J.-J. Isolation of Lignin from Wood. *Bachelor's Thesis*, Saimaa University of Applied Science: Imatra, Finland, 2011; p 14.
(144) Iatridis, B.; Gavalas, G. R. *Ind. Eng. Chem. Prod. Res. Dev.* **1979**, *18* (2), 127.
(145) Chan, R.W-C.; Krieger, B.B. J. *Appl. Polym. Sci.* **1981**, *26*, 1533.
(146) Nunn, T. R.; Howard, J. B.; Longwell, J. P.; Peters, W. A. *Ind. Eng. Chem. Process Des. Dev.* **1985**, *24*, 844.
(147) Caballero, J. A.; Font, R.; Marcilla, A. *J. Anal. Appl. Pyrol.* **1996**, *36*, 159.
(148) Ferdous, D.; Dalai, A. K.; Bej, S. K.; Thring, R. W. *Energy Fuels* **2002**, *16*, 1405.
(149) Wang, S.; Wang, K.; Liu, Q.; Gu, Y.; Luo, Z.; Cen, K.; Fransson, T. *Biotechnol. Adv.* **2009**, *27*, 562.
(150) de Wild, P.; Van der Laan, R.; Kloekhorst, A.; Heeres, E. *Environ. Prog. Sustainable Energy* **2009**, *28*, 461.
(151) Beis, S. H.; Mukkamala, S.; Hill, N.; Joseph, J.; Baker, C.; Jensen, B.; Stemmler, E. A.; Wheeler, M. C.; Frederick, B. G.; van Heiningen, A.; Berg, A. G.; DeSisto, W. J. *BioResources* **2010**, *5*, 1408.
(152) Guerra, A.; Filpponen, I. *J. Agric. Food Chem.* **2006**, *54*, 5939.
(153) Li, C.-Z.; Gaines, A. F.; Güell, A. J.; Kandiyoti, R. *Proc. Int. Conf. Coal Sci.* **1991**, 723.
(154) Dyrkacz, G. R.; Horwitz, E. P. *Fuel* **1982**, *61*, 3.
(155) Dyrkacz, G. R.; Bloomquist, C. A. A.; Ruscic, L. *Fuel* **1984**, *63*, 1367.
(156) Yang, H.; Yan, R.; Chen, H.; Lee, D.-H.; Zheng, C. *Fuel* **2007**, *86*, 1781.
(157) Couhert, C.; Commandre, J.-M.; Salvador, S. *Fuel* **2009**, *88*, 408.
(158) Collot, A.-G.; Zhuo, Y.; Dugwell, D. R.; Kandiyoti, R. *Fuel* **1999**, *78*, 667.
(159) Brownsort, P. A. *UKBRC Working Paper 5*; 2009; www.biochar.org.uk.
(160) Mohan, D.; Pittman, C. U., Jr.; Steele, P. H. *Energy Fuels* **2006**, *20*, 848.
(161) Brammer, J. G.; Bridgwater, A. V. *Renewable Sustainable Energy Rev.* **1999**, *3*, 243.
(162) Klass, D. L. *Biomass for Renewable Energy, Fuels and Chemicals*; Academic Press: San Diego, 1998.
(163) Mochida, I.; Sakanishi, K. *Adv. Catal.* **1994**, *40*, 39.
(164) Mochida, I.; Sakanishi, K. *Fuel* **2000**, *79*, 221.
(165) Li, J.; Yang, J.; Liu, Z. *Fuel Process. Technol.* **2009**, *90*, 490.
(166) Kan, T.; Wang, H.; He, H.; Li, C.; Zhang, S. *Fuel* **2011**, *90*, 3404.
(167) Lei, Z.; Gao, L.; Shui, H.; Chen, W.; Wang, Z.; Ren, S. *Fuel Process. Technol.* **2011**, *92*, 2055.
(168) Song, C.; Nihonmatsu, T.; Hanaoka, K.; Nomura, M. *Prepr. Pap.—Am. Chem. Soc., Div. Fuel Chem.* **1991**, *36*, 542.
(169) Song, C.; Nihomnatsu, T.; Nomura, M. *Ind. Eng. Chem. Res.* **1991**, *30*, 1526.
(170) Song, C.; Hanaoka, K.; Nomura, M. *Energy Fuels* **1992**, *6*, 619.
(171) Huber, G. W.; Iborra, S.; Corma, A. *Chem. Rev.* **2006**, *106*, 4044.
(172) Diebold, J. P. NREL 2000, NREL/SR-570-27613; Contract No. DE-AC36-99-GO10337.
(173) Pindoria, R. V.; Megaritis, A.; Herod, A. A.; Kandiyoti, R. *Fuel* **1998**, *77*, 1715.
(174) Furimsky, E. *Appl. Catal., A* **2000**, *199*, 147.
(175) Elliott, D. C.; Schiefelbein, G. F. *Prepr. Pap.—Am. Chem. Soc., Div. Fuel Chem.* **1989**, *34*, 1160.
(176) Sanna, A.; Andrésen, J. M. *ChemSusChem* **2012**, *5*, 1944.
(177) Huber, G. W., Vispute, T.P.; Routray, K. *Production of hydrogen, liquid fuels, and chemicals from catalytic processing of bio-oils*; University of Massachusetts: USA, 2010; p 54. Patent application.
(178) Boocock, D. G. B.; Konar, S. K.; Mackey, A.; Chang, P. T. C.; Liu, J. *Fuel* **1992**, *71*, 1291.
(179) Vispute, T. P.; et al. Renewable chemical commodity feedstocks from integrated catalytic processing of pyrolysis oils. *Science (Washington, DC)* **2010**. *330*, 1222.
(180) Baker, E. G.; Elliott, D. C., Catalytic hydrotreating of biomass-derived oils. In *Pyrolysis Oils from Biomass*; ACS Symposium Series 376; Soltes, J.; Milne., T. A., Eds.; American Chemical Society: Washington, DC, 1988; p 228.
(181) Baker, E. G.; Elliott, D. C. In *Research in Thermochemical Biomass Conversion*; Bridgewater, A. V.; Kuester., J. L., Eds.; Elsevier Applied Science: London and New York, 1988; p 883.
(182) Sharma, R. K.; Bakhshi, N. N. *Energy Fuels* **1993**, *7*, 306.
(183) Sharma, R. K.; Bakhshi, N. N. *Can. J. Chem. Eng.* **1991**, *69*, 1083.
(184) Sharma, R. K.; Bakhshi, N. N. *Can. J. Chem. Eng.* **1991**, *69*, 1071.
(185) Katikaneni, S. P. R.; Adjaye, J. D.; Bakhshi, N. N. *Energy Fuels* **1995**, *9*, 1065.
(186) Adjaye, J., Sharma, R.; Bakhshi, N. N. Upgrading of biomass-derived oils to fuels and chemicals: the effect of temperature. In *Energy from Biomass and Waste*; Klass, D. L., Ed.; Institute of Gas Technology: Chicago, 1991; Vol. *XV*, p 783.
(187) Jiang, J.; Yu, J.; Corma, A. *Angew. Chem., Int. Ed.* **2010**, *49*, 3120.
(188) Diebold, J. P.; Bridgewater, A. V.; Beckman, D.; Elliott, D. C.; Solantausta, Y. In *Advances in Thermochemical Biomass Conversion*; Bridgewater., A. V., Ed.; Blackie Academic and Professional: Glasgow, 1994; Vol. *2*, p1325.
(189) Diebold, J.; Scahill, J. In *Pyrolysis from Biomass*; ACS Symposium Series 376; Soltes, L.; Milne, T. A., Eds.; American Chemical Society: Washington, DC, 1988; Vol. 23, p 264.
(190) Diebold, J.; Phillips, S.; Tyndall, D.; Schaill, J.; Feik, C.; Czernik, S. *Prepr. Pap.—Am. Chem. Soc., Div. Fuel. Chem.* **1994**, *39*, 1042.
(191) Bain, R.; Diebold, J.; Overend, R.; Rejai, B.; Power, A. J. The production of reformulated gasoline components from biomass and

rdf. In *Energy from Biomass and Waste*; Klass, D. L., Ed.; Institute of Gas Technology: Chicago, IL, 1993; Vol. *XVI*, p 753.
(192) Agblevor, F. A.; Rejai, B.; Evans, R. J.; Johnson, K. D. Pyroltic analysis and catalytic upgrading of lignocellulosic materials by molecular beam mass spectrometry. In *Energy from Biomass and Waste*; Klass, D. L., Ed.; Institute of Gas Technology: Chicago, IL, 1993; Vol. *XVI*, p 767.
(193) Evans, R. J.. Milne, T. A. In *Pyrolysis Oils from Biomass*; ACS Symposium Series 376; Soltes, E. J.; Milne., R. J., Ed.; American Chemical Society: Washington, DC, 1988; p 311.
(194) Rejai, B.; Evans, R. J.; Milne, T. A.; Diebold, J. P.; Scahill, J. W. The conversion of biobased feedstocks to liquid fuels through pyrolysis. In *Energy from Biomass and Waste*; Klass, D. L., Ed.; Institute of Gas Technology:Chicago, IL, 1991; Vol. *XV*, p 855.
(195) Diebold, J.; Phillips, S.; Tyndall, D.; Scahill, J.; Feik, C.; Czernik, S. *Prepr. Pap.—Am. Chem. Soc., Div. Fuel Chem.* **1994**, *39*, 1043.
(196) Connors, W. J.; Johanson, L. N.; Sarkanen, K. V.; Winslow, P. *Holzforschung* **1980**, *34*, 29.
(197) Lappas, A. A.; Kalogiannis, K. G.; Iliopoulou, E. F.; Triantafyllidis, K. S.; Stefanidis, S. D. *WIREs Energy Environ.* **2012**, *1*, 285.
(198) Carlson, T. R.; Cheng, Y.-T.; Jae, J.; Huber, G. W. *Energy Environ. Sci.* **2011**, *4*, 145.
(199) Aho, A.; Kumar, N.; Lashkul, A. V.; Eranen, K.; Ziolek, M.; Decyk, P.; Salmi, T.; Holmbom, B.; Hupa, M.; Murzin, D. Y. *Fuel* **2010**, *89*, 1992.
(200) Foster, A. J.; et al. *Appl. Catal., A* **2012**, *423*−*424*, 154.
(201) Zhang, H.; et al. *Energy Environ. Sci.* **2011**, *4*, 2297.
(202) Zhang, H.; et al. *Green Chem.* **2012**, *14*, 98.
(203) Cheng, Y.-T.; et al. *Angew. Chem., Int. Ed. Engl.* **2012**, *51*, 11097.
(204) Zubkova, V. *Anal. Bioanal. Chem.* **2011**, *399*, 3193.
(205) Herod, A. A.; Bartle, K. D.; Kandiyoti, R. *Energy Fuels* **2007**, *21*, 2176.
(206) Herod, A. A. *Rapid Commun. Mass Spectrom.* **2010**, *24*, 2507.
(207) Karaca, F.; Islas, C. A.; Millan, M.; Behrouzi, M.; Morgan, T. J.; Herod, A. A.; Kandiyoti, R. *Energy Fuels* **2004**, *18*, 778.
(208) Paul-Dauphin, S.; Karaca, F.; Morgan, T. J.; Millan, M.; Herod, A. A.; Kandiyoti, R. *Energy Fuels* **2007**, *21*, 3484.
(209) Karaca, F.; Millan-Agorio, M.; Morgan, T. J.; Bull, I. D.; Herod, A. A.; Kandiyoti, R. *Oil Gas Sci. Technol.-Rev. Inst. Fr. Pet.* **2008**, *63*, 129.
(210) Berrueco, C.; Venditti, S.; Morgan, T. J.; Álvarez, P. P.; Millan, M.; Herod, A. A.; Kandiyoti, R. *Energy Fuels* **2008**, *22*, 3265.
(211) Zander, M.; Haenel, M. W. *Fuel* **1990**, *69*, 1206.
(212) Li, C.-Z.; Wu, F.; Cai, H.-Y.; Kandiyoti, R. *Energy Fuels* **1994**, *8*, 1039.
(213) Xu, B. *Ph.D. Thesis*, University of London: London, 1995.
(214) Bartle, K. D.; Taylor, N.; Mulligan, M. J.; Mills, D. G.; Gibson, C. *Fuel* **1983**, *62*, 1181.
(215) Li, C.-Z.; Bartle, K. D.; Kandiyoti, R. *Fuel* **1993**, *72*, 3.
(216) Nali, M.; Calemma, V.; Montanari, L. *Org. Mass Spectrom.* **1994**, *29*, 607.
(217) Herod, A. A.; Johnson, B. R.; Bartle, K. D.; Carter, D. M.; Cocksedge, M. J.; Domin, M.; Kandiyoti, R. *Rapid Commun. Mass Spectrom.* **1995**, *9*, 1446.
(218) Merdrignac, I.; Truchy, C.; Robert, E.; Guibard, I.; Kressmann, S. *Pet. Sci. Technol.* **2004**, *22*, 1003.
(219) Ben, H.; Ragauskas, A. J. *Energy Fuels* **2011**, *25*, 2322.
(220) Fahmi, R.; Bridgwater, A. V.; Donnison, I.; Yates, N.; Jones, J. M. *Fuel* **2008**, *87*, 1230.
(221) Li, J.; Yang, J.; Liu, Z. *Catal. Today* **2008**, *130*, 389.
(222) Herod, A. A.; Zhang, S.-F.; Johnson, B. R.; Bartle, K. D.; Kandiyoti, R. *Energy Fuels* **1996**, *10*, 743.
(223) Johnson, B. R.; Bartle, K. D.; Herod, A. A.; Kandiyoti, R. *J. Chromatogr., A* **1997**, *758*, 65.
(224) Herod, A. A.; Islas, C.; Lazaro, M. J.; Dubau, C.; Carter, J. F.; Kandiyoti, R. *Rapid Commun. Mass Spectrom.* **1999**, *13*, 201.
(225) Islas, C. A.; Suelves, I.; Li, W.; Morgan, T. J.; Herod, A. A.; Kandiyoti, R. *Fuel* **2003**, *82*, 1813.
(226) Groenzin, H.; Mullins, O. C. *Energy Fuels* **2000**, *14*, 677.
(227) Morgan, T. J.; Millan, M.; Behrouzi, M.; Herod, A. A.; Kandiyoti, R. 2005, *19*, 164
(228) Karaca, F.; Morgan, T. J.; George, A.; Bull, I. D.; Herod, A. A.; Millan, M.; Kandiyoti, R. *Rapid Commun. Mass Spectrom.* **2009**, *23*, 2087.
(229) Morgan, T. J. *Ph.D. Thesis*, University of London: London, 2008.
(230) Morgan, T. J.; George, A.; Davis, D. B.; Herod, A. A.; Kandiyoti, R. *Energy Fuels* **2008**, *22*, 1824.
(231) George, A.; Morgan, T. J.; Alvarez, P.; Millan, M.; Herod, A. A.; Kandiyoti, R. *Fuel* **2010**, *89*, 2953.
(232) Herod, A. A.; Kandiyoti, R.; Lazaro, M. J.; Dubau, C.; Richaud, R.; Shearman, J.; Card, J.; Jones, A. R.; Domin, M.; Suelves, I. *Energy Fuels* **2000**, *14*, 1009.
(233) Domin, M.; Li, S.; Lazaro, M. J.; Herod, A. A.; Larsen, J. W.; Kandiyoti, R. *Energy Fuels* **1998**, *12*, 485.
(234) Millan, M.; Morgan, T. J.; Behrouzi, M.; Karaca, F.; Galmes, C.; Herod, A. A.; Kandiyoti, R. *Rapid Commun. Mass Spectrom.* **2005**, *19*, 1867.
(235) Islas, C. A.; Suelves, I.; Millan, M.; Apicella, B.; Lazaro, M.-J.; Herod, A. A.; Kandiyoti, R. *J. Sep. Sci.* **2003**, *26*, 1422.
(236) Islas, C. A.; Suelves, I.; Apicella, B.; Herod, A. A.; Kandiyoti, R.; Carter, J. F.; Li, W. *Combust. Sci. Technol.* **2003**, *175*, 775.
(237) Li, W.; Morgan, T. J.; Herod, A. A.; Kandiyoti, R. *J. Chromatogr., A* **2004**, *1024*, 227.
(238) Herod, A. A.; George, A.; Islas, C. A.; Suelves, I.; Kandiyoti, R. *Energy Fuels* **2003**, *14*, 862.
(239) Karaca, F.; Behrouzi, M.; Morgan, T. J.; Herod, A. A.; Kandiyoti, R. *Energy Fuels* **2005**, *19*, 187.
(240) Islas, C. A.; Suelves, I.; Li, W.; Morgan, T. J.; Herod, A. A.; Kandiyoti, R. *Prepr. Pap.—Am. Chem. Soc., Div. Fuel Chem* **2002**, *47* (2), 647−648.
(241) Morgan, T. J.; George, A.; Alvarez, P.; Millan, M.; Herod, A. A.; Kandiyoti, R. *Energy Fuels* **2008**, *22*, 3275.
(242) Suelves, I.; Lazaro, M.-J.; Begon, V.; Morgan, T. J.; Herod, A. A.; Kandiyoti, R. *Energy Fuels* **2001**, *15*, 1153.
(243) Morgan, T. J.; George, A.; Alvarez-Rodriguez, P.; Millan, M.; Herod, A. A.; Kandiyoti, R. *J. Chromatogr., A* **2010**, *1217*, 3804.
(244) Strausz, O. P.; Safarik, I.; Lown, E. M.; Morales-Izquierdo, A. *Energy Fuels* **2008**, *22*, 1156.
(245) da Silva-Souza, R.; Nicodem, D E.; Garden, S. J.; Correa, R. J. *Energy Fuels* **2010**, *24*, 1135.
(246) Yamaguchi, Y.; Matsubara, Y.; Ochi, T.; Wakamiya, T.; Yoshida, Z. *J. Am. Chem. Soc.* **2008**, *130*, 13867.
(247) Hanson, K.; Roskop, L.; Djurovich, P. I.; Zahariev, F.; Gordon, M. S.; Thompson, M. E. J. *Am. Chem. Soc.* **2010**, *132*, 16247.
(248) Begon, V.; Islas, C. A.; Lazaro, M.-J.; Suelves, I.; Herod, A. A.; Dugwell, D. R.; Kandiyoti, R. *Eur. J. Mass Spectrom.* **2000**, *6*, 39.
(249) Mercedes Maroto-Valer, M.; Andrésen, J. M.; Dilcio Rocha, J.; Snape, C. E. *Fuel* **1996**, *75*, 1721.
(250) Solum, M. S.; Pugmire, R. J.; Grant, D. M. *Energy Fuels* **1989**, *3*, 187.
(251) Morgan, T. J.; Alvarez-Rodriguez, P.; George, A.; Herod, A. A.; Kandiyoti, R. *Energy Fuels* **2010**, *24*, 3977.
(252) Snape, C. E.; Ladner, W. R.; Bartle, K. D. *Fuel* **1985**, *64*, 1394.
(253) McKelvy, M. L.; Britt, T. R.; Davies, B. L.; Gillie, J. K.; Lentz, L. A.; Leugers, A.; Nyquist, R. A.; Putzig, C. L. *Anal. Chem.* **1996**, *68*, 93R.
(254) McKelvy, M. L.; Britt, T. R.; Davies, B. L.; Gillie, J. K.; Graves, F. B.; Lentz, L. A. *Anal. Chem.* **1998**, *70*, 119R.
(255) Gillie, J. K.; Hochlowski, J.; Arbuckle-Keil, G. A. *Anal. Chem.* **2000**, *72*, 71R.
(256) Guillen, M. D.; Iglesias, M. J.; Dominguez, A.; Blanco, C. G. *Energy Fuels* **1992**, *6*, 518.
(257) Guillén, M. D.; Iglesias, M. J.; Domínguez, A.; Blanco, C. G. *Fuel* **1995**, *74*, 1595.

(258) Socrates, G. *Infrared and Raman Characteristic Group Frequencies: Tables and Charts*, 3rd ed.; Wiley: New York, 2001.
(259) Painter, P. C.; Coleman, W. M. *Fuel* **1979**, *58*, 301.
(260) Krzton, A.; Cagniant, D.; Gruber, R.; Pajak, V.; Fortin, F.; Rouzaud, J.-N. *Fuel* **1995**, *74*, 217.
(261) Sobkowiak, M.; Painter, P. C. *Fuel* **1992**, *71*, 1105.
(262) Parker, J. E.; Johnson, C. A. F.; John, P.; Smith, G. P.; Herod, A. A.; Stokes, B. J.; Kandiyoti, R. *Fuel* **1993**, *72*, 1381.
(263) Herod, A. A.; Ladner, W. R.; Stokes, B. J.; Berry, A. J.; Games, D. E.; Hohn, M. *Fuel* **1987**, *66*, 935.
(264) Herod, A. A.; Ladner, W. R.; Stokes, B. J.; Major, H. J.; Fairbrother, A. *Analyst* **1988**, *113*, 797.
(265) Herod, A. A.; Stokes, B. J.; Schulten, H.-.R. *Fuel* **1993**, *72*, 31.
(266) Bartle, K. D. *Handbook of Polycyclic Aromatic Hydrocarbons*; Marcel Dekker: New York, 1985; Vol. 2, Chapter 6.
(267) Romanowski, T.; Funcke, W.; Grossmann, I.; Koenig, J.; Balfanz, E. *Anal. Chem.* **1983**, *55*, 1030.
(268) Herod, A. A.; Millan, M.; Morgan, T.; Li, W.; Feng, J.; Kandiyoti, R. *Eur. J. Mass Spectrom.* **2005**, *11*, 429.
(269) Herod, A. A.; Kandiyoti, R. *J. Chromatogr., A* **1995**, *708*, 143.
(270) Wu, Z. G.; Rodgers, R. P.; Marshall, A. G. *Anal. Chem.* **2004**, *76*, 2511.
(271) Wu, Z. G.; Jernstrom, S.; Hughey, C. A.; Rodgers, R. P.; Marshall, A. G. *Energy Fuels* **2003**, *17*, 946.
(272) Herod, A. A.; Stokes, B. J.; Tye, R. E.; Kandiyoti, R.; Gaines, A.; Li, C.-Z. *Fuel* **1993**, *72*, 1317.
(273) Herod, A. A.; Zhang, S. F.; Carter, D. M.; Domin, M.; Cocksedge, M. J.; Parker, J. E.; Johnson, C. A. F.; John, P.; Smith, G. P.; Johnson, B. R.; Bartle, K. D.; Kandiyoti, R. *Rapid Commun. Mass Spectrom.* **1996**, *10*, 171.
(274) Johnson, B. R.; Bartle, K. D.; Cocksedge, M.; Herod, A. A.; Kandiyoti, R. *Fuel* **1998**, *77*, 1527.
(275) Acevedo, S.; Gutierrez, L. B.; Negrin, G.; Pereira, J. C.; Mendez, B.; Delolme, F.; Dessalces, G.; Broseta, D. *Energy Fuels* **2005**, *19*, 1548.
(276) Boenigk, W.; Haenel, M. W.; Zander, M. *Fuel* **1990**, *69*, 1226.
(277) Morgan, T. J.; George, A.; Alvarez, P.; Herod, A. A.; Millan, M.; Kandiyoti, R. *Energy Fuels* **2009**, *23*, 6003.
(278) Lafleur, A. L.; Nakagawa, Y. *Fuel* **1989**, *68*, 741.
(279) Pindoria, R. V.; Chatzakis, I. N.; Lim, J.-Y.; Herod, A. A.; Dugwell, D. R.; Kandiyoti, R. *Fuel* **1999**, *78*, 55.
(280) Al-Muhareb, E. M.; Karaca, F.; Morgan, T. J.; Herod, A. A.; Bull, I. D.; Kandiyoti, R. *Energy Fuels* **2006**, *20*, 1165.
(281) Wiehe, I. A. *Process Chemistry of Petroleum Macromolecules*; CRC Press, Taylor and Francis: Boca Raton, FL, 2008; Chapter 2.6.3.
(282) Omais, B.; Courtiade, M.; Charon, N. g.; Thiébaut, D.; Quignard, A. *Energy Fuels* **2010**, *24*, 5807.
(283) Omais, B.; Charon, N.; Courtiade, M.; Ponthus, J.; Thiébaut, D. *Fuel* **2013**, *104*, 805.
(284) Herod, A. A.; Li, C.-Z.; Xu, B.; Parker, J. E.; Johnson, C. A. F.; John, P.; Smith, G. P.; Humphrey, P.; Chapman, J. R.; Kandiyoti, R. *Rapid Commun. Mass Spectrom.* **1994**, *8*, 815.
(285) Domin, M.; Moreea, R.; Lazaro, M-J; Herod, A. A.; Kandiyoti, R. *Rapid Commun. Mass Spectrom.* **1997**, *11*, 638.
(286) Lazaro, M. J.; Herod, A. A.; Domin, M.; Zhuo, Y.; Islas, C. A.; Kandiyoti, R. *Rapid Commun. Mass Spectrom.* **1999**, *13*, 1401.
(287) Dickinson, E. M. *Fuel* **1980**, *59*, 290.
(288) Rongbao, L.; Zengmin, S.; Bailing, L. *Fuel* **1988**, *67*, 565.
(289) Guillen, M.; Blanco, J.; Canga, J.; Blanco, C. *Energy Fuels* **1991**, *5*, 188.
(290) Marsh, H.; Neavel, R. C. *Fuel* **1980**, *59*, 511.
(291) Zhang, H.; Carlson, T. R.; Xiao, R.; Huber, G. W. *Green Chem.* **2012**, *14*, 98.
(292) Seshadri, S. K.; Ruberto, R. G.; Jewell, D. M.; Malone, H. P. *Fuel* **1978**, *57*, 549.
(293) Swanslger, J. T.; Best, H. T.; Danner, D. A.; Youngless, T. L. *Anal. Chem.* **1982**, *54*, 2576.
(294) Yokono T.; Miyazawa K.; Obara T.; Sanada Y.; Marsh H. *15th Biennial Conference on Carbon*; American Carbon Society: Lexington, KY, 1981; Vol. *134*.
(295) Yokono, T.; Marsh, H.; Yokono, M. *Fuel* **1981**, *60*, 607.
(296) Gould, K. A.; Wiehe, I. A. *Energy Fuels* **2007**, *21*, 1199−1204.
(297) Joseph, J.; Baker, C.; Mukkamala, S.; Beis, S. H.; Wheeler, M. C.; DeSisto, W. J.; Jensen, B. L.; Frederick, B. G. *Energy Fuels* **2010**, *24*, 5153.
(298) Strahan, G. D.; Mullen, C. A.; Boateng, A. A. *Energy Fuels* **2011**, *25*, 5452.
(299) Christensen, E. D.; Chupka, G. M.; Luecke, J.; Smurthwaite, T.; Alleman, T. L.; Iisa, K.; Franz, J. A.; Elliott, D. C.; McCormick, R. L. *Energy Fuels* **2011**, *25*, 5462.
(300) Prauchner, M. J.; Pasa, V. M. D.; de Menezes, S. M. C. *J. Wood Chem. Technol.* **2001**, *21*, 371.
(301) Falco, C.; Perez Caballero, F.; Babonneau, F.; Gervais, C.; Laurent, G.; Titirici, M.-M.; Baccile, N. *Langmuir* **2011**, *27*, 14460.
(302) Strausz, O. P.; Safarik, I.; Lown, E. M. *Energy Fuels* **2009**, *23*, 1555.
(303) Bermejo, J.; Menéndez, R.; Fernández, A. L.; Granda, M.; Suelves, I.; Herod, A. A.; Kandiyoti, R. *Fuel* **2001**, *80*, 2155.
(304) Belkina, T. V.; Lur'e, M. V.; Stepanenko, M. A. *Kimiya Tverdogo Topliva* **1981**, *15*, 143.
(305) Cheshko, F. F.; Pityulin, I. N.; Pyrin, A. I.; Shustikov, V. I. *Coke Chem.* **1995**, *7*, 36.
(306) Fernandez, A. L.; Granda, M.; Bermejo, J.; Menendez, R. *Carbon* **1999**, *37*, 1247.
(307) Álvarez, P.; Granda, M.; Sutil, J.; Menendez, R.; Fernández, J. J.; Viña, J. A.; Morgan, T. J.; Millan, M.; Herod, A. A.; Kandiyoti, R. *Energy Fuels* **2008**, *22*, 4077.
(308) Fernández, A. L.; Granda, M.; Bermejo, J.; Menéndez., R. *Carbon* **2000**, *38*, 1315.
(309) Bermejo, J.; Fernández, A. L.; Granda, M.; Rubiera, F.; Suelves, I.; Menéndez, R. *Fuel* **2001**, *80*, 1229.
(310) Ben, H.; Ragauskas, A. J. *ChemSusChem* **2012**, *5*, 1687.
(311) Dufour, A.; Castro-Diaz, M.; Brosse, N.; Bouroukba, M.; Snape, C. *ChemSusChem* **2012**, *5*, 1258.
(312) Dufour, A.; Castro-Díaz, M.; Marchal, P.; Brosse, N.; Olcese, R.; Bouroukba, M.; Snape, C. *Energy Fuels* **2012**, *26*, 6432.
(313) Fletcher, T. H.; Pond, H. R.; Webster, J.; Wooters, J.; Baxter, L. L. *Energy Fuels* **2012**, *26*, 3381.
(314) Bertoncini, F. *Abstracts of Papers*; 232nd National Meeting of the American Chemical Society, San Francisco, CA, Sept 10−14, 2006; American Chemical Society: Washington, DC, 2006; p 1.
(315) Fong, W. S.; Peters, W. A.; Howard, J. B. *Fuel* **1986**, *65*, 251.